KU LEUVEN

ARENBERG DOCTORAL SCHOOL
Faculty of Engineering Science

Optimal operation of hybrid AC/DC meshed grids

Johan Rimez

Supervisory Committee:
Prof. dr. ir. J. Vandewalle, chair
Prof. dr. ir. R. Belmans, supervisor
Prof. dr. ir. D. Van Hertem, co-supervisor
Prof. dr. ir. J. Driesen
Prof. dr. ir. W. D'haeseleer
Prof. dr. ir. R. Sabariego
Prof. ir. W. L. Kling
(TU Eindhoven, The Netherlands)
Prof. dr. ir. O. Gomis-Bellmunt
(UPC Barcelona, Spain)

Dissertation presented in partial fulfillment of the requirements for the degree of Doctor in Engineering Science

March 2014

Optimal operation of hybrid AC/DC meshed grids

Johan RIMEZ

Supervisory Committee:
Prof. dr. ir. J. Vandewalle, chair
Prof. dr. ir. R. Belmans, supervisor
Prof. dr. ir. D. Van Hertem, co-supervisor
Prof. dr. ir. J. Driesen
Prof. dr. ir. W. D'haeseleer
Prof. dr. ir. R. Sabariego
Prof. ir. W. L. Kling
(TU Eindhoven, The Netherlands)
Prof. dr. ir. O. Gomis-Bellmunt
(UPC Barcelona, Spain)

Dissertation presented in partial fulfillment of the requirements for the degree of Doctor in Engineering Science

March 2014

D/2014/7515/35
ISBN 978-94-6018-811-4

Preface

-A PhD is a license to do research, Dirk Van Hertem

Starting a PhD research after already eight years of working in the industry is not evident. At the end of 2007, the Belgian Transmission System Operator, Elia, my employer at that time, had just finished a huge project with installing three of the biggest phase shifting transformers, and the step for even more challenging technology was very close by. The experiences I gathered while working with these devices, convinced me that, if I could reorganise my working habits slightly and put just a little more pressure on myself, I could combine this research together with my normal full-time job. Almost against good judgement, completely intuitively, I made the step to the K.U.Leuven and professor Ronnie Belmans, and started officially in January 2008.

The first three years are characterised by learning to use a whole set of new tools (load flow calculations, optimal power flow, grid dynamics) and an (unforeseen) change of organisation within the expertise department. My job definition changed, I needed to learn to use new tools there as well, these were not the optimal conditions to start the PhD.

The last three years of the PhD, roughly starting in 2011, were the most productive ones. I mastered the tools, learned to play with them and started to add one by one the new functionalities to the original programming code.

I'm very grateful to have such a fantastic partner of life, Erika, who day by day, stands by my side and supported me with every aspect of this research. My promoters Ronnie Belmans and Dirk Van Hertem: without your energy, enthusiasm, dedication and wondrous insights, I wouldn't have finished this work. Also the ESAT-Electa researchers, Jef, Hakan, Simon, David and Steven, you were always there to help me with the academic aspects of doing research, writing papers and concluding this work.

I wish to thank all my colleagues at Elia's: you were always very positive and supportive to my work and gave me the opportunity to, condition-less, combine both work and research. My gratitude goes especially to professor Markus Berger, COO, Mr. Didier Wiot, head of the Expertise department (called TGX) and finally my two direct chiefs Dr. Cédric Moors and Dr. Benjamin Genêt who were extremely patient with me.

Furthermore, I thank all the members of the jury. Their remarks and suggestions are essential to the quality of this work.

Abstract

Direct Current (DC) technology has already a long history for long distance bulk transmission of electric power. As technological developments in this field progressed, applications based on the Voltage Source Converter schemes became available combining independent control of active and reactive power with the possibility for multi-terminal layouts. Meshed DC grids operating as an overlay or a parallel path to the existing alternating current (AC) high voltage systems are becoming a reality now.

Calculation methodologies and simulation tools to analyse the static and dynamic behaviour of such DC systems are a crucial aspect for planning, development and operation of hybrid grids.

The main contribution of this research is the development of mathematical methodologies and applications for the optimal power flow of the hybrid, meshed AC/DC system for normal and security constrained cases. A unified approach has been followed for fast convergence of the optimisation algorithms. The developed functionalities give flexibility to the optimality objectives so that multi-objective analyses can be performed as well. As an application, the thesis combines all added functionalities into a single tool, proposing the grid operator the most useful control actions to get the high voltage grid back into a healthy state after an incident occurred.

The development and verification of the methodologies are done with MatPower, an open-source power flow and optimal power flow calculation tool for the Matlab environment.

Beknopte samenvatting

De gelijkstroom- (DC) technologie heeft al een lange weg achter de rug voor toepassingen waar het transport over lange afstanden met hoge elektrische vermogens centraal staan. Door voortdurende technologische ontwikkelingen zijn nieuwe toepassingen, gebaseerd op het spanningsbron-convertor concept, mogelijk geworden. Hierbij worden onafhankelijke regeling van actief en reactief vermogen gecombineerd met verbindingen waarop meer dan twee convertor-installaties in parallel worden aangesloten. Vermaasde gelijkstroomnetwerken die als bovenliggend net samenwerken met het bestaande wisselspanningsnet (AC) of er een parallelle verbinding mee vormen, worden in de nabije toekomst realiteit.

Berekeningsmethodologieën en simulatieprogramma's om het statisch en dynamisch gedrag van deze gelijkspanningssystemen te bestuderen, zijn cruciaal voor planning, ontwikkeling en uitbating van dergelijke hybride netwerken.

De hoofdbijdrage van deze thesis is de ontwikkeling van wiskundige methodes en toepassingen voor de optimale uitbating van hybride AC/DC netwerken in normale toestand en rekening houdend met de nodige redundantie voor een veilige uitbating. Er werd een gecombineerde aanpak gevolgd voor snelle convergentie van de optimalisatie-algoritmes. Deze ontwikkelde functionaliteiten geven flexibiliteit aan de objectieffuncties zo dat ook multi-objectief analyses kunnen doorgevoerd worden. Als toepassing combineert dit onderzoek alle toegevoegde functionaliteiten in een tool die aan de netwerkbeheerder toelaat om de meest efficiënte regeling uit te voeren om het net terug in een veilige toestand te brengen nadat er een incident heeft plaatsgevonden.

De ontwikkeling en verificatie van de methodologieën werden gedaan met

MatPower, een openbronsoftware-pakket voor netwerkbelastings- en optimalisatieberekeningen in de Matlab-omgeving.

List of abbreviations

AC	Alternating Current
CAPEX	CAPital EXpenditures
CCC	Capacitor Commutated Converter
CIGRE	International council on large electric systems (French: *Conseil International des Grands Réseaux Électriques)*
CWE	Central Western European (control zone)
DAFC	Day-Ahead Congestion Forecast
DC	Direct Current
ENTSO-e	European Network of Transmission System Operators for Electricity
FACTS	Fast/Flexible AC Transmission Systems
HV	High Voltage
HVDC	High Voltage Direct Current
IEEE	Institute of Electrical and Electronics Engineers
IGBT	Insulated Gate Bipolar Transistor
KKT	Karush-Kuhn-Tucker (conditions)
LCC	Line Commutated Converter
MI	Mass Impregnated (cables)
MIPS	MATLAB Interior Point Solver
MMC	Multi-level Modular Converter
PCC	Point of Common Coupling
PF	Power Flow calculation
PFC	Power Flow Controlling devices
PWM	Pulse Width Modulation
OPEX	OPerating EXpenditures

SCR	Short Circuit Ratio
SCOPF	Security Constrained Optimal Power Flow calculation
STATCOM	STATic COMpensator
SVC	Static Var Compensator
SM	SubModule
SSSA	Steady State Security Analysis
TSO	Transmission System Operator
VSC	Voltage Source Converter
XLPE	Cross Linked PolyEthylene (cables)

List of mathematical symbols and subscripts

A star (*) as unit means that the unit depends on the context.

Symbol	*Usage*	*Unit*
B	Barrier function or susceptances, depending on the context	* or pu
C	Cost factor or the connection matrix, depending on the context	* or -
c	Vector of arbitrary constants	*
f	Objective function of an optimisation case	*
G	Conductance	pu
g	Equality constraint function vector	*
h	Inequality constraint function vector	*
J	Jacobian matrix	*
H	Hessian matrix	*
I	Current	pu
L	Vector with limit values	pu
P	Active power	pu
Q	Reactive power	pu
R	Resistance	pu
s	Vector of slack variables	*
U	Voltage	pu
u	Vector of non-automatic control variables	*
W	Global weighting factor	-
w	Individual weighting factor	-
X	Subspace with $x \in X$, or reactances depending on the context	* or pu

x	Vector of state variables	pu
Y	AC or DC system admittance matrix, depending to the context	pu
z	Vector of state variables	pu
ϵ	Parameter sequence $\{\epsilon_k\}$	-
ϕ	Argument of a complex number	$^\circ$
λ	Lagrange multipliers associated to the inequality constraint function vector f	-
μ	Lagrange multipliers associated to the equality constraint function vector g	-
Θ	Phase angle vector	$^\circ$
θ	Phase angle	$^\circ$
ω	AC grid pulsation	$^\circ/s$
∇	Nabla operator	
$\jmath$	Imaginary unit for complex numbers	
$\mathfrak{L}$	General symbol for the Lagrangian function	
$\mathbf{x} = [x_i]$	For some mathematical developments, a clearer distinction between full matrices and their elements is made for easy readability	
	Subscripts	
$_{a,b,c}$	Phases a, b or c	
$_{a}$	Attractor value	
$_{br}$	Branch element	
$_{c}$	Converter side	
$_{DC}$	DC quantity	
$_{g}$	Generator	
$_{i,j}$	i^{th} or j^{th} element in the set	
$_{l}$	Grid load	
$_{m}$	Magnitude of a vector or complex number	
$_{P}$	Equations for active power	
$_{Q}$	Equations for reactive power	
$_{s}$	Source or grid side	
*	value of the associated vector at the optimum	

Contents

List of Figures

List of Tables

Chapter 1

Introduction

1.1 Situation and context

Technological advancement and project development always go together in engineering. No single project, with its specific technical challenges, is possible without the backup of research and development efforts. It is always satisfactory for researchers, both in the academia and industry to see innovations materialise into huge and prestigious realisations with a real societal impact.

This is certainly true for the electricity transmission business. Handling high currents at high voltages is a very specific action field with a high impact on society and the environment. The ambition to be more efficient, more reliable, more manageable and flexible, while limiting visible, audible and environmental impacts, makes this domain very relevant for engineers and academia.

Many company initiatives and research projections foresee huge shifts in the current mindset on the development and operation of the High Voltage Grid. Up till now, the main solution to connect generation sites and load centres are the classic Alternating Current (AC) high voltage grids. For some specific cases where long distance bulk transport is needed, point-to-point Direct Current (DC) connections were installed. Already new applications emerge in this field e.g. the integration of DC links into a meshed AC grids. Instead of transferring power to islands or asynchronous grids (e.g. NorNed [1, 2] 700 MW between The Netherlands and Norway, IFA2000 (2000 MW) between France and England, Nemo (1000 MW) between Belgium and England [3]), these new links (the

projects ALEGrO [4], Inelfe [5] amongst others) are going to be operated parallel with the existing 400 kV interconnection grid with the explicit aim for the controllability of the HVDC installations [6].

It is expected that these first DC links are the beginning of the concept of the Direct Current grids. Multi-terminal applications for the Line Commutated Converter have been installed and already commissioned: the SACOI link (connecting the Italian mainland with Corsica and Sardinia [7] is the first one ever installed (1987) and the Québec-New England connection (2000 MV, commissioned in 1992) [8] is the largest LCC multi-terminal in service today. One project, the South-West Link [9], a point-to-point Direct Current connection with the two converter stations in the Swedish meshed AC grid, was first announced to have one future extension into the Norwegian grid. This would have been the first announced multi-terminal application using the Voltage Source Converter (VSC) technology.

In their 2013 grid development plan, the four German transmission system operators (TSOs) propose to install four north-south corridors, with a total length of 2100 km and total capacity of 12GW [10]. A multi-infeed scheme in this outline for the time horizon 2023 is foreseen (figure 1.1). International bodies (CIGRE, ENTSO-e) are working on frameworks to accommodate complete DC grids into the existing high voltage AC transmission system [11, 12]. The MEDGRID project [13] develops an even more challenging scheme to connect all countries around the Mediterranean Sea (time horizon 2020-2025).

Yet an additional dimension to this already complex matter, is that many initiatives, like the European Supergrid initiative [14, 15, 16, 17, 18], foresee the implementation of HVDC installations on offshore platforms. This concept has many advantages, e.g. the connection of nearby offshore wind power plants [15, 19] or the construction of backbone grids, e.g. the Atlantic Wind Connection [20] in order to avoid congestion in the on-land AC grid. However, offshore applications of HVDC installations bring along a high number of conceptual issues [21] together with high investment costs.

New theoretical models and simulation techniques for the static, dynamic and transient behaviour to study the interaction of the DC and AC network are needed. These algorithms are needed at every stage of modelling, planning, installation and operation of the individual point-to-point DC links or the fully developed DC grid, taking into account the difference in nature of the AC and DC power flow. The AC power flow is determined by the injections in the buses and the impedances of its branches and the inputs and outputs at its nodes,

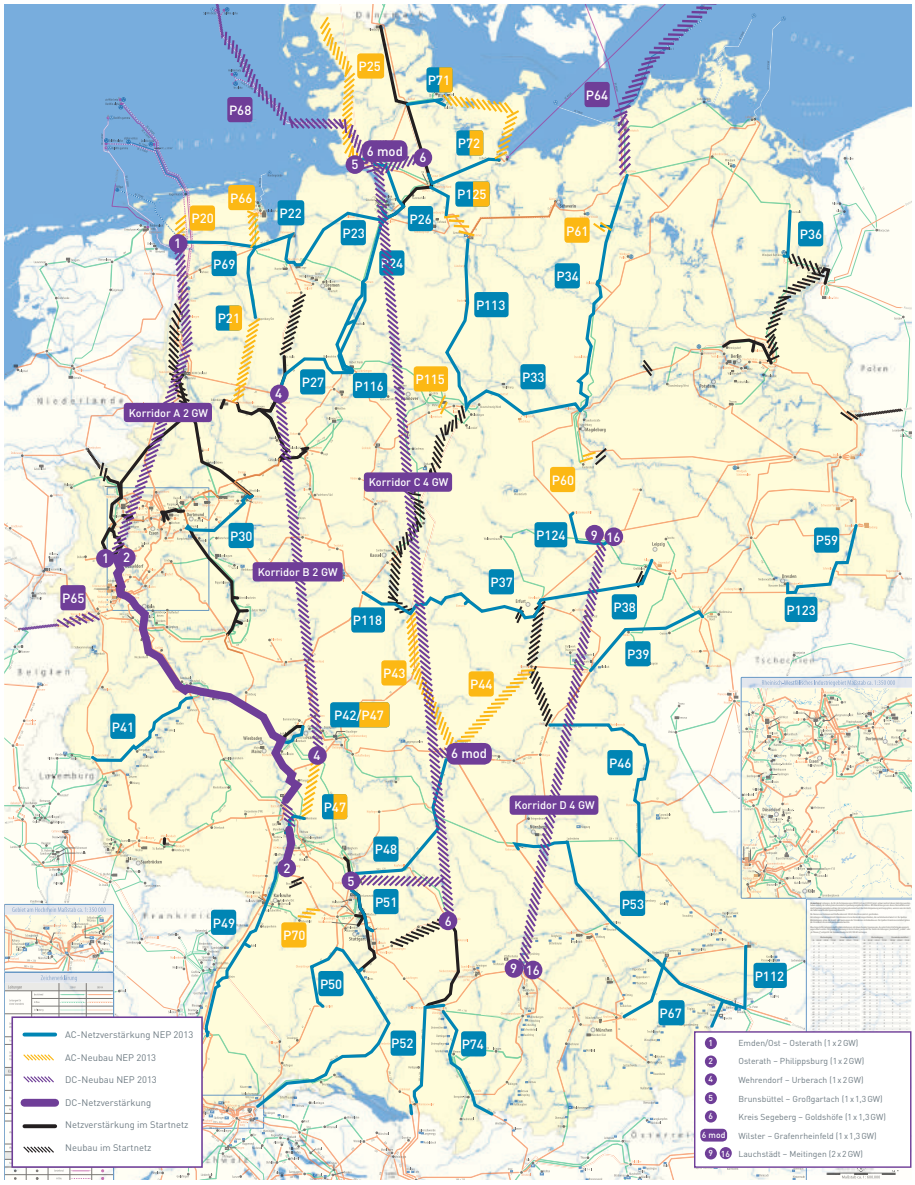

Figure 1.1: German grid development plan 2013, horizon 2023, version March 2013, source: www.netzentwicklungsplan.de

whereas the power flow through the AC/DC converters are controlled to given setpoints. This results in controlled exchanges between the AC and DC power flows. The introduction of semiconducting devices implies indeed the use of fast programmable, often project specific control systems which should possess at least the same robustness and stability of the existing AC grid.

The contribution of this research is the development of fundamental mathematical methodologies and calculation techniques for the optimal steady-state behaviour of meshed AC and DC grid operated in parallel while taking security constraints into account.

More in particular, the research has extended the classic formulation of the AC grid optimisation with new functionalities: modelling hybrid meshed AC/DC grids and their simultaneous optimisation, optimisation with contingency constraints and applications for the optimisation objectives: customisation of the cost function, multi-objective optimisations, constraining state variables to defined values and calculating power flow by optimal power flow algorithms.

In principle, the conclusions of this work hold for both types of converter technologies, Line Commutated (LCC) and Voltage Source Converter (VSC), as long as they are able to inject or absorb the active and reactive power resulting from the calculations. Here, the voltage source converter topology has a natural advantage over the LCC technology: as long as the requested power flow stays within their ratings, the converters have full independent control over both active and reactive power exchange. Furthermore, voltage source converters allow for multi-terminal grids at the AC side.

1.2 Main contributions

The main contribution of the thesis is to develop a methodology to perform security constrained optimisation of hybrid AC/DC grids, taking into account both corrective and preventive actions. A second objective of the work was to extend the methodologies into an open-source grid optimisation tool which is capable of integrating a wide range of DC grid topologies and security constrained OPF. This tool was built as a fundamental extension of an existing open-source tool, MatPower, reusing its data structures, design methodology

and numerous sample systems.

The development of OPF routines for hybrid AC/DC systems is an ongoing research topic, with several researchers working on it. This work exceeds current studies by integrating state-of-the-art research of AC optimisation with the integration of state-of-the-art VSC HVDC systems. This has resulted in developed algorithms and methodologies which are implemented into one unique and robust calculation tool.

The specific contributions are:

- whereas most OPF software optimises one AC system at a time, the security constrained optimal power flow for the preventive measures, demands an extension for which several slightly different AC systems are optimised simultaneously. The number of parallel optimisation cases is only limited by the robustness and efficiency of the optimisation algorithm. The methodology used compiles the different cases into one global optimisation, which calls the individual cases using the traditional OPF routines.

- the second pillar of this research was the extension of the AC system with a DC overlay grid of any topology, whether it be a single point-to-point connection, multi-terminal scheme, ring structure or the most complex meshed DC grid of any size and complexity (Figure 1.2). With the developed methodologies, it is even possible to define a number of independent DC grids laid over the same AC grid or to connect separate AC grids using the DC grid. To define the DC grids, data structures analogous to their AC counterpart are constructed. The innovative aspect of this work is setting up the system equations for the DC grid and AC/DC converters and correctly linking them to the AC network. The same problem reduction philosophies (discarding outaged generators, branches and buses) as for the AC grid had to be followed.

- the implementation of these first two algorithms had to be such that they were not mutually exclusive: the implementation of the optimisation case is independent when none, only one of them or both functionalities are requested by the user.

- A flexible approach for the cost function has been implemented, giving the user a wider and extendible range of cost functions using any state variable (in comparison to the standard approach where only piece-wise linear or polynomial functions can be included).

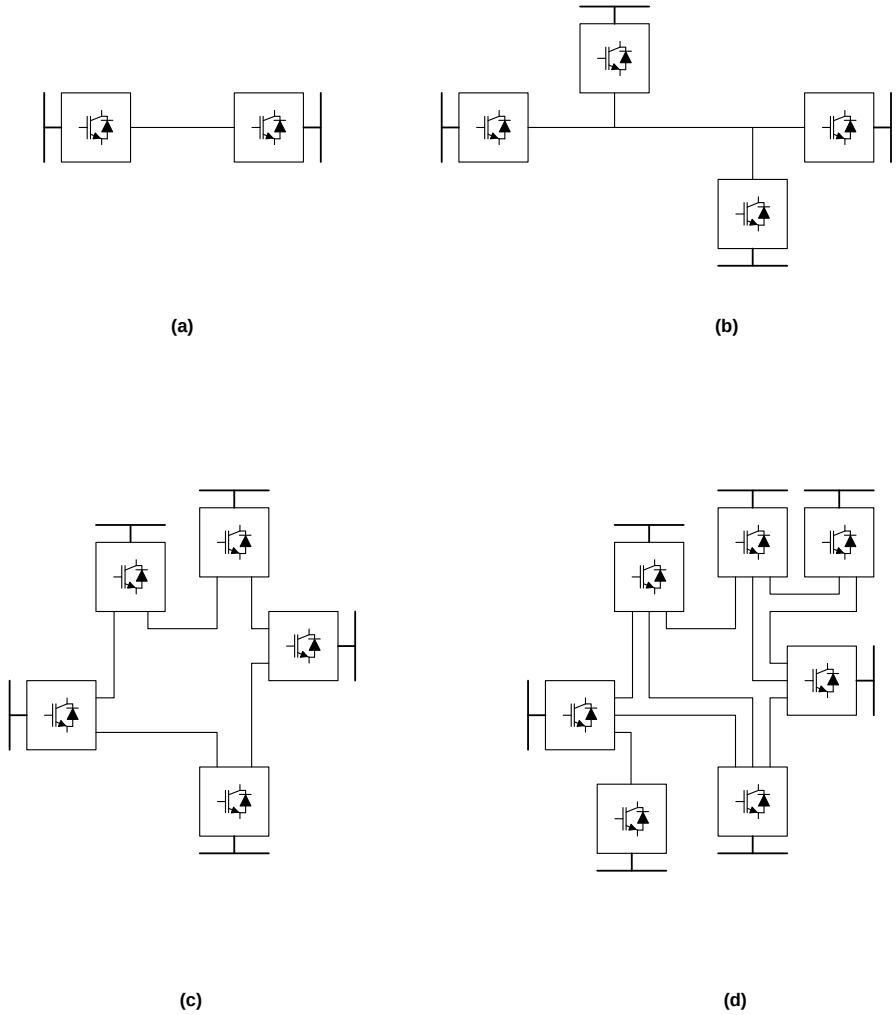

Figure 1.2: DC grid topologies: (a) point-to-point, (b) multi-terminal, (c) radial and (d) complex meshed grid configurations

Altering the optimisation routines for better performance and convergence acceleration was not an objective of this thesis. Nevertheless, the obtained tool performs well and sufficiently fast, through the use of adequate solvers and methodologies which are computational effective.

1.3 Objectives and tools

The main objectives of this research are the development of sound fundamental methodologies and mathematical tools to model meshed DC overlay grids in an existing AC system and to optimise them together as one unified optimisation case. This is done without and with security constraints. On top of the original cost functions programmed in MatPower, a wider range of cost function primitives has been implemented. Their weighted summation enables the multi-objective optimality analyses.

To test the implementation of the developed methods, only open-source power system software is used. MatPower, [22], has been chosen as the basis on which the developments have been built. The function calling prioritisation of Matlab has been extensively used to program a shell around the original MatPower routines and to entirely reuse the routines for the AC networks, providing replacement routines where appropriate.

All routines presented are to work together as one combined algorithm. The modules alter the program flow based on model specifications and settings provided by the user. The developed routines are created to be independent from custom-made optimisation routines, to guarantee maximum exportability and flexible use.

As with the existing MatPower routines, the methods developed in this research are not able to cope with discrete state variables (e.g. discrete positions of transformer tap changers and circuit breaker positions), since it is a mathematical problem that falls outside the scope of this work.

All algorithms have been successfully tested on three sample systems, which are presented in appendix A.

1.4 Overview of the text including appendices

This chapter, provides the context of the research and own contributions to the topics. Chapter 2 gives a brief overview of the current state-of-the-art of AC/DC converter technology and DC equipment relevant to this work.

In chapter 3, the reader finds the general discussion on the context and use of optimal power flow calculations in the wider range of power system calculations. The relevant topics of the optimisation theory for systems with non-linear cost functions and constraints are given together with theorems to answer questions on convergence and local and global optima of the problems. A method is discussed on how to extend a ready-made optimisation problem with additional equality and inequality constraints as input for the following chapters. The choice of the cost function, general aspects of multi-objective optimisation and the related Pareto fronts are discussed. Finally, two special applications are developed: keeping state variables at defined values and applying the optimal power flow to a classic power flow problem.

Chapter 4 is dedicated to the contingency constrained optimal power flow (OPF). Besides an overview of the current developments on this topic, the classic AC optimal power flow is extended to simultaneously take contingencies into account, thus defining the preventive security constrained optimal power flow. The proposed formulation is general, so that the DC grid from chapter 5 is automatically included.

Chapter 5 extends the AC optimisation problem with AC/DC converters and two distinct methods to formulate the DC network topology into a set of non-linear equality constraints. To parallel the AC network, power flow limits have been implemented in the converters, DC bus voltages and DC branch flows, by means of non-linear inequality constraints.

Chapter 6 discusses how each of the implementations of the features of previous chapters interact and form one combined algorithm. For demonstration purposes, a search algorithm is proposed to combine DC grids, contingency constrained optimisations and custom-made objective functions as a decision aid to the system operator to get the system back to a safe state after a grid incident.

Chapter 7 summarises the main achievements of this work and discusses further developments.

This work also presents four appendices. They are an integral part of this work, rendering it a self-sustainable text for which the reader does not necessarily need to have other reference works at hand. However their content is not essential for the good understanding and reading of the different chapters.

- Appendix A discusses the base functionalities of MatPower and the added methodologies developed here. An overview of three sample networks to test the new algorithms is given.
- Appendix B gives a complete iterative optimisation routine using the Barrier method.
- Appendix C develops the non-linear equality constraint equations to describe the AC grid topology and branch impedances.
- Appendix D completely states all relevant equations for the AC/DC converter model .
- Appendix E gives an overview of the implemented routines and data structures of the developed optimisation functionalities.

Chapter 2

HVDC technology: converter and DC grids

2.1 Goal

This chapter gives a historical overview of the technological evolutions of the most applied High Voltage Direct Current technologies and a qualitative rationale behind the DC transmission systems. Several variants for both line commutated (LCC) and voltage source (VSC) converter types as well as a qualitative comparison between both technologies are discussed. The chapter concludes with reference material on underground DC cables.

2.2 Historical background and rationale

2.2.1 Parallelism of AC and DC grids

Alternating current (AC) is the main technology for all electricity transmission and distribution networks nowadays. This technology has predominated direct current (DC) over the years, although both technology streams were developed and proposed as the ultimate solutions for electrical generation, transmission and distribution system in the beginning of the electricity era, around the late 1880s.

At that time, the American inventor and businessman Thomas Edison (°1847 - †1931), promoted systems based on direct current. Edison had an interest in a few electrical companies which merged into The General Electric Company (GE). The main loads were small DC motors and incandescent light bulbs. Cities started to get electrified with a DC grid, but as soon as a large expansion of the grid had to be envisaged, technical problems arose. The rated voltages of these grids remained fairly low though long distance transportation had to be established. Only small consumption islands around the generation plants could be connected.

The other camp in "The War of the Currents" was situated around the entrepreneur George Westinghouse Jr. (°1846 - †1914) and the inventor Nikola Tesla (°1856 - †1943). They were in favour of the at that time less advanced AC appliances, but over the years, as motors and eventually transformers became available, their solution had natural advantages for rapid expansion of the electricity grid.

Nevertheless for the electricity grids, demanding the transportation of huge amounts of energy over very long distances, DC grids were not completely pushed away. Still today in Europe, almost all metro, tramways, trolley buses and a significant part of the electrified railway lines use DC. Only after the invention of a whole set of power electronic components and appliances (variable speed drives), high-speed railways supplied by AC current emerged.

Electricity grid developers have always accepted the natural advantages of DC voltages: in steady-state conditions, overhead lines and underground cables do not require a charging current, neither do they exhibit an inductive voltage drop, making the technology interesting for e.g. very long distance transmission. This is why, starting from the 1950s, research and development have been done to still be able to develop high voltage DC equipment primarily in combination with long distance overhead lines. In this period, the first commercial HVDC connections were installed: an undersea cable connection between the mainland of Sweden and the Gotland island was commissioned in 1954 (20 MW, 90 km) [23] and a mixed overhead line/underground cable connection of 30 MW for 125 km was built in Russia between the cities of Moscow and Kashira (1959) [24]. Both installations used mercury arc valves.

2.2.2 Technological evolution of DC grid equipment

The first developments in this field were rotating DC machines. The rated voltages were limited, due to insulation constraints. The mere use of moving equipment, and specifically the commutator, did not add to the reliability of the equipment either. Not being able to produce high voltages, the practical radius for a well-developed distribution system was fairly limited.

Later on, in the 1920s, mercury arc valves became available, both for public transport applications as for the electricity transmission business. A big disadvantage of this technology (besides having to manipulate large quantities of the heavily disputed chemical element mercury), are the so-called arc-back faults, caused by high inversely polarised voltages, leading to backwards directed current.

With the rise of the (static) semiconductors, the thyristor based converter appeared. The first project using this type of technology was the Eel River back-to-back scheme, rated 320 MW, commissioned in 1972 [25]. These installations are based on robust operating principles and materials: they cancel out the arc-back faults of the mercury valves in a natural way. However, the trade-off using thyristor technology is the generation of a lot of (other) inconvenient issues, especially regarding harmonics on the grid and the inherent constant need for reactive power. These converters need the grid to which they connect, to be up and running, as their principle to commute from one conducting thyristor to the next one, requires the zero crossing of the line voltage. The common name for this type of installation is derived from this operating principle: Line Commutated Converter (LCC). This principle renders the LCC installation inadequate for feeding into weak networks or for black start[1].

As LCC installations are growing even higher in voltage and rating, a second movement in the market asked for smaller installations, with a more limited impact on footprint, harmonics and reactive power: the voltage source converter (VSC). Having taken inspiration from AC motor drives, the transistor based converter made its appearance, as an outscaled version of a variable speed drive, to deliver power from the mainland of Sweden to the island Gotland [26]. In the beginning the technology used Pulse Width Modulation (PWM) converters and later the Multi-level Modular Converter (MMC) type appeared as discussed further in this chapter. Voltage source converters, by controlling the voltage of

[1] Black start is the procedure to have one or more generation units injecting into a grid that has partially or completely been shut down after a major incident.

the DC system at high and stable values, are more suitable for multi-vendor applications, multi-infeed topologies and eventually meshed DC grids.

2.2.3 Qualitative rationale behind DC transmission systems

Even though alternating current was chosen as the preferred technology, in certain circumstances and applications, direct current still has benefits over its AC counterpart. These are listed in the list below.

- Improved **Controllability** of power through the converter. When comparing an AC overhead line or underground cable with a point to point DC connection, it is not guaranteed for the AC variant to be able to operate at its maximum rating. Instead, the flow through the link depends on the power flow in the close electrical vicinity of that link: the bus voltage angles of its connecting substations are the determining factor. Some investments could prove less useful in AC technology. On the other hand, using DC technology, the operator is able to impose the power flow through that link surrounded by other parallel (AC or DC) links, by setting the proper setpoint. Steady-state overloading of the converters or connections is impossible. The link simply takes over a controlled part of the flow taken by these other branches. One application is the Inelfe-project [23].
- **Asynchronous interconnections**: indeed, the converters on either side can properly operate at the local AC frequency independently from the other converters. An application to obtain this effect is the back-to-back configuration: two converters situated next to each other with only a very short DC bus in between them. Even a transition between a 50 and 60Hz system is possible (Saoudi Arabia, Japan, Brasil-Argentina)
- **Reduced propagation of grid faults**. With proper design of the DC transmission system, the connected AC grids become less vulnerable to grid events on the other converters (e.g. voltage collapses, symmetrical and asymmetrical faults).
- **Rapid control action**, especially true for VSC type converters. The converters provide a whole range of new control possibilities. Amongst others: system oscillation damping through voltage support and active power modulation, stepless local reactive power and voltage control, and black start capability (VSC only)
- **Ecological alternative** for a power plant next to a very important network load situated in an ecological sensitive region (e.g. a large city

as Paris or London). Instead of installing complete new corridors of HV cables or lines through that area, installing a converter next to these loads can often be a solution, e.g. the BritNed [27] and the NEMO connection [3].

- **No continuous reactive charging current** is required to operate the DC link, contrarily to their AC counterparts. For long AC connections, overhead lines and underground cables, two effects provoked by the reactive charging current require additional investments to be viable. The Ferranti effect causes the intermediate voltages to raise (even beyond acceptable equipment levels). At systematic intervals, the grid developer needs to install reactive compensators (e.g. shunt reactors, series FACTS devices), in order to properly energise and operate the link [25]. This additional equipment in turn may cause undesired secondary effects (e.g. subsynchronous resonance). The second effect of the reactive charging currents is that from certain distances onwards, the reactive current exceeds the current rating of the cable or overhead line itself, thus rendering these link inoperatable. DC technology does not experience these effects. Practically no distance limit is encountered, as a DC loaded cable just needs to be charged during energisation. This process can be controlled with minimal stress for equipment and network. The link does not require any charging current in steady-state and in unloaded conditions, the voltages are constant over the link with VSC applications.

- **Long subsea connections** are only possible using DC cable technology, as demonstrated by many recent projects: not only power transmission projects to link AC grids, but also offshore oil rigs (e.g. the Troll A oil rig [28]) are starting to use DC installations as a non-polluting means of high power supply.

- **Transmission losses** are lower for DC than for AC links with equal voltage and power rating. Again, the reactive charging current and reactive series losses add to the active power current and AC effects like the proximity-effect and the skin-effect alter the uniform current distribution in the conductors and push the current more towards the conductor surfaces, invoking more resistive losses.

- **Investment costs** for DC transmission lines and cables are lower, resulting in lower investment costs. As the investment cost for DC substations and the converter in particular, is considerably higher, a break-even point exists beyond which the DC variant is cheaper. The break-even point differs for each project, with respect to the connection length, rated voltage and power, overhead line and cable. Even when

disregarding the issues which arise with reactive loading current, DC technology uses only two conductors instead of three for the AC grid.

Still, when dealing with DC transmission technology, some disadvantages arise:

- **Investment costs**, especially the converter stations take a significant share of the project budget. The additional advantages, black start capability, flexible control possibilities and voltage regulation might result in a lower OPEX for the grid. However they are less quantifiable and thus more difficult to defend toward regulators and investors as the income is often regulated based on invested capital.
- **Engineering costs**. High level competences, vision change for maintenance and emergency interventions, extensive use of offline and real-time simulations for grid dynamics and electromagnetical transients are required for choosing operation setpoints and researching dynamic behaviour (e.g. maximum ramp rates), fault-ride-through capabilities, Power Quality requirements, generation of electromagnetic fields, electromagnetic interference with other installations, DC stray currents, asymmetrical fault behaviour. All items need to be researched, either in-house if the future owner is capable to do so, or by hiring external research or engineering companies. The engineering costs are expected to be considerably higher than in AC systems where the TSO has a long standing experience.
- **Switching losses** in the converters are prone to lower with the development of new topologies, but are still high (up to about 1 % of the rated power) compared to AC grid equivalents. The losses in the converters need to be evacuated by means of a complex and redundant cooling system, requiring a new range of auxiliary equipment.
- **Availability and reliability**, the presence of the elevated number of components: converters, cooling system, AC and DC switchyards, control cubicles, specially designed power transformers and so on, have an impact on the failure rate of the complete installation. With the modular design of the semiconductor bridges and control equipment nowadays, the whole installation can be designed towards a predefined rate of availability and reliability, but at the expense of higher investment costs. Redundancy of components leads to a better overall availability level, but the higher number of components requires more maintenance.
- **DC breaking units** are under development, but the first commercially operational unit still needs to be put into service. The whole idea around

meshed DC overlay grids depends on the availability of such breaker technology. Without it, the complete DC grid is outaged by a short-circuit at the DC busbar or on one of the DC links.

- **DC/DC converters** at the levels required for use in a DC grid, the direct equivalent of the AC phase shifting transformers and fast controls (or series FACTS devices), are less crucial in the development of a meshed DC grid: they control the current flowing in dedicated meshes. Still, their availability could greatly improve the viability of the overall concept.

From the previous discussion, it is clear that there are as many points supporting as well as opposing the choice for the DC technology to build new network branches or a complete overlay grid. Nevertheless, referring again to the extensive list of DC reference projects, this technology proves in some business cases to be the most suitable one.

2.3 Line Commutated Converter

2.3.1 Current state of developments

Recent development of the semiconductors allows the manufacturing of thyristors with a blocking voltage of 8.5 kV and current rating of 4kA [29]. The highest ratings for DC transmission installations already installed and in operation reach ±800 kV and 7.2GW. New developments for even higher characteristics go up to ±1100 kV and beyond 10GW [30].

2.3.2 Semiconducting elements: thyristor

The thyristor is a semiconducting device, which in a normal state blocks the current (open switch), and can be closed when positively biased (i.e. when the resulting, upcoming current would flow from the anode to the cathode (from the P- to the N-side of the semiconducting junction). A current pulse from the control mechanism initiates the conduction.

The thyristor only stops conducting, as with a diode, when the current flowing through it, would reverse its direction. This is beyond the control of the device and is why a thyristor cannot properly function without any AC source: it is needed for the current commutation, the process where the conduction is handed over from one thyristor to the next one in the sequence by opening

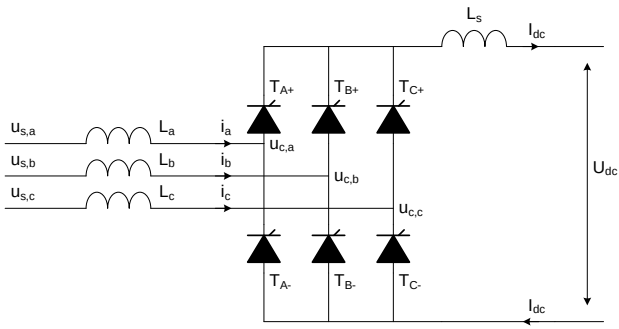

Figure 2.1: Basic 6-pulse LCC setup, Graetz bridge

the second and therefore (in a natural way) closing the first one. An external voltage delivers the necessary alternating wave shapes to let this happen.

A big advantage of the semiconductor technology, is that all devices can be integrated into stacking elements. By stacking them in series, higher voltages can be reached. The upper and lower half of the bridge assembly for one phase is called a *valve*. This is the most common practice to meet high power ratings. Elements can be connected in parallel as well to obtain higher currents.

In the LCC converters, the current in the DC system does not change polarity. The DC voltage polarity reverses the power direction. The control mechanisms primarily act on the DC current setpoint.

2.3.3 Typical schemes and topologies

At the basis of all subsequent LCC schemes, lies the Graetz bridge, a three-phase full-wave 6-pulse[2] converter (figure 2.1). By varying the so-called firing angle (the angle in electrical degree measured from the start of the conduction period of one thyristor) to shorten the conduction interval of each thyristor, one can inject or extract active power to or from the AC grid. As the direction of the current cannot change, power reversal implies a voltage polarity reversal.

[2]Pulse number is counted as the number of repeating DC voltage ripples per power frequency period.

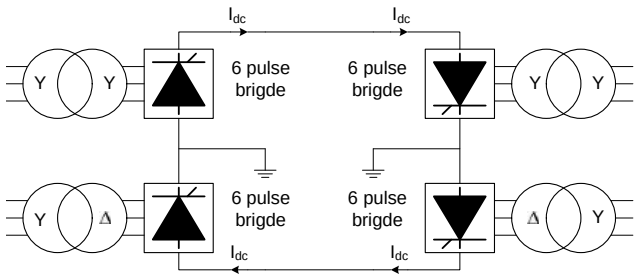

Figure 2.2: LCC Monopole configuration, with the midpoints grounded

Connecting this scheme generates an intolerable amount of current and voltage harmonics in the feeding AC grids, caused by the block-like wave shapes of the phase currents. In order to cancel out all multiples of the third harmonic, two Graetz bridges are connected in series at the DC side to jointly form the monopolar LCC scheme. When using one power transformer with its converter side winding using Y configuration and the other Δ connected (both with the same rated secondary voltage and with a fixed phase shift of 30°), the multiples of the third harmonic are cancelled. Only the $(12n \pm 1)$-harmonics of the power frequency (with $n \in \mathbb{N}_0$) remain ([25], p.525) and should be dealt with by means of AC filters to cope with the imposed Power Quality requirements. This combination is called a 12-pulse bridge[3].

The commutation between two subsequently conducting thyristors, incited by the firing angle always comes with a phase lag with respect to the line voltage, both in rectifier and inverter mode. LCC type converters are in any operation mode a net absorber of reactive power, varying with the firing angle and thus with the DC power setpoint. So, on top of the filter requirements described above, reactive compensation must be foreseen. Shunt capacitors are the most common solution. They can be integrated into the harmonic filters. STATCOM and synchronous condensers are other options.

Figure 2.2 shows this monopole configuration with the center points (a connection between the two Graetz bridges) grounded by a high impedance or by means of a harmonic filter (e.g. tuned to cancel out the $6^t h$ harmonic). The connections of both DC polarities have the same voltage amplitudes. In steady-state, no (DC) current flows through the earthing of the DC circuit.

[3]Some industrial applications which need an even more stable DC output, form 24- or 48-pulse bridges, requiring transformers shifting voltages down to 15° or 7.5°.

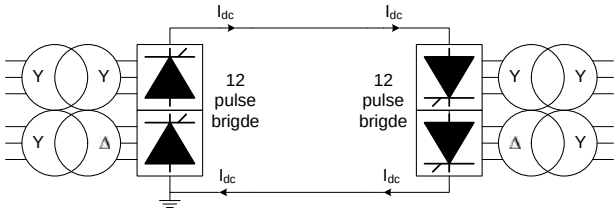

Figure 2.3: LCC Monopole configuration, with metallic ground return

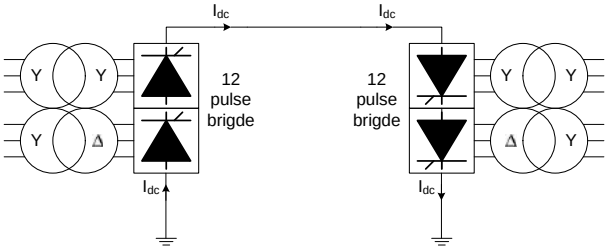

Figure 2.4: LCC Monopole configuration, with ground return using electrodes

Both converter halves handle half of the DC voltage, and thus half of the DC power as well.

On the other hand, figures 2.3 and 2.4 show that an asymmetrical setup is also possible for which one of the DC polarities remains at (or close to) the earth potential. The first figure still uses a metallic return, by means of a conductor insulated at low or medium voltage level. A compact way for the earth potential conductor is to be integrated as an additional layer in the same cable composition as the high voltage conductor [31]. The use of earth electrodes (figure 2.4), has the advantage to save one conductor (only the high voltage one remains), but due to electrode corrosion, compass deviation regulations and the adverse effect of vagabonding currents in the ground and seabed or other conducting assets, this variant is usually not allowed.

The power transformers need to be specifically designed for this application, as every converter side winding is additionally stressed by a permanent DC bias resulting in a more complex and expensive setup of the insulation system. The AC side harmonics flow through these converter transformers, causing additional hysteresis and eddy current losses. Harmonics of the DC side are smoothed

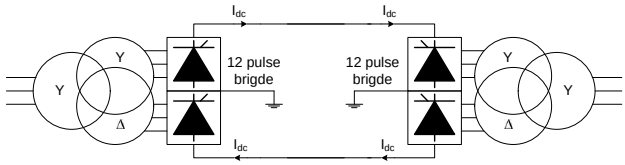

Figure 2.5: LCC Symmetric Monopole configuration with midpoints grounded

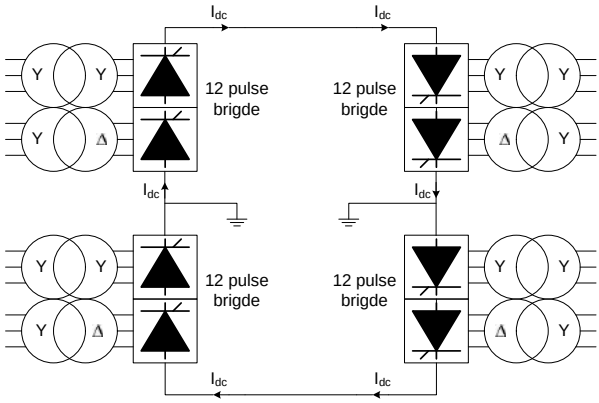

Figure 2.6: LCC Bipole configuration using two 12-pulse converters on each side

by the DC series reactor L_{DC} and by additional filters e.g. on the grounding points. Another variant is the symmetrical monopole configuration (figure 2.5). The previous setup uses independent 6-pulse bridges, and in case of failure in one part, after reconnection, it is possible to restart with the healthy half of the converter depending on the control. For the symmetrical monopole, this is not true. The power transformer has now three windings, is more complicated to build and transport and the converters cannot physically be separated. This configuration has the advantage to rely on less equipment (lower failure rate), but operates on an all-or-nothing setting [1]. An additional advantage is that in this case, only one transformer type is used, rendering spare part management easier.

An even more extended configuration is given by the bipolar transmission schemes, where two independent monopolar installations are combined in series (figure 2.6).

2.3.4 Main features

The need for filtering at the AC and DC side and the constant need for reactive power were already described in previous sections.
Another phenomenon called *commutation failure* endangers the proper operation of the LCC. This is initiated by certain circumstances, and happens when the commutation voltage reverses polarity before the commutation has properly ended. The thyristor valve starts conducting again, creating a DC side short-circuit between two of the arms.

The fail-safe mode of a thyristor is to get short circuited by itself. In the valves, as a precaution to natural failure phenomena, like commutation failure, a surplus number of semiconducting units is installed, so that only after a certain predefined number of thyristor failures, the complete installation must be outaged and the failed units replaced. Commutation failures are more likely to happen in inverter mode operation, with lower AC voltage amplitudes and with higher DC current setpoints with sudden changes in amplitudes and phase angles (coming with AC grid faults) as the trigger.

High power ratings for the converter can only be applied when connected to a strong grid, i.e. a grid with a relatively low short circuit impedance. The short circuit ratio (SCR), i.e. the ratio between the short circuit power level of the grid and the rated power of the LCC installation, gives the relative strength of the grid at the Point of Common Coupling (PCC). The converter has less impact on the grid for high numbers, and a lot of Power Quality issues may arise below certain values [25, 32]: voltage flicker, voltage instability, harmonic resonances, an increased probability of commutation failure, and (when applicable) also undesired resonance interaction with HVDC schemes nearby. An alternative scheme, the Capacitor Commutated Converter (CCC) has been developed and put into service, especially to deal with these low SCR problems (e.g. the Rio Madeira project [33]).

The overall footprint of this type of installation, especially the filtering of harmonics on the AC side, makes this technology less useful for places where ground or platform surface usage is critical.

LCC HVDC is a robust technology, in use for many years. During the last

years, with the introduction of the improved VSC schemes, this converter type is directed into the niche of ultra high voltage bulk transmission over long distances.

2.4 Voltage Source Converters

The development of high power transistors in the 1990s opened the way for a new direction in the HVDC technology [34, 35]. Based on the variable speed drives for induction and synchronous motors, upscaled versions led to the first grid applications. The first commercial application was the link to the Swedish Gotland island, at a rating of 50 MW using subsea cables at ±80 kV, commissioned in 1999 [26].

With the arrival of the Insulated Gate Bipolar Transistor (IGBT), switching schemes could be developed where the ability to open and close the transistor at fast speeds is essential. The IGBT has the advantage to produce low conduction losses and high switching speed and this at higher voltages and currents.

Three-phase converters using these semiconducting devices are generally called Voltage Source Converters (VSC) because they can be modelled as a controllable voltage source at the point of common coupling (PCC).

2.4.1 Current state of developments

The latest developments for the IGBT are gate voltages up to 6.5 kV and current ratings up to 3.6kA. Current commissioned converter configurations go up to ratings of 400 MW and ±200 kV. Links up to 1000 MW and ±320 kV are under construction. Even parallel LCC-VSC configurations are possible: the Skagerrak 4 VSC link (in operation 2014) is planned to operate in a bipole configuration using the same cable routing and connected to the same substations in Denmark and Norway as the Skagerrak 3 LCC connection [36]. Both links operate independently, however the controls of both projects need to be tuned to avoid interference.

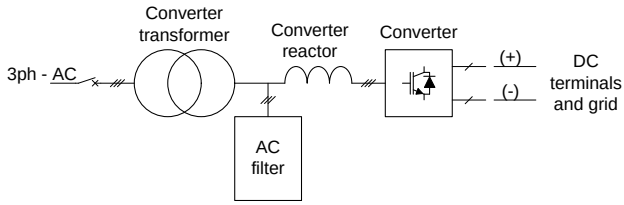

Figure 2.7: Base Voltage Source Converter equipment

2.4.2 Typical schemes and topologies

A typical converter station configuration is shown in figure 2.7. It is made up of the following parts:

- **Three-phase AC switchyard**, connecting with the point of common coupling (PCC).
- **Converter transformer**, essential to optimise the operation of the converter itself by matching the rated grid voltage with the operational voltages of the converter. Contrarily to the converter transformers meant for the LCC technology, the transformer windings are not stressed by a permanent DC bias, making them less complicated to design and manufacture.
- **AC filters** are less critical as only high order frequencies are generated by the switching actions which are easier to filter (with a low-pass filter) compared to the filter needs for the LCC technology.
- **The converter phase reactor** is one of the key elements of the installation. The main principle of the active and reactive current controls is to dynamically fine-tune the voltage drop over this reactor.
- **The IGBT Converter** is able to generate an arbitrary voltage waveshape: frequency, amplitude and phase angle are controlled. In combination with the impedance of the converter reactor and the AC grid voltage, independent control of active and reactive power is established.

The IGBT converter topologies mainly split into three mainstream directions, roughly following the chronological order of development.

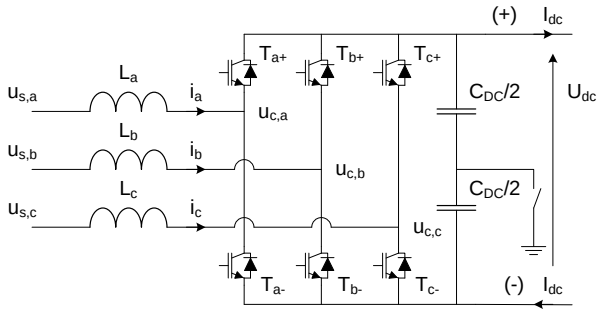

Figure 2.8: Two level Voltage Source Converter

Two-level converter

Figure 2.8 shows the typical 2-level voltage source converter topology. It consists of 6 IGBT-Freewheel Diode combinations acting as fast bidirectional switches. The switches in one phase (e.g. T_{a+} and T_{a-}) have an opposite status connecting their midpoint always to the half positive or half negative DC voltage. The reference voltage signal is translated into a series of positive and negative pulse blocks, using the Pulse Width Modulation (PWM) technique ([37], p.225). Even more advanced modulation techniques (e.g. Space Vector Modulation) for three-phase converters have been developed. A sample of the voltage output signals of the converter is shown in figure 2.9.

This technology is widely used for (large) motor drives. For HVDC transmission systems, there is a set of issues to be considered:

- **Switching losses** - To obtain high AC phase voltages, several stacks of IGBTs need to switch simultaneously at the switching instant. Switching causes losses depending on the switching frequency. A possibility to lower the switching losses is to lower the switching frequency, resulting in a higher voltage harmonic content.
- **Harmonics** - Square waves generate a high amount of additional harmonics to be filtered. As the switching frequency being higher than with the LCC technology, the needed filter capacity is less.
- **Material availability** - In order to obtain perfectly aligned switchings along each phase so that all IGBTs are evenly stressed, they need to have exactly the same characteristics. The operator needs to be sure

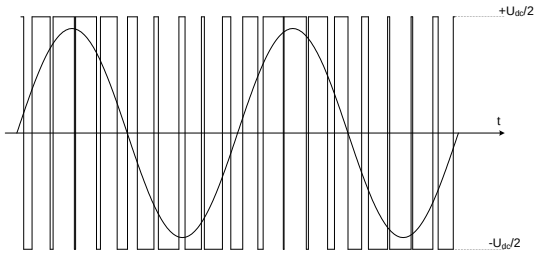

Figure 2.9: Phase-to-ground wave shapes for the 2-level VSC converter

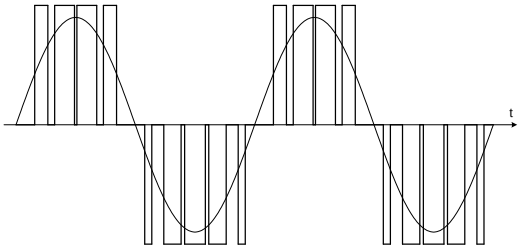

Figure 2.10: Phase-to-ground wave shapes for the 3-level VSC converter with clamped neutral point

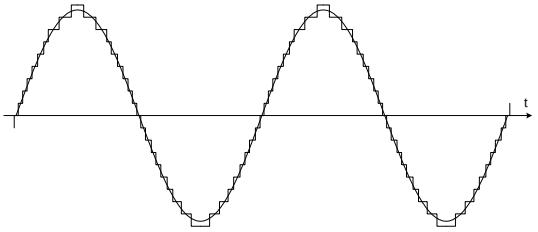

Figure 2.11: Phase-to-ground wave shapes for the VSC with the Modular Multilevel Converter Configuration

that correct spare parts are available during the whole lifetime of the installation.

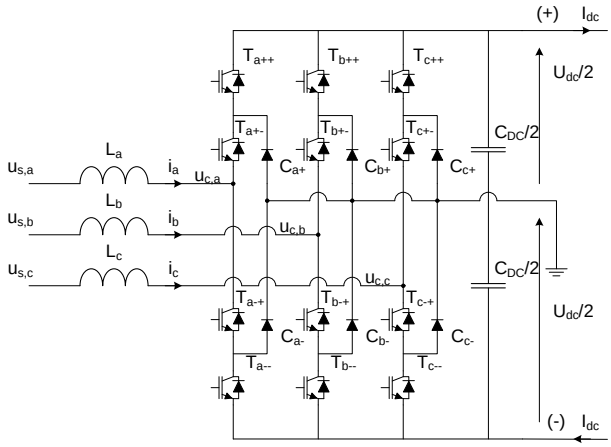

Figure 2.12: Three level Voltage Source Converter with clamped neutral point

Three-level converter

The topology for the three-level Voltage Source Converter with clamped neutral is shown in figure 2.12, the corresponding wave shapes in figure 2.10. This scheme is derived from the former two-level topology. However the upper and the lower half of the AC wave shape are generated by two half two-level converters. Clamping diodes balance the whole setup to the neutral point. This setup has the advantage that the converter output voltage can be either half positive, half negative or zero. The voltage stress on each individual PWM converter is cut in half and the switching losses drop in this scheme as roughly only half of the IGBTs need to switch at the same time compared to the equivalent two-level converter.

The disadvantage of this setup is its complexity and the use of a higher number of components, compared to the two-level converter. Variants of this configuation (e.g. without the clamped neutral point) have also been developed.

Multilevel Modular Converter

The latest developments in converter topologies aim to answer the needs of the modern system operators: reduction of the system (switching) losses, low demand for maintenance, high availability and reliability of the installations and

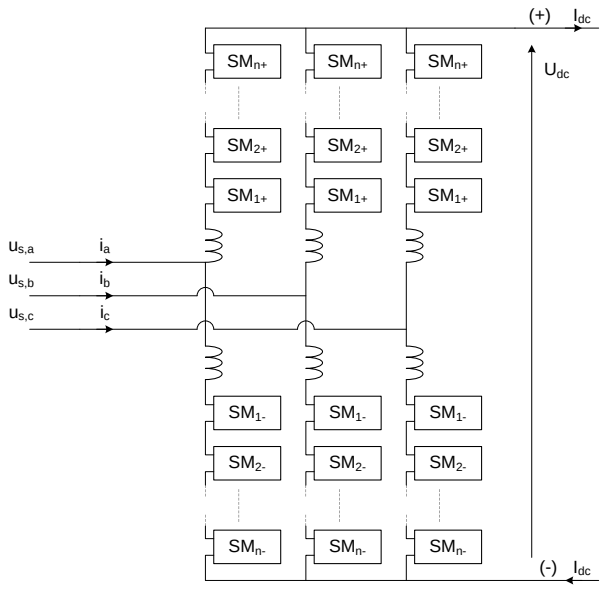

Figure 2.13: Voltage Source Converter with the Modular Multilevel Converter Configuration

spare components. Around 2005 - 2007, the first applications were developed for the new generation of topologies, leaving the former principle that all switchings need to happen simultaneously. Using principles invented more than 5 decades before, but infeasible at that time by the lack of computational power and power electronic components, the Multilevel Modular Converter (MMC) was introduced. Figure 2.13 shows the possible setup (without the clamped neutral point; variants with a fixed neutral point have also been developed) and figure 2.11 the typical output wave shape. One can see that each valve consists of several modules each responsible for a distinct voltage step. Depending on the output voltage, a number of steps is switched in, the rest are put on stand-by. Calculation power is needed to monitor the internal voltage of each step, to charge and discharge the power capacitor and to assess which steps are best to be used in order to generate the desired wave shape.

Two examples of the internal module setup are shown in figures 2.14 and 2.15. Variations amongst manufacturers exist. The first configuration, the *half-bridge module*, consists of one power capacitor and two IGBT-Diode combinations for switching. When no control signals are sent to the IGBTs, the whole

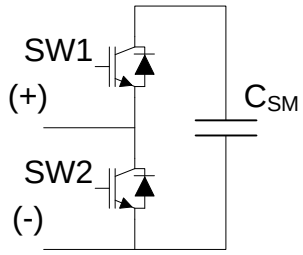

Figure 2.14: Half-bridge module of a Modular Multilevel Converter Configuration

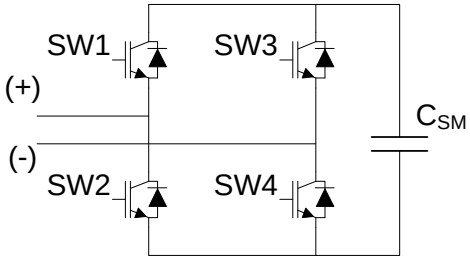

Figure 2.15: Full-bridge module for the the Modular Multilevel Converter Configuration

configuration is dominated by the freewheeling-diode of SW2. When the converter is fed from the AC side alone, without control actions or with the IGBTs blocked, it degenerates to a classic AC/DC rectifier. At start-up, the DC cable is automatically charged, and with any DC fault, each converter (through this rectifier mode) injects inevitably a fault current[4]. This disadvantage is inexistent with the LCC technology: when no control pulses are sent to the thyristors, the current conduction is automatically halted. The half-bridge module converter is not able to interrupt by itself the fault current flowing to a DC fault. This can only be achieved by breaking the current using an AC circuit breaker or DC breakers.

As an alternative, the full-bridge module has been developed. Twice as many switching devices are used (hence, the switching losses are approximately doubled

[4]The same holds for the two- and three-level converters

as well), but the natural rectifier mode has been eliminated. This installation is able to interrupt the fault current for a fault on the DC side, so it incorporates the functionality of a DC breaker.

2.4.3 Comparing the LCC and VSC technology

The following advantages of the VSC over the LCC technology can be identified:

- **Independent reactive power control** is one of the fundamentals of the control actions for the VSC technology. In theory, when sufficient DC capacitance is installed at the DC side of a VSC converter, it is even possible to operate it as a STATCOM, without the need for a link with another converter station. By controlling the absorption or injection of reactive power, control loops are able to control the PCC bus voltage amplitude. Reactive power control becomes important for AC grid faults: the exchange of active power is blocked and the reactive current injection into the fault is maximised, for classic protective relays to better detect and localise that fault. The working principles for the LCC type converter are less flexible on this point: it always consumes reactive power which has to be compensated locally (see also section 2.3).
- **Weak system connections** and under certain circumstances a grid with only passive loads can be fed by a VSC converter. The first installations to connect large offshore wind power plants to the onshore grid using VSC HVDC technology are being built, e.g. the DolWin 1 project [38]. As already mentioned in section 2.3, the LCC converter type, needs an AC source in all cases for proper commutation. Additional equipment needs to be installed should LCC technology be connected to passive loads or a grid with a low short circuit level.
- **Black-start capability**: the same issue arises with LCC converters to deliver the black start capability. The VSC converter can be set into frequency control mode to keep the balance between load and active power injection.
- **Other ancillary services**, such as flicker mitigation, harmonic resonance damping, unbalanced power compensation, become available using the fast control mechanisms of the VSC technology. LCC technology is a net generator of harmonics, that need to be locally mitigated.

On the other hand, the LCC still offers some other advantages over the voltage source converters.

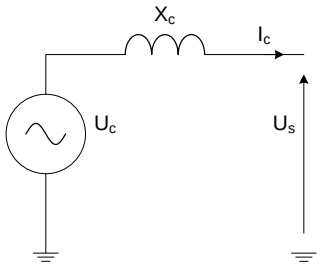

Figure 2.16: Steady-state equivalent for the balanced Voltage Sourced Converter

- **Robustness and maturity** for LCC technology is higher rated than for the VSC type converters. Only recently, considerable ratings for VSC became available and many research and improvement initiatives are taken to further optimise the system losses and number of system components.
- **Rating and bulk transmission** remain the advantage of the LCC technology. VSC technology offers many side advantages useful for the AC grid operator, but when only bulk transmission over very long distances is envisaged, thyristor technology is the only viable option nowadays.

2.4.4 Operating principles of the VSC technology

As the Voltage Source Converter has quasi complete freedom over frequency, voltage amplitude and phase angle within its operational limits, the same working and control principles apply as for classic AC generators. Figure 2.16 shows the steady-state equivalent of the complete VSC installation. It consists of a conventional voltage source and the total installed series impedance. For most steady-state calculations (i.e. power flow and optimal power flow) it is common, as applied throughout the remainder of the text, that the converters are only modelled by an impedance-less voltage source.

This series reactance, however, plays a major role in the control of the current and power exchange of the grid and thus for the dynamic and transient simulations

of the converters [25], p.250:

$$P_s = \frac{U_c U_s \sin\theta_c}{X_c} \tag{2.1a}$$

$$Q_s = \frac{U_c U_s \cos\theta_c - U_s^2}{X_c} \tag{2.1b}$$

In these equations, $\overline{U_s} = U_s \angle 0$ is the (source) grid voltage at the point of common coupling (PCC) and $\overline{U_c} = U_c \angle \theta_c$, the output voltage controlled by the converter, is leading the grid voltage by an angle θ_c. The general principle to control the power output of the converter is by adjusting the voltage drop across the converter reactance.

A difference between the HVDC converters (and similarly for the full-converter wind turbines) and the classic AC generators is the behaviour in case of AC faults. For the generators, it is common to consider the unchanged voltage source and to simulate the transition from the subtransient to the steady-state reactance for the equivalent model. However, for the VSC HVDC installations, as all voltage waveform output is a function of the control loop settings, special care should be taken by the operator and manufacturers to properly design and tune suited control loops for AC fault handling. Grid codes, aiming at specifying these functions in a uniform way, are being established [11].

Figure 2.17 shows the principles of generating and absorbing reactive power of the HVDC installation. Similar to the over-excitation of the AC generators, imposing an in-phase converter voltage higher than the grid voltage amplitude generates reactive power and vice versa: absorption is obtained by a converter voltage lower than the grid voltage.

The same parallel for the active power exchange can be drawn (2.18): imposing a voltage with a leading/lagging angle to the grid voltage reference, results in injection/absorption of active power. Figure 2.19, shows the sign convention of the full four-quadrant control of a VSC converter. The installation can function either in inverter/rectifier mode and independently inject (capacitive behaviour) or extract (inductive behaviour) reactive power from the grid.

To conclude, only a few notions on the control principles are given, as this is not the main target of this research. All control loops are designed to control DC quantities. Therefore, all AC quantities (voltages, currents) of the system need to be transformed into DC quantities. The Park and Clarke

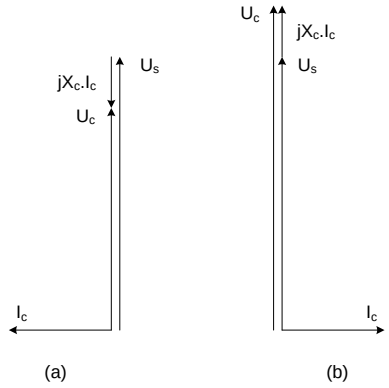

Figure 2.17: Principle for (a) absorption of reactive power and (b) generation of reactive power

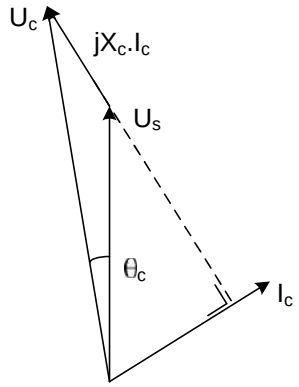

Figure 2.18: Principle for generation of active and reactive power

transformations are used, the first to reference the three-phase quantities (the (abc)-system) into the auxiliary ($\alpha\beta 0$)-referencing system transforming the 120° shifted signals into a perpendicular system. Secondly, this ($\alpha\beta 0$) system, using the Clarke-transformation, is projected into the synchronously rotating (dq0)-system rendering all 50Hz-signals as DC quantities, the input signals for the control loops. The inverse transformations need to be done as well, in order

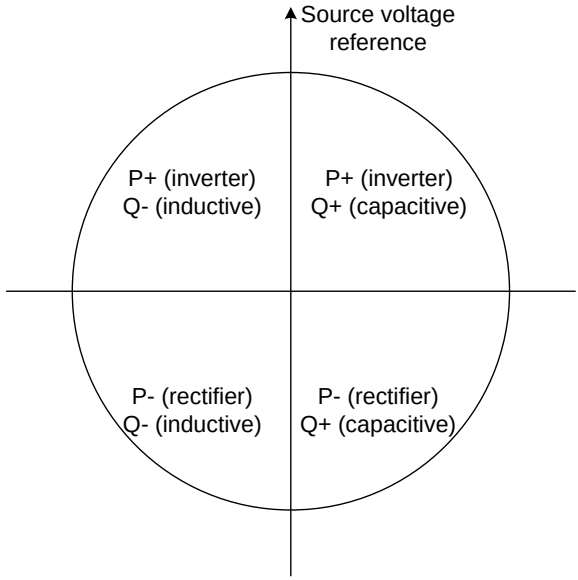

Figure 2.19: Sign conventions for absorbtion and generation of active and reactive power

to convert the DC setpoints for the voltage output back to AC signals. Figure 2.20, gives an overview of the different reference systems and projections. The $(\alpha\beta)$ axis are standing still, the (dq)-axis are rotating with the grid pulsation. The grid voltage angle is taken as a reference, the vector $\overline{U_s}$ is always aligned with the q-axis.

2.5 Power cables

The DC connection of the converters can either be an overhead line or an underground (even subsea) cables. The advantage of the DC operation of the links is that no reactive current is needed. As a result, no real physical length limit restrictions are imposed. Choosing overhead lines for the links needs to be well considered, as due to lightning strokes, many DC faults can occur.

For the underground cables: the Mass Impregnated (MI) cables as well as the extruded Cross Linked Polyethylene (XLPE) can be used. Accumulated space

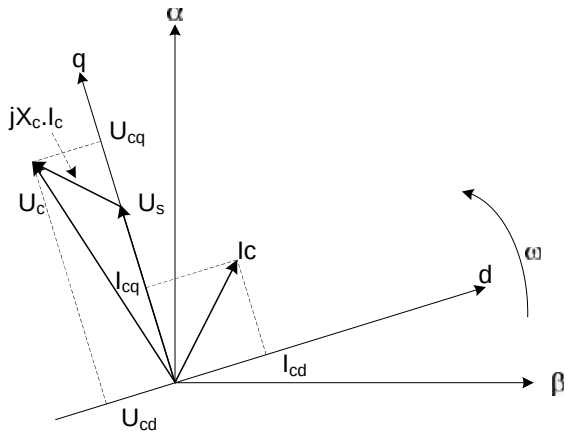

Figure 2.20: Projection from the $\alpha\beta$-reference frame to the dq-reference frame

charges in the XLPE cable insulation make this type of cable vulnerable to rapid polarity reversals and thus this type of cable is unsuitable to be combined with the LCC converter type. On the other hand, the solid insulation of this cable type is has important advantages over its MI counterpart:

- Environmental friendlier: no risk of oil leakage in case of rupture.
- Smaller bending radii, making installation easier.
- Repair jointing is easier: pre-fabricated pieces are used instead of impregnated paper strips.
- Cheaper than the mass-impregnated cable.

At the time of writing, the maximum DC voltage rating of the MI cables is 500 kV and 320 kV for the XLPE cable. Research is being done on insulation materials for both cable types to reach even higher voltage ratings [12].

2.6 Conclusions

This chapter started with a brief history and the technological evolutions of the HVDC technology and a qualitative rationale for their use in high voltage grids.

Next, different topologies for the line commutated converter and voltage source converters and a state-of-the-art comparison have been discussed. This chapter concludes with a discussion and reference material about DC underground cables.

Chapter 3

Optimal Power Flow for AC networks

-Essentially, all models are wrong, but some are useful. - George E.P.Box

3.1 Goal

This chapter places the Optimal Power Flow (OPF) in its larger electrical simulation context starting from the classic Power Flow (PF) calculations. A more general overview on this matter is provided in the literature [39],[40]. Next, the general formulation of the non-linear optimisation problem is given together with the necessary and sufficient conditions with which a solution should comply and the iterative methods to calculate local and global optimal solution points. In a separate section, a theory is developed to be used when one wants to extend an existing case with supplementary non-linear equality and inequality constraints.

After the theoretical section, the optimal power flow case is transformed into an optimisation problem. An overview is given of the choice of state variables, their limits and the definition of linear and non-linear equality and inequality constraint equations.

A separate section treats the choice of the cost function and the chapter ends with the possibilities when several concurring cost functions are to be considered together, the so-called multi-objective problems, and adds a conclusion.

3.2 Qualitative comparison of power flow and optimal power calculations

The optimal power flow (OPF) and power flow (PF) calculations are a subset of the whole range of simulations and calculations that are normally performed for planification, protection and operation of High Voltage (HV) networks.

Both tools are dealing with steady-state (and quasi steady-state) behaviour of power systems, and although very similar in the base data set (starting with the same network model), they have different goals and approaches.

Perhaps the best way to introduce the strengths and particularities of the Optimal Power Flow is taking a small step back and start with a quantitative introduction of the more classic Power Flow calculations.

For this type of calculations, all structural electrical elements and their impedance properties and the topology of the AC network need to be defined. The busbars or network nodes play a major role, as connection points of all network branches (transformers, overhead lines, underground cables, coupling bays, shunt capacitors and shunt reactors), the electrical loads and the generators. For each node of the network, two equations are written out stating that the balance of active and reactive needs to be preserved: the Kirchhof's Current Law (Appendix C)

$$\begin{aligned} P_i(\Theta, \mathbf{U}, \mathbf{P}) &= P_{br,i} + P_{l,i} - P_{g,i} \\ &= \sum_{j=1}^{n_b} Y_{ij} U_i U_j \cos\left(\theta_i - \theta_j - \varphi_{ij}\right) + P_{l,i} - P_{g,i} = 0 \end{aligned} \tag{3.1a}$$

$$\begin{aligned} Q_i(\Theta, \mathbf{U}, \mathbf{Q}) &= Q_{br,i} + Q_{l,i} - Q_{g,i} \\ &= \sum_{j=1}^{n_b} Y_{ij} U_i U_j \sin\left(\theta_i - \theta_j - \varphi_{ij}\right) + Q_{l,i} - Q_{g,i} = 0 \end{aligned} \tag{3.1b}$$

These equations take into account the bus voltage amplitudes U and angles Θ, the active and reactive power injections and extractions of the connected branches, loads and generators (P_{br}, P_l and P_g) respectively. The branch powers only depend on the voltages amplitudes and angles of the buses connected to. The network loads are considered to be constant. This leads to a situation where per node, 4 independent parameters are defined (U, Θ, P_g and Q_g) with only 2 equations. In order to obtain a solvable system of equations (with as many parameters as equations), two parameters per node still need fixed values. The other two are solution results. Three different bus types are defined:

- PQ-nodes: active and reactive generator power exchange are set, i.e. P_g and Q_g are known, typically nodes where no active generation or generation without automatic voltage control is present.
- PV-nodes: active generation power P_g together with the bus voltage amplitude U_m are specified, in order to represent the power generation and its voltage control.
- SB-node (Slack Bus): voltage amplitude and reference angle are specified; per network there is only one node of this type, serving to balance the active power in the network.

This non-linear calculation problem has one non-trivial solution and is typically solved by an iterative process. It disregards branch loading, generation and bus voltage limits. Furthermore, for all but one generator, the active power output needs to be given at the start of the calculation.

The power flow calculation is a powerful tool to generate network snapshots, but is less useful when a solution needs to be found taking into account all element limitations or when it is not desired to explicitly specify the output power of each generator upfront. This can be the case when one is interested in knowing what the generator ideal output should be in the case when a given optimisation criterion has to be met. The need to set values for two of the four bus parameters becomes irrelevant for the optimal power flow: all four are taken as state variables and are adapted by the solver to meet all given limits, and when specified, the best network state amongst all feasible ones (following a predefined ranking criterion) is proposed as solution.

The next section treats the optimisation problem in its most general form and proposes solution methods. After that in section 3.4, the optimal power flow case is developed as a specific application of the general, theoretical form.

3.3 General optimisation theory

In this section, a number of solution methods for the above optimisation problem, are treated. There are a large number of optimisation methods and algorithms available, depending on the nature of the problem.

- Linear problems. Cost function and constraints are linear functions of the optimisation variables.
- Non-linear problems without constraints.
- Non-linear problems with a non-linear cost function but with linear constraints.
- Non-linear problems with a non-linear cost function and constraints.
- Mixed integer non-linear problems combining real number and discrete state variables. It is not an objective of this work to implement this type of optimisation algorithms. The discrete state variables are used for switched elements, e.g. circuit breakers, transformer tap changers (section 3.6.1); the extension of the methodologies with discrete state variables is proposed as a further development.

The Optimal Power Flow problem is of the last type in this list. The cost function can be a linear function of the optimisation variables, e.g. a simple sum of the generator output, but the power flow equations (equality constraints) and the branch flow limitations (inequality constraints) are always non-linear unless the DC approximation is used. This research is based on the full AC network equations.

The most common method to solve non-linear objectives and to integrate the constraints is using the so-called Lagrangian function.

To give a condensed overview on how constraints are integrated in the optimisation problem, the case with only equality constraints is treated in subsection 3.3.1, and extended with the inequality conditions in subsection 3.3.2. Comprehensive overviews and theoretical developments are given in [41], [42], [43] and [40].

3.3.1 Optimisation with equality constraints

Assume an optimisation case where the cost function $f(x)$ is to be minimised and that m (non-linear) equality constraints $g_i(x) = 0$ with $i = 1 \dots m$ are

defined. The vector x is called a state variable vector and has n elements. A new function, combining these equations, is constructed and new variables μ (m elements) are introduced. This function $\mathfrak{L}(x,\mu)$ is called the Lagrangian function.

$$\mathfrak{L}(x,\mu) = f(x) + \mu^T g(x) = f(x) + \sum_{n}^{i=1} \mu_i g_i(x) \tag{3.2}$$

$\mathfrak{L}(z) = \mathfrak{L}(x,\mu)$ is again to be minimised and has, compared to the original problem $n+m$ optimisation variables: n from the original $x \in \Re^n$ vector and m additional parameters from the $\mu \in \Re^m$ vector, the Lagrange parameters or also Lagrange multipliers.

It is useful to state the Lagrange theorem (without proof, [42], p.287) giving insights for the later parts of this manuscript.

Let $x^\star$ be a local minimum of the optimisation problem and moreover a regular point. f and g are continuously differentiable functions, at least in the local neighbourhood of the point $x^\star$. Then there exists a unique set of scalars such that

$$\nabla\mathfrak{L}(x^\star,\mu^\star) = \nabla f(x^\star) + \sum_{i=1}^{m} \mu_i^\star \nabla g_i(x^\star) = 0 \tag{3.3}$$

And, if in addition f and g are twice continuously differentiable, then

$$\forall y \text{ with } \nabla g(x^\star)^T y = 0 : \tag{3.4}$$

$$y^T \nabla^2 \mathfrak{L}(x^\star,\mu^\star) y = y^T \left(\nabla^2 f(x^\star) + \sum_{i=1}^{m} \mu_i^\star \nabla^2 g_i(x^\star) \right) y \geq 0 \tag{3.5}$$

Furthermore, the first derivative of the Lagrangian function can be written as

$$\nabla\mathfrak{L}(x^\star,\mu^\star) = \begin{bmatrix} \nabla_x \mathfrak{L}(x^\star,\mu^\star) \\ \nabla_\mu \mathfrak{L}(x^\star,\mu^\star) \end{bmatrix} = 0 \tag{3.6}$$

A *regular* point of a function means that the first derivatives of the function in that point are linearly independent. All functions to describe the optimal power

flow for AC grids and all additional functionalities developed in this research are twice differentiable.

The lower part of (3.6) is the expression for the constraints:

$$\nabla_\mu \mathfrak{L}(x^\star, \mu^\star) = g_i(x^\star) = 0 \tag{3.7}$$

so when $z^\star = (x^\star, \mu^\star)$ is a local solution of the Lagrangian function, implicitly all equality constraints are satisfied as well.

The above statement gives the necessary (or minimum) conditions for a solution of the optimisation problem. Next, the sufficient conditions are given. When a solution complies with the sufficient conditions ([42], p.296), one is certain to have found an optimum of the optimisation problem.

Assume that f and g are twice differentiable and let $x^\star$ and $\mu^\star$ satisfy

$$\nabla_x \mathfrak{L}(x^\star, \mu^\star) = 0$$

$$\nabla_\mu \mathfrak{L}(x^\star, \mu^\star) = 0$$

$$y^T \nabla^2 \mathfrak{L}(x^\star, \mu^\star) y > 0 \ , \ \forall y \neq 0 \text{ with } \nabla g(x^\star)^T y = 0$$

Then $x^\star$ is a strict local minimum of f subject to $g(x) = 0$.

The sufficient conditions do not require the optimum point $x^\star$ to be regular.

Graphical example

Figure 3.1 illustrates the different elements used for the non-linear optimisation problem. Assume the following setup: a person needs to travel from the point A to B, thereby taking into account that he must stop once on the curve g (a river for example). The travelled distance needs to be minimised.

The objective function f, with respect to the point P at an arbitrary location in the two-dimensional space, can be expressed by equation

$$f(P) = \|AP\| + \|BP\| \tag{3.8}$$

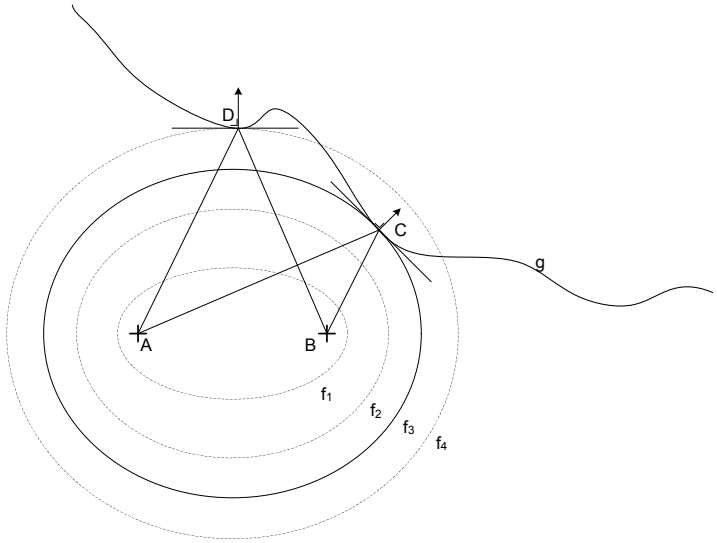

Figure 3.1: Example for a non-linear optimisation problem: minimise the sum of the distances from point A and B to a point on the curve g

The iso-lines of the objective function $f(P)$ (i.e. the curves with the same value of that function) are ellipses with A and B as their focal points. In the figure, 4 different iso-lines (f_1 to f_4) are drawn. The condition that the person needs to stop at least in the curve g is mathematically expressed by

$$g(P) = 0 \tag{3.9}$$

The expression is an equality constraint, as it imposes the point P (to where the distances AP and BP are measured) to be situated exactly on that curve.

The Lagrangian function for this sample problem is

$$\mathfrak{L}(P) = f(P) + \mu g(P) \tag{3.10}$$

Equation (3.3) states that for an optimal point, the gradient vector of the objective function $f(P)$ and the gradient of the constraint function $g(P)$ have the same or opposite direction, depending on the sign of the Lagrange multiplier μ. As the gradient vector of a function always is perpendicular to its associated

function, the previous statement implies that the optima are those points where the iso-lines of the objective function are tangent to all equality constraint functions.

For the example figure, already two points, C and D, comply with this condition. The global minimum of this optimisation case is C, but, as indicated by the drawing, point D complies to the Lagrange theorem as well. Point D is a local optimum.

It can be concluded that, when an algorithm is able to find a point that complies with the Lagrange theorem, no guarantee can be given whether that point is a mere local or the global optimum point of the optimisation problem. Depending on the starting position of the iterative algorithm, the solution point can be attracted by a certain local optimum, rendering the whole optimisation problem dependent on the choice of the starting point.

Sensitivity

Sensitivity in this context is meant as the influence of the variation of the constraints on the cost function. Suppose the following optimisation problem

$$\min f(x) \tag{3.11}$$

$$g(x) = c_i \tag{3.12}$$

with $i = 1 \dots m$ and furthermore that $z^\star = (x^\star, \mu^\star)$ is a local solution of the corresponding Lagrangian function in the case that $c_i = 0$ (3.3). The change of the cost function result when the vector c changes, is to be assessed.

$$\begin{aligned} \frac{\mathrm{d}f(x^\star)}{\mathrm{d}c_i} &= \nabla_x f(x^\star) \cdot \frac{\mathrm{d}x^\star}{\mathrm{d}c_i} \\ &= -\mu^\star \cdot \nabla_x g(x^\star) \cdot \frac{\mathrm{d}x^\star}{\mathrm{d}c_i} \\ &= -\mu^\star \cdot \frac{\mathrm{d}g(x^\star)}{\mathrm{d}c_i} \\ &= -\mu^\star \end{aligned} \tag{3.13}$$

In this derivation, the Lagrange theorem $\nabla_x f(x^\star) = -\mu^\star \cdot \nabla_x g(x^\star)$ is used and from $g_(x) = c_i$ follows that $\dfrac{\mathrm{d}g(x^\star)}{\mathrm{d}c_i} = 1$.

The Lagrange multipliers $\mu^\star$ at the local minimum $x^\star$ give an indication on the constraints in this point:

- Suppose a positive μ_i, a positive change of c_i results in a lower cost function.
- The higher the absolute value of μ_i, the more a particular constraint is restraining the optimisation algorithm in finding lower values of the cost function.

Care should be taken in interpreting the absolute value of μ_i. It depends directly on the formulation of $g_i(x) = 0$:

$$g_{i,k}(x) = k \cdot g_i(x) = 0 \text{ with } k \in \Re_0 \tag{3.14}$$

The corresponding multipliers are then inversely scaled by that same factor $\mu^\star_{i,k} = \frac{\mu^\star_i}{k}$.

3.3.2 Optimisation including inequality constraints

Implementing inequality constraints is more complex to take care of, as it is impossible to identify from the beginning of the algorithm which conditions hit their limit and which ones can be neglected in the optimisation problem. These inequality constraints are said to be *active* and are treated as normal equality constraints. Several approaches to deal with inequality constraints are treated hereafter.

The first approach discussed, treats the inequalities as equations, neglecting those that do not reach the upper limit. Take the following optimisation problem

$$\min_x f(x) \tag{3.15}$$

$$g(x) = 0 \tag{3.16}$$

$$h(x) \leq 0 \tag{3.17}$$

with $f : \Re^n \mapsto \Re$, $g : \Re^m \mapsto \Re$, $h : \Re^r \mapsto \Re$. The functions have to be continuously differentiable[1].

An inequality constraint is said to be *active* when at the point x the function equals the upper limit $h(x) = 0$. If $x^\star$ is a local minimum, the active constraints h_i are treated as equality constraints. The Lagrangian function is expanded with the inequality constraints using an additional multiplier vector λ:

$$\mathfrak{L}(x, \mu, \lambda) = f(x) + \mu^T g(x) + \lambda^T h(x) \tag{3.18}$$

The equivalent for the Lagrange theorem here, are the Karush-Kuhn-Tucker (KKT) necessary conditions ([42], p.310).

When $x^\star$ is a local minimum and regular, there exists a unique Lagrange multiplier vector $(\mu^\star, \lambda^\star)$ such that

$$\nabla_x \mathfrak{L}(x^\star, \mu^\star, \lambda^\star) = 0 \tag{3.19}$$

$$\text{with } \lambda_i^\star = 0, \text{ for } \forall i \text{ with } h_i(x^\star) < 0 \tag{3.20}$$

$$\lambda_i^\star > 0, \text{ for } \forall i \text{ with } h_i(x^\star) = 0 \tag{3.21}$$

If in addition f, g and h are twice differentiable, and $\forall y \in \Re^n$ with

$$\nabla g(x^\star)^T y = 0 \tag{3.22}$$

$$\nabla h(x^\star)^T y = 0 \text{ for } \forall i \text{ with } h_i(x^\star) = 0 \tag{3.23}$$

then

$$y^T \nabla^2_{xx} \mathfrak{L}(x^\star, \mu^\star, \lambda^\star) y \geq 0 \tag{3.24}$$

[1] All functions used in this work are continuously differentiable

The two conditions (3.22) and (3.23) are rewritten as

$$\lambda_i^\star \geq 0 \tag{3.25}$$

$$h_i(x^\star) \leq 0 \tag{3.26}$$

$$h_i(x^\star) \cdot \lambda_i^\star = 0 \tag{3.27}$$

In order to avoid confusion, the last equation is treated for each individual element i (and not an implicit inner product of the elements).

And finally, the general sufficiency conditions for the optimisation problem are given below ([42], p.316).

Assume the problem

$$\min_x f(x) \tag{3.28}$$

$$x \in X \tag{3.29}$$

$$g(x) = 0 \tag{3.30}$$

$$h(x) \leq 0 \tag{3.31}$$

with $f : \Re^n \mapsto \Re$, $g : \Re^m \mapsto \Re$, $h : \Re^r \mapsto \Re$ and X a given subset of $\Re^n$. Let $x^\star$ be a feasible vector. A feasible vector is a vector satisfying all constraints. When it satisfies together with the vectors $\mu^\star$ and $\lambda^\star$ the following conditions

$$\lambda_i^\star = 0, \text{ for } \forall i \text{ with } h_i(x^\star) < 0 \tag{3.32}$$

$$\lambda_i^\star > 0, \text{ for } \forall i \text{ with } h_i(x^\star) = 0 \tag{3.33}$$

and minimises the Lagrangian function (3.18) over $x \in X$:

$$x^\star = \arg\min_{x \in X} \mathfrak{L}(x, \mu^\star, \lambda^\star) \tag{3.34}$$

Then $x^\star$ is a *global* minimum of the problem.

Sensitivity

The same reasoning as described in section 3.2 is valid for the sensitivity nature of the Lagrange multipliers λ_i. For the inactive inequality constraints, the multiplier $\lambda_i = 0$, i.e. they do not have an impact on the cost function value for small changes.

The expression (3.13) applies also to the active constraints with $\lambda_i > 0$. Because these Lagrange parameters are always positive, relaxing the limits of an inequality constraint has a lowering effect on the cost function.

3.3.3 Optimisation problem transformation

So far in the development of this chapter, the only method that can be used to solve the optimisation problem is by analytically solving the necessary conditions, taking them as a system of equations. In this subsection, the optimisation case, including equality and inequality constraints, is transformed to be fit to use by iterative computer algorithms. The Barrier ([42], p.370) and the Penalty ([42], p.395) methods are described here as an illustration. They are the most commonly used in commercial software. Appendix B gives a complete worked out algorithm [40]. The standard built-in solver of MatPower, the MatPower Interior Point Solver (MIPS, [44]) and the KNITRO solver [45] use the Barrier method as prime method as well.

The Barrier method considers the inequality constraints to be equality constraints and add to the cost function a barrier function that becomes very high when one inequality constraint approaches its limit. The Penalty method uses non-negative slack variables to transform the inequality to equality constraints together with applying a quadratic penalty function to each constraint, aiming to prioritise the constraint functions in the optimisation process.

Barrier method

Assume again the optimisation problem

$$\begin{aligned} \min_x & f(x) \\ x & \in X \\ g(x) & = 0 \\ h(x) & \leq 0 \end{aligned} \tag{3.35}$$

with $f : \Re^n \mapsto \Re$, $g : \Re^m \mapsto \Re$, $h : \Re^r \mapsto \Re$ and X a closed subset[2] of $\Re^n$. The *interior region* S of the set X defined by the inequality constraints is

$$S = \{x \in X : h_i(x) < 0, \forall i\} \tag{3.36}$$

It is assumed that S is non-empty and that any feasible point not lying in S (i.e. the vectors for which $h_i(x) = 0$), can be approached arbitrarily near by another vector in S.

To the cost function, a *barrier* function is added. It is defined and continuous within S and goes to ∞ when one of the constraints $h_i(x)$ approaches 0 from negative values: the two most used barrier functions are

$$B(x) = -\sum_{i=1}^{r} \ln\left(-h_i(x)\right) \tag{3.37a}$$

$$B(x) = -\sum_{i=1}^{r} \frac{1}{h_i(x)} \tag{3.37b}$$

Furthermore, a parameter sequence $\{\epsilon_k\}$ (3.38) approaches 0 with each iteration step and combined together with a barrier function:

$$0 < \epsilon_{k+1} < \epsilon_k \ , \ k = 0, 1, \ldots \tag{3.38}$$

The method consists of finding the optima of

$$x_k = \arg\min_{x \in S} \left(f(x) + \epsilon_k B(x)\right) \ , \ k = 0, 1, \ldots \tag{3.39}$$

[2] A closed set contains its own boundary

The step size and initial point must be selected in such a way that the successive points of the iteration steps must be interior points since the barrier function is only defined in the interior region S. For all points x_k lying within S, the barrier term goes to 0 as ϵ_k becomes smaller with every step. For the points lying on the boundary of S (where one or more constraint functions reach their limit), the individual components of the barrier function get an increasingly unpredictable behaviour: the barrier function components in (3.37a) or (3.37b) for these constraints go to infinite but the second term in (3.39), $\epsilon_k B(x)$, stabilises on a finite value when k progresses.

The following statement gives the main convergence result.

Every limit point of a sequence $\{\epsilon_k\}$ generated by a barrier method is a global minimum of the original constrained problem (3.35).

Penalty method

A second methodology is to convert the inequalities from (3.35) into equality constraints using slack variables $s \in \Re^r$. The inequality constraints $h_i(x) \leq 0$ are transformed into the following set $h_i(x)+s_i^2 = 0$. The practical disadvantage of this method is that these slack variables c_i define another r state variables.

The Lagrangian function becomes

$$\mathfrak{L}(x, \mu, \lambda, s) = f(x) + \sum_{i=1}^{m} \mu_i g_i(x) + \sum_{j=1}^{r} \lambda_j \left(h_j(x) + s_j^2\right) \tag{3.40}$$

Quadratic penalty functions are added to (3.40), constructing the *augmented* Lagrangian function:

$$\bar{\mathfrak{L}}_c(x, \mu, \lambda, s, c) = \mathfrak{L}(x, \mu, \lambda, s) + \frac{c}{2} \sum_{i=1}^{m} g_i(x)^2 + \frac{c}{2} \sum_{j=1}^{r} \left(h_j(x) + s_j^2\right)^2 \tag{3.41}$$

Optimising the constrained system (3.35) equals finding the optimum of the unconstrained augmented Lagrangian function with respect to all its parameters

and the penalty multiplier c. A possible approach to solve this optimisation problem, is first eliminating the slack variables s by minimising (3.41) with respect to s and then by minimising the resulting Lagrangian function:

$$\mathfrak{L}_c(x, \mu, \lambda) = \min_s \bar{\mathfrak{L}}_c(x, \mu, \lambda, s, c) \tag{3.42}$$

It is proven that for a parameter sequence $0 < c_k < c_{k+1}$ (for all k), every limit point $\{x_k\}$ is a global minimum of $\mathfrak{L}_{c_k}(x, \mu, \lambda)$ and thus of the original constrained problem (3.35) ([42], p.391).

3.3.4 Iterative solution methods

Once a suitable function has been determined to be minimised, the next step is to set up computational algorithms to find the minimum. Many reference works have been written on various methods and their characteristics. A few of the basic algorithms are treated in this section.

First-order Lagrangian method

As the name implies, only the first derivatives of the optimisation function $\mathfrak{L}(x)$ to its parameters need to exist in the neighbourhood of the optimum state. The information of the second derivatives is neglected. The idea of the first-order Lagrangian method is that at any given point, the vector of first derivatives $\nabla_x \mathfrak{L}(x)$ is pointing to the direction of the steepest upwards slope, hence the name *steepest descend method*. So, when taking a step in the reverse direction, one would expect to end in a new position with a function value lower than the previous one:

$$x_{k+1} = x_k - \alpha \nabla_z \mathfrak{L}(z) \tag{3.43}$$

with step size $\alpha > 0$.

With a step size α sufficiently small, $\mathfrak{L}(x_{k+1}) \leq \mathfrak{L}(x_k)$. Note that the step size may vary at every step. Whereas larger step sizes are interesting for quicker convergence, the inconvenience is that it risks to jump too much back and forth or even jump "over" the local minimum without gradually converging to that point.

Without taking into account inequality constraints, the solutions for the Lagrangian function

$$\mathfrak{L}(x, \mu,) = f(x) + \mu^T g_i(x) \tag{3.44}$$

are given by the iteration algorithm

$$\begin{aligned} x_{k+1} &= x_k - \alpha \nabla_x \mathfrak{L}(x_k, \mu_k) \\ \mu_{k+1} &= \mu_k - \alpha \ g(x_k) \end{aligned} \tag{3.45}$$

The convergence of this first-order algorithm is linear [42]. It converges to the closest local minimum as seen from the entry point of the sequence. Furthermore, when the Lagrangian function is twice continuously differentiable, there exists an upper limit for the step size for which an optimal point is always found.

Second-order method

Originally developed to find the roots of an analytic function, the method is applied in the optimisation environment to find the roots of the first derivative of the function to be minimised. For this, the Lagrangian function needs to be at least twice differentiable to all its parameters in the neighbourhood of the local optimum. A drawback of the method is that it is attracted by local minima and only local convergence is guaranteed. It is almost obligatory to start the searching sequence sufficiently close to the real optimum. The region of convergence can be enlarged using a merit function ([42], p.454). Moreover a number of functions have been developed to let the Newton-Raphson method (further named the Newton method) converge to the global solution.

The purpose of the Newton method is to find the roots $x^\star$ of a given function $F(x)$: $F(x^\star) = 0$. For the optimisation case, not the function itself (the Lagrangian function $\mathfrak{L}$) but its first derivative needs to be set to zero.

$$\nabla_x \mathfrak{L}(x) = 0 \tag{3.46}$$

As the function $F : \Re^n \mapsto \Re$ has n variables, (3.46) is implicitly a system of n equations. To solve this set of equations, the Newton method states:

$$x_{k+1} = x_k + \Delta x_k \tag{3.47}$$

with Δx_k as the solution of

$$\nabla^2 \mathfrak{L}(x_k) \cdot \Delta x_k = -\nabla \mathfrak{L}(x_k) \tag{3.48}$$

It can be proven that if the optimal solution $x^\star$ is indeed existing, the function $\nabla^2 F(x)$ is invertible in the neighbourhood of $x^\star$. The point sequence given by the Newton iteration is in this case said to be *well-defined*. The convergence to the local minimum is super-linear and at least of the second order if $\nabla^2 F(x)$ is Lipschitz continuous[3] in the neighbourhood of $z^\star$.

Searching global convergence

The Newton method has a few drawbacks

- When the inverse of $\nabla_x^2 F(x)$ in a particular region does not exist (for instance the optimising function can become linear ($\nabla_x^2 F(x) = 0$), it is impossible for the iteration process to make a next step.
- It is not guaranteed that the sequence of optimisation function values descends at each step.
- Local extrema (minima as well as maxima) attract the solution when the starting point is close enough to one of them, even when they are not the global optimum.
- No guarantee is given that the real global minimum is found.

The general idea to cope with the drawbacks of the Newton method, is to make an interpolation of both the steepest descent method (first-order method) and (gradually) switch to the Newton method.

In order to make, at least for the first steps of the iteration process, the left-hand side of the change vector calculation invertible, a method often used is to manipulate the diagonal of this matrix so that it becomes positive definite (and as a consequence also invertible).

The modified direction calculation becomes

$$\left(\nabla^2 F(x_k) + \Gamma_k\right) \Delta x_k = -\nabla F(x_k) \tag{3.49}$$

with Γ_k a diagonal matrix, chosen such that the matrix $\nabla^2 F(z_k) + \Gamma_k$ is positive definite.

[3] Lipschitz continuity is a strong form of function continuity where no gradient between two arbitrary points within the region is larger than a certain real number.

An easy understandable algorithm, developed in [46], is to take for

$$\Gamma_k = \gamma_k \cdot I \tag{3.50}$$

with I the identity matrix of the appropriate size.

Taking the positive scalar parameter γ_k very high compared to the elements of $\nabla^2 F(x_k)$, the total matrix becomes automatically positive definite. However, the solution of the step size Δx_k becomes small. With $\gamma_k = 0$, the method falls back to the normal Newton formulation.

A possible algorithm is the following:

- With a very high value of γ, calculate the step and do a provisional step forward.
- Accept the step when the optimisation function decreased, lower the value of γ, e.g. divide by 10.
- Refuse the step when the function increased, take a higher value for γ, e.g. multiply by 10.

As already pointed out, the algorithm takes small steps in the beginning, dictated by the steepest slope method. When the iterations progress, the Newton's elements in the left-hand side of the step equation become predominant. As mentioned earlier, in the close vicinity of a minimum, the Hessian $\nabla^2 F(x_k)$ is invertible as well. However, this demonstration algorithm is not robust enough to solve complicated cases: when applying constraint functions, the algorithm becomes indecisive (i.e. the magnitude order of γ does not decrease significantly over the iterations) to activate the second order convergence and successive iteration go back and forth without advancing to an optimum. This effect is due to the multiplication of the Lagrange multipliers with the constraint functions. The method described in Appendix B applies step size control to add robustness in case the Lagrange parameter step updates are fluctuating (subsection B.3.3).

3.4 Extending the formulation

In order to provide additional functionalities to an existing optimisation case, e.g. the extension of an AC grid with a DC grid, often a definition of new state variables is needed. This procedure is quite straightforward in theory, but not

many commercial software packages allow such an extension by user-defined parameter variables. Some, e.g. MatPower, allow the user to define additional state variables and the related linear equality and inequality constraints [47]. However, nothing has been foreseen for the user to implement his own non-linear equations. This research specifically required that functionality.

Assume an optimisation case with its state variable vector x (n_x elements) and the vector of the additional state variables z (n_z elements):

$$x_n = \begin{bmatrix} x \\ z \end{bmatrix} \tag{3.51}$$

The optimisation case definition is affected as well, as the use of new state variables comes together with an additional set of equality and inequality constraints and a new cost function f_n, function of the original and the new state variables. The subscript o is used for the original constraint functions and n for the added ones. The extended optimisation case is

$$\min_{x,z} f_n(x,z) \tag{3.52}$$

$$g(x_n) = \begin{bmatrix} g_o(x) \\ g_n(x,z) \end{bmatrix} = 0 \tag{3.53}$$

$$h(x_n) = \begin{bmatrix} h_o(x) \\ h_n(x,z) \end{bmatrix} \leq 0 \tag{3.54}$$

$$x_{min} \leq x \leq x_{max} \tag{3.55}$$

$$z_{min} \leq z \leq z_{max} \tag{3.56}$$

Whatever optimisation algorithm is used, the non-linear programming techniques require to extend the Jacobian and Hessian matrices for parameter functions g_n and h_n with each iteration step. A combination of submatrices depending on the original and the additional constraint vectors needs to be evaluated. Assume the original Jacobian ($n_o \times n_x$ matrix) matrix

$$J_o = {}_{n_o}\{ \begin{bmatrix} \overbrace{\dfrac{\partial g_o}{\partial x}}^{n_x} \end{bmatrix} \tag{3.57}$$

The number of functions in the original equality constraint vector g_o is assumed n_o and n_n for the extension constraint vector g_n. The extended Jacobian starts from previous expressions and adds all other necessary derivatives of the new constraints.

$$J = \begin{matrix} \\ n_o\{ \\ n_n\{ \end{matrix} \begin{bmatrix} \overbrace{}^{n_x} & \overbrace{}^{n_z} \\ J_o & 0 \\ \frac{\partial g_n}{\partial x} & \frac{\partial g_n}{\partial z} \end{bmatrix} \tag{3.58}$$

The Hessian matrix for a function vector is in theory three-dimensional, expressing the possible combinations of the second derivatives to its parameters (3.59). The Hessian consists of n_n "layers", with n_n the combined number of (non-linear) functions in the function vector for which the calculation of its Hessian matrix is desired. Each $(n_x + n_z) \times (n_x + n_z)$ sized layer corresponds to all the second derivatives of one of these functions. Here, $n_x + n_z$ is the combined number of the original and new state variables of the optimisation case.

$$H(x) = \left[\frac{\partial^2 g_i}{\partial x_{n,j} \partial x_{n,k}} \right] \tag{3.59}$$

The Hessian is calculated for each of the layers separately. For some computer applications (e.g. in the case for MatPower) it is required to calculate the dot-product of the Hessian with a given column vector (for example the vector of the corresponding Lagrange parameters). The result is a more conventional 2-dimensional matrix

$$\mu \cdot H(x_n) = \sum_{i=1}^{n_o+n_n} \mu_i \left[\frac{\partial^2 g_i}{\partial x_{n,j} \partial x_{n,k}} \right] \tag{3.60}$$

The same matrix constructions apply for the Jacobian and the Hessian of the inequality function vector $h(x)$.

3.5 Optimisation and electrical networks

This section describes the purpose and added-value of optimisation for electrical networks. Not only the power flow of the networks, which is the main focus of this research, can be optimised. Economical dispatch of generating units,

environmental impact and market regulation [48] are cast into optimisation cases as well.

This section focusses on the goals, time frames, control possibilities and coordination issues of the optimal power flow applications.

3.5.1 Goal of the OPF calculation

Even when the core of the optimal power flow case is the power grid itself, there are still different approaches or goals that can be obtained. The following subsections give an overview.

Determining the optimal state

An optimisation goal is given to localise the best point within the boundary region. In a standard OPF definition, the optimal point is found when a given cost function is minimized and when the solution fulfils all constraints: nodal voltage magnitude, generator loading and branch loading limitations. The set of different possibilities for the cost function, as well as weighted combinations of cost functions, are treated in section 3.7.

The chosen cost function depends on the motivation of the calculation by the user (non-exhaustive):

- Economical optimisations (minimal grid losses, generation cost) [40, 49, 50].
- Optimising secondary voltage and reactive power control [51].
- Optimising the use and setpoint of FACTS devices [52, 53].
- Optimising network investments (e.g. location for reactive power compensation devices).
- Maximising cross-border transit capacity.
- Emergency grid operation.
- Maximising the import of renewable energy sources.
- Environmental impact: minimising exhaust gases (CO_2, NO_x, SO_x), de-favouring high polluting power plants.

- Starting point for further power flow and security constrained optimal power flow calculations.

Feasible operation of the network

An optimal power flow can also be run without an optimisation criterion (or a goal function) to find a safe or feasible operation point for the system. A viable working state within the given boundaries is then iteratively searched depending on the initial state of the algorithm. An application is discussed in subsection 3.7.6 where the viable state closest to the initial state is searched.

Security constraints can be set in the optimal power flow case as well (chapter 4).

Determine the marginal cost of the network boundaries

The marginal costs at the boundaries are the same as the sensitivities treated in section 3.3. Each Lagrange multiplier of the inequality constraints (describing the grid element limitations) states their respective marginal cost. Comparing them, gives an indication of which limit relaxations have the most effect on the cost function. The following items describe the use of these marginal costs:

- **Grid investment justification**. Network branches with a positive marginal cost (or Lagrange multiplier for their constraints) are loaded at their maximum. Uprating the branches with the highest marginal costs is more beneficial for a reduced congestion, higher social welfare and thus a lower objective function value.
- **Voltage support** Installing voltage support installations at those nodes with high marginal reactive power costs is economically more justified.

3.5.2 OPF for different time frames

Power system operations is a term which encompasses an entire range of activities performed by the different stakeholders. The activities of the operation fall within a time frame of several weeks, days or hours in advance, up to real time (figure 3.2, [54]).

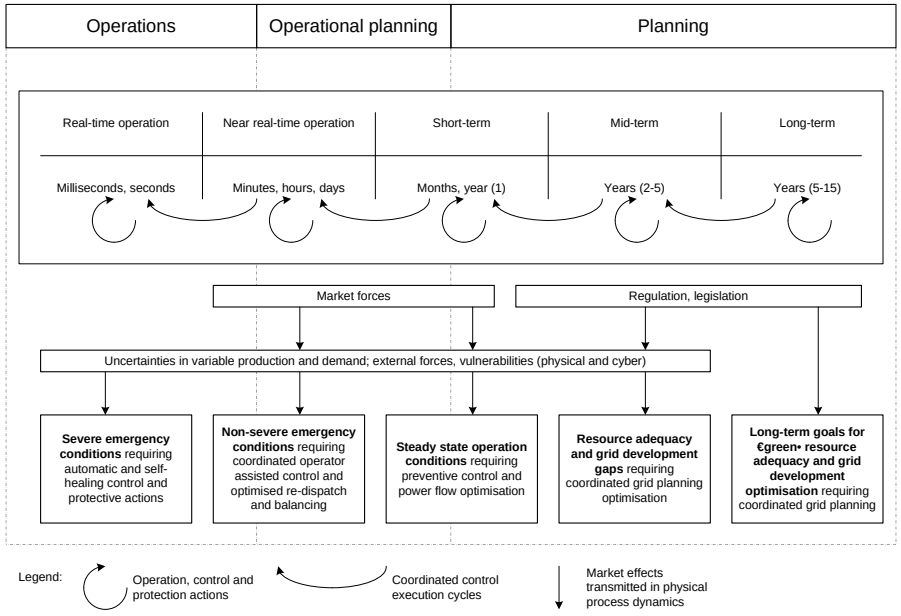

Figure 3.2: Smart Operation and Planning time frames

Months to days in advance, the operational planning of the power system focusses on maintenance, long-term generation scheduling and assessing the grid capacity between zones. Closer to actual operations (D-2), the guaranteed available system capacity between zones is determined and given to the market. Based on this input, market participants make offers to the market. The bids for the actual day come in the day before the actual operation (D-1), before gate closure. The different system operators perform the Day-Ahead Congestion Forecast (DACF) to determine whether the provided generation schedule can be maintained or whether there are adjustments needed. The DACF forecasts the system flows for each individual hour, while taking into account "N-1" constraints. The DACF also includes the expected generation from renewable energy sources. These adjustments can be done through market actions, or through TSO preventive actions such as the control of power flow controlling devices (PFCs). The DACF forms the basis for the security assessment done by the TSO. During the day itself, the TSO monitors the grid behaviour, which in normal operation always differs to a certain extent from the predicted state due to contingencies in the system, unforeseen generation shifts (possibly due to weather conditions), and changes in demand amongst others.

Furthermore, the system continuously changes its operating state because of the numerous variables in the system. If the predictions are close enough to the actual operation point, the TSO performs its planned operation. Generators (and other market participants) might also trade electricity intraday, resulting in possible changes from the foreseen schedules. Regular energy trade and balancing actions occur throughout the day. Larger shifts from the predicted operating point might occur as well. This can happen through large deviations in generation or load (due to an outage or unforeseen shifts in generation) or through outages in the grid. Such larger shifts can cause the system to move beyond the secure operating boundaries of the system. At such occasions, the system operator takes action through additional preventive actions or even corrective actions [55].

This discussion also reflects on the type of studies done with optimal power flow calculations. For **long-term studies** in an unbundled market situation, the generation of active power is in the hands of the generation companies and market players. The transmission system operator needs to develop his system in order to operate his network in a stable way. One of the aspects is having correct voltage ranges on each of the network nodes, taking into account different grid loading patterns. The nodal voltages are linked to the generation of reactive power. To manage this, the operator has proper means at hand: switching shunt reactors and capacitor banks. Another share of the reactive power generation comes from the generator units themselves. Optimal power flow calculations are used to estimate the minimum amount of reactive power from generator production units to guarantee correct bus voltages, taking into account sufficient margin on reactive power in case of grid emergencies. Securing sufficient transmission capacity, both internally and for international transit, taking security constraints into consideration, defines the second most important long-term studies from the operator point of view. Typically, these long-term optimisation calculations are run once each half to full year. The results are announced to the market players and serve as base cases for short-term studies.

The **short-term** calculations are typically performed one to two days before the studied date in a day-to-day cycle. They consider the actual state of the network with all current outages. The active power is nominated again by the market and the cross-border transfer capacities are maximised by the TSO. This type of optimisations and verification calculations is routinely done for each month, week and day.

The optimisation tools can also play a crucial rule for the real-time **grid operations**: one example is the gradual curtailment of dispersed generation. In order to provisionally accommodate more generation than can be allowed for safe operation in a security constrained situation, the owners of the generation units agree to curtail their output in case of a specific contingency. The grid operator sends maximum output setpoints which are the result of optimisation calculations initiated immediately after a grid incident has occurred. As such, more generation is allowed with the trade-off to be curtailed temporarily depending on the time to establish the safe state of the local network.

All calculation tools give at the desired time intervals a global picture on how the grid can be operated in an optimal way by means of setpoints for power and phase shifting transformers, output of generators and setpoints for converters. It is up to the human operator to perform the necessary switchings, tap position and setpoint changes in order to shift the grid state to its optimal point taking into account the inherent control restrictions. At all times, weather conditions and unforeseen outages are interacting with this process.

3.5.3 Control variables

It is only an utopian case that the operator can decide the setpoints for every element in the network. The current grid situation and policy dictate the control possibilities of the Optimal Power Flow case. Care must be taken which devices may be used for the grid optimisation.

Control possibilities of TSOs before unbundling

In the early stage of the electricity grid development, where generation, transmission and distribution were grouped together into vertically integrated corporations, there has traditionally been a good coordination between location choice of generation with respect to the grid, easy and predictable economical dispatch and easy fine-tuning of the reactive power balance. A global optimisation with generation and network capabilities was possible. It reflected into the optimal power flow case by giving output freedom to all generators linked to the network.

Control constraints of TSOs after unbundling

Due to unbundling, generation, transmission and distribution reside in independent companies. The Transmission System Operator does no longer have unlimited freedom. Generators in the internal network, owned by independent companies, are to be considered as units with a contractually fixed active output power. Deviations from these setpoints are possible to prevent dangerous network operation modes, but at a considerable cost. This deviation cost can be taken into the objective function as well.

Exclusive control for TSOs

Transmission System Operators have, generally speaking, unlimited access to the network elements they own. They can manage these devices continuously, quasi-continuously or in a discrete manner.

- Tapping of the classic power transformers, interaction on the reactive power flow in meshed networks and direct voltage control of the radial distribution grids.
- Energising shunt capacitors and reactors, impact on the local reactive power balance.
- Switching of network elements: typically overhead lines, underground cables, coupling bays, power transformers. This has an impact on the power flow and possible influence on the short circuit power management.
- Setpoints and ramping rates of the FACTS, phase shifting transformers and the HVDC installations.
- Generator voltage setpoints cannot be automatically controlled: the operator forwards new setpoints to the generation companies.

Grid loads

Under normal circumstances of network operation, loads are taken as given when starting an OPF calculation. No variation of their setpoints is considered, as the main task of the TSO is to supply electrical power under a wide range of operating states. However, care should be taken when choosing different scenarios, as different load patterns (night/day, winter/summer, working day/weekend day) result in different optimal working points.

3.5.4 Grid coordination

A very important issue with electrical grids is their mutual interaction. As pointed out by [56] and [57], the Transmission System Operators controlling active power by means of Phase Shifting Transformers or faster acting installations (FACTS, HVDC) are not only acting on the energy flows in their own grid or control zones. Due to the transnational grid meshes, every control action has implications on neighbouring grids. Avoiding loop flows in the grid of Party A can cause severe overloading on branches of the grid of Party B which are not even monitored by the operators of Party A. Interactions between the control of Belgian phase shifting transformers and the power flow of the German-Austrian transborder power flow have been reported in [57].

Power flow controlling devices, e.g. phase shifting transformers, are acting on the quasi steady-state behaviour of the grid and are most often manually controlled by the grid operator. Installations applying fast controls, using semi-conductor technology, can induce unexpected transient stresses on the neighbouring networks with even the possibility of tripping generators.

Coordination between all grid parties is the key to solve these issues. Transnational organisations, e.g. ENTSO-e, Coreso, the CWE control zone amongst others, provide different platforms for cooperation and awareness that no interconnected grid can be regarded as an isolated electrical island without any interaction with the neighbouring grid operators and generation companies.

These aspects reflect in the approach on how the optimal power flow cases are set up. Taking the example of the Belgian grid, optimising the overall grid losses by avoiding overloads on the 380 kV grid, implies that parts of the grids of The Netherlands, Germany, Luxembourg and France are to be taken into the grid model. Optimising only for the Belgian internal grid, may compromise the safe operation of the Dutch grid and vice versa. When a party optimises its own grid, no global optimisation is reached due to the illusion that the neighbouring grid Operator would just accept its grid to be overloaded or even operated in a less secure state for the benefit of the first.

The picture gets even more complicated when, as pointed out in chapter 2, an independent DC overlay grid operator connects its grid to the existing AC grids. The active power exchange, contrarily to the passive AC networks, is controlled. In order not to jeopardise the power supply anywhere, a global coordination must be assured and legally formalised.

Tools that can take care of very large grids, including meshed AC and DC grids, AC/DC converters (both LCC and VSC types) with good data exchange capabilities so the models can be fed on regular basis by many different parties, are of utmost importance.

3.6 Mathematical formulation of the optimal power flow

In this section, the standard optimal power flow case definition is given for the sake of completeness, readability and easy referencing of the equations in the remainder of this manuscript. It also helps to introduce a series of parameter vectors, their related vector functions and respective element sizes.

The description implicitly assumes that all state variables have a deterministic nature. When dealing with probabilistic quantities, e.g. the active output power of renewable energy sources, other aspects need to be implemented as well. One way to deal with this, is the formulation of the so-called probabilistic optimal power flow (P-OPF), [48], and the use of probability density functions.

It should be noted that this part is only describing an OPF for a classic AC network without security constraints. In the following chapters, the additional functionalities are introduced as an expansion of the formulation. Furthermore, the cost functions f are defined and described separately, although they appear in the general formulation in their most generic way.

Most of the available algorithms, when converting network data into an OPF case to be optimised by a generic solver, perform a number of simplifications, in order not to unnecessary overgrow the matrices and element vectors and to improve calculation speed. Some useful simplifications are discussed below as well.

Assume a generic AC grid which contains the following network elements

- n_b, number of nodes in service.
- n_l, number of network branches in service, typically overhead lines, underground cables, power transformers and phase shifting transformers. Before the optimisation algorithm is launched, the branches not in service, are discarded.

- n_g, number of active generators. Different generators connected to the same node could be aggregated to one single unit as a first simplification.
- Passive shunt elements, like capacitor banks and shunt reactors, which can only be switched on and off, are aggregated per node and treated in the same way as in power flow calculations: they interact only with the active and reactive power equalities in each node. Some software packages offer the possibility for switched shunt elements. In this case, this aggregation becomes more complex.
- Active regulated shunt elements, SVCs, STATCOM, ... are modelled as special purpose network generators on a PV node.

When a real substation consists of more than one busbar, it can be modeled as one node, except in the case when the substation is operated with independent uncoupled busbars. Some packages take coupling bays as independent network element into account. This has only a useful meaning in the post-treatment of the calculation when comparing the loading of this bay against its thermal characteristics. The added value of including coupling bays into the model, is to decide whether or not to split or join the nodes of the different busbars depending on their open or closed position.

3.6.1 State variables

The purpose of the OPF calculation is to find a set of state variables, defining a viable working point of the network complying with the imposed constraints and which is the minimum of the defined cost function.

The state variable vector used for the optimal power flow formulation is

$$x = \begin{bmatrix} \Theta \\ U \\ P \\ Q \end{bmatrix} \tag{3.61}$$

where Θ are the n_b bus voltage angles, U the n_b bus voltage magnitudes, P the n_g generator active and Q the n_g reactive power injections. The length of the vector x is thus $2n_b + 2n_g$ and contains only continuous values.

In order to build a more realistic model, the state vector x needs to be extended with a set of discrete value parameters: e.g. tap position of power and phase shifting transformers, state of capacitor banks. This extension of the optimisation formulation is not implemented in this work (section 1.3).

3.6.2 Linear constraints

Linear and non-linear constraints have to be imposed on the optimisation parameters in order not to exceed physical or other limitations of the network elements, and as such to find acceptable working points.

The upper and lower limits of the individual state variables are expressed as linear constraints:

- For the bus voltage angle vector Θ, in the normal case, only the voltage angle of the slack bus (SB) is set to 0°.
- Minimum and maximum voltage limitations are used for each of the bus voltage amplitudes U_i following operational experience and grid codes. The maximum value is given by the equipment insulation level, the minimum lower the risk of voltage collapse.
- Limitations on the vectors P and Q, the active and reactive power output of the network generators give the power range for proper operation of that specific power plant. This rectangular set of limitations is not limiting the thermal generator output power $S = \sqrt{P^2 + Q^2} \leq S_{max}$, a non-linear inequality constraint (subsection 3.6.3).

The linear constraints thus create the following set of $2 + 2n_b + 4n_g$ linear inequality constraints

$$\begin{aligned} \Theta_{SB} &= 0 \\ U_{i,min} \leq U_i &\leq U_{i,max} \\ P_{i,min} \leq P_i &\leq P_{i,max} \\ Q_{i,min} \leq Q_i &\leq Q_{i,max} \end{aligned} \tag{3.62}$$

Linear equality constraints, such as the first equation of the slack bus reference in the set (3.62), are rewritten as (3.63) and count as a double linear inequality constraint.

$$x = x_0 \Leftrightarrow x_0 \leq x \leq x_0 \tag{3.63}$$

3.6.3 Non-linear constraints

So far, only linear constraints are treated, whereas no distinction is made between the linear and non-linear constraints by most optimisation algorithms

(e.g. the one described in Appendix B). Other software algorithms however, such as MatPower, have implemented a different treatment of the linear and non-linear constraints and their clear distinction must be maintained.

Non-linear equality constraints

The AC network configuration, the branch impedances, active and reactive power absorbed by the network loads and the injections of the connected generators are mathematically described by non-linear equality constraints. These expressions are the very same as the power flow equations, stating the active and reactive power balance in each node. Contrarily to the power flow calculation, only the reference bus angle, the network loads and branch configuration are usually fixed. The notions slack bus, PV node and PQ node are undefined in this context. As such, the expressions for all nodes, independent of their Power Flow context, are treated in the same uniform way (section 3.2). An additional advantage of splitting the equations into their active and reactive part, is that direct calculation with complex numbers is avoided.

For a network with n_b buses, a total of $2n_b$ equality constraints is defined

$$\mathbf{g}_P\left(\Theta, \mathbf{U}, \mathbf{P}\right) = 0 \tag{3.64a}$$

$$\mathbf{g}_Q\left(\Theta, \mathbf{U}, \mathbf{Q}\right) = 0 \tag{3.64b}$$

With the aid of the calculations of Appendix C, the expressions for $\mathbf{g}_P(\Theta, \mathbf{U}, \mathbf{P})$ and $\mathbf{g}_Q(\Theta, \mathbf{U}, \mathbf{Q})$ from the previous two equations are expanded and written out for an arbitrary node i.

$$\begin{aligned} g_{P,i}(\Theta, \mathbf{U}, \mathbf{P}) &= P_{br,i} + P_{l,i} - P_{g,i} \\ &= \sum_{j=1}^{n_b} Y_{ij} U_i U_j \cos\left(\theta_i - \theta_j - \varphi_{ij}\right) + P_{l,i} - P_{g,i} \end{aligned} \tag{3.65a}$$

$$\begin{aligned} g_{Q,i}(\Theta, \mathbf{U}, \mathbf{Q}) &= Q_{br,i} + Q_{l,i} - Q_{g,i} \\ &= \sum_{j=1}^{n_b} Y_{ij} U_i U_j \sin\left(\theta_i - \theta_j - \varphi_{ij}\right) + Q_{l,i} - Q_{g,i} \end{aligned} \tag{3.65b}$$

In these equations, for the node i, the active and reactive power flowing away through the branches (to other nodes as well as to shunt elements connected to that node) are noted as $P_{br,i}$ and $Q_{br,i}$. Expressions (C.17a) and (C.17b) are used to give their relation with bus voltages and network admittance matrix Y (C.12).

$P_{l,i}$ and $Q_{l,i}$ are fixed values (for the OPF standard case used in this research) and state the sum of active and reactive power extractions of the network loads connected to the AC bus i. And finally, $P_{g,i}$ and $Q_{g,i}$ are the total power *injections* (hence the minus sign) by the combined generators in that bus.

As these equations are forced to be zero, the optimisation algorithm is forced to use the actual grid definition and power balance, hence the use of equality constraints. They are sufficient for the whole AC OPF case [40].

Other non-linear equality constraints for the AC network case may apply, only (3.65a) and (3.65b) are used in this research and by the MatPower tool.

Non-linear inequality constraints

Inequality constraints are used to limit computed function values using state variables to upper and lower bounds, instead of fixing them to predefined values. Direct limitations on the state variables are already introduced by the linear equation set (3.62).

Network branches (overhead lines, underground cables, power transformers, phase shifting transformers) have also their specific thermal limitations. Some network management software packages give the user the possibility to specify current limitations for different conditions (e.g. Elia, the Belgian TSO, defines three limits, for summer, winter and two intermediate seasons).

The limits taken into account are the long-term loading capabilities. In chapter 4, for the general case of the OPF case with contingency constraints (equations 4.1a to 4.1h), different maximum load current values for the different time frames are given. They depend on the thermal time constants of the individual elements. For the base case however, they are not taken into account.

On the other hand, overloading shunt elements is not considered. Their loading depends only on the bus voltage amplitudes, with fixed upper limits.

Looking only at the passive network branches, current or power limits can be applied. Because of the two connection points, each branch adds two constraints to the OPF case: the current or power flowing into the link from the from (k)- and the to (l)-bus. Equation (C.9) from Appendix C states the set of these two current equations.

These currents can be either positive or negative, depending on the current flow direction. One can set an upper and lower bound, multiplying the number of inequality constraints by two. The expression and the corresponding limits are squared, resulting for the branch i together with its current limit value $I_{max,i}$ in

$$\begin{cases} h_{2i-1}(\mathbf{x}) & = \left|\overline{I}_{i,k}\right|^2 - I_{max,i}^2 = I_{i,k}^2 - I_{max,i}^2 \leq 0 \\ h_{2i}(\mathbf{x}) & = \left|\overline{I}_{i,l}\right|^2 - I_{max,i}^2 = I_{i,l}^2 - I_{max,i}^2 \leq 0 \end{cases} \tag{3.66}$$

Here, $i = 1 \ldots n_l$, n_l being the number of 2-node branches in the AC system and the number of these constraints is $2n_l$.
Alternatively, when it is desired not to limit the current, but the apparent power $S_{i,k}$ and $S_{i,l}$ (with the limitation $S_{max,i}$) flowing into the branch i, one can express the inequality constraints by

$$\begin{cases} h_{2i-1}(\mathbf{x}) & = S_{i,k}^2 - S_{max,i}^2 = \left(U_k I_{i,k}\right)^2 - S_{max,i}^2 \leq 0 \\ h_{2i}(\mathbf{x}) & = S_{i,l}^2 - S_{max,i}^2 = \left(U_l I_{i,l}\right)^2 - S_{max,i}^2 \leq 0 \end{cases} \tag{3.67}$$

Note the use of the amplitudes of the complex values of current, voltage and power.

Other inequality constraints may apply: when the apparent power of the grid generators is to be limited (subsection 3.6.2), the corresponding constraints need to be added to the OPF case. For an arbitrary generator i, with its maximum apparent power $S_{max,i}$, the following expression is used.

$$h_{g,i}(\mathbf{x}) = S_{g,i}^2 - S_{max,i}^2 = P_{g,i}^2 + Q_{g,i}^2 - S_{max,i}^2 \leq 0 \tag{3.68}$$

3.6.4 Reference formulation

Putting all the above together, the base OPF case can be generically stated as an optimisation problem:

$$\min_x f(x) \tag{3.69}$$

$$g(x) = 0 \tag{3.70}$$

$$h(x) \leq 0 \tag{3.71}$$

$$x_{min} \leq x \leq x_{max} \tag{3.72}$$

The full overview of all first and second derivatives needed to compile the Jacobian and Hessian matrices of the above system to be implemented in the optimisation algorithm is found in [41].

3.6.5 Implementation of the routines

Figure 3.3 shows the normal course of the Optimal Power Flow algorithm as implemented in MatPower in its standard form. It starts and ends with the proper MatPower routines for case preparation (specifying default values, filtering out outaged buses, generators and AC branches) and post-processing. The proper optimisation process is performed by a solver routine (user-selectable), which on its turn calls MatPower routines with each iteration step for the construction of function vectors of the cost function and the non-linear equality and inequality constraints, their first derivatives for the Jacobian and their summed contribution to the Hessian matrix.

The definition of additional state variables and linear equality and inequality constraints is already foreseen in the MatPower extended OPF formulation. However, no option is given to directly add non-linear inequality and equality constraints and to define cost functions other than the polynomial and piece-wise linear generation costs of active and reactive power.

When adding supplementary non-linear constraints is desired, the normal course of the optimisation solver needs to be altered (figure 3.4). After each call to MatPower routines, to calculate the necessary function vectors for the AC network, the additional values, vectors and matrices are calculated and compiled in the way described in section 3.4. The routines developed for this research, intercept the original MatPower routines, by altering the function calling priority, as foreseen in Matlab. The altered algorithm flow and the developed program block are drawn with bold lines. Altering the algorithm course by

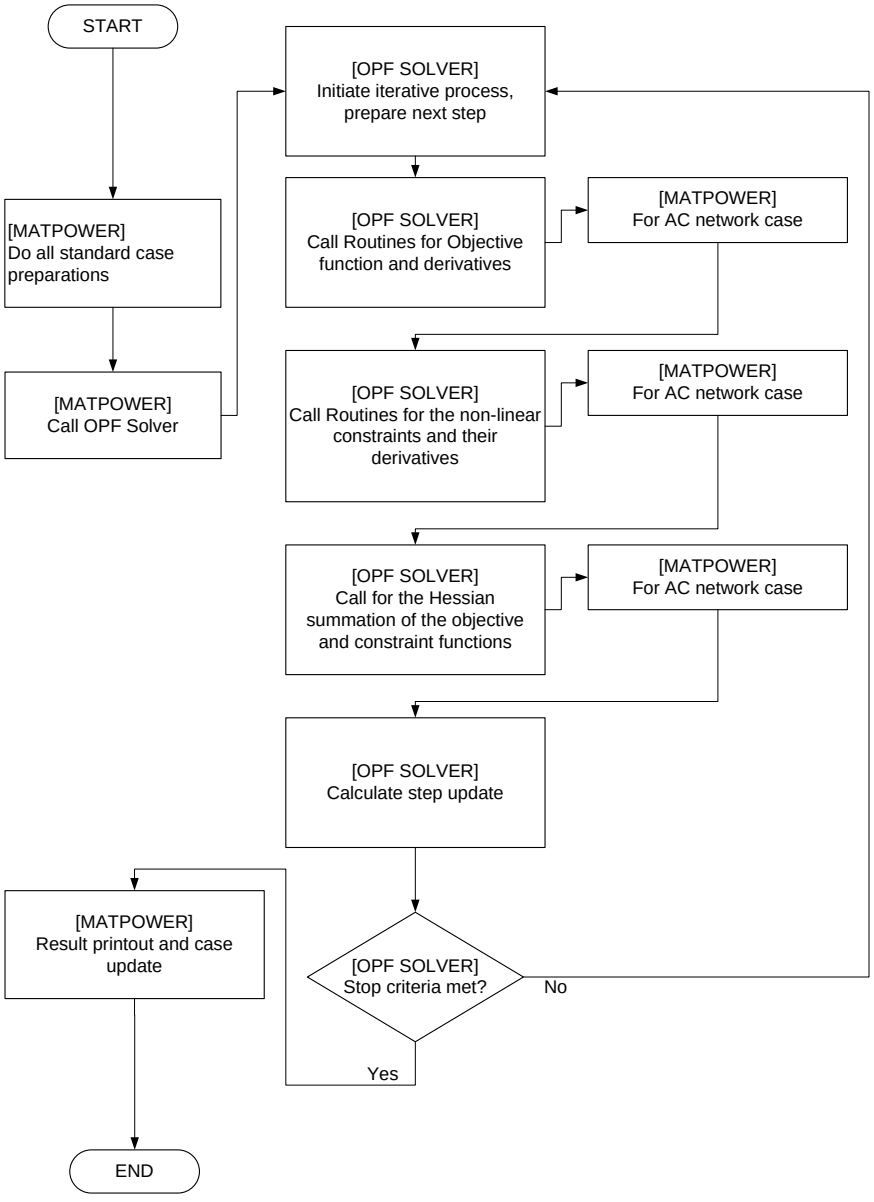

Figure 3.3: Unaltered MatPower flowchart for the Optimal Power Flow

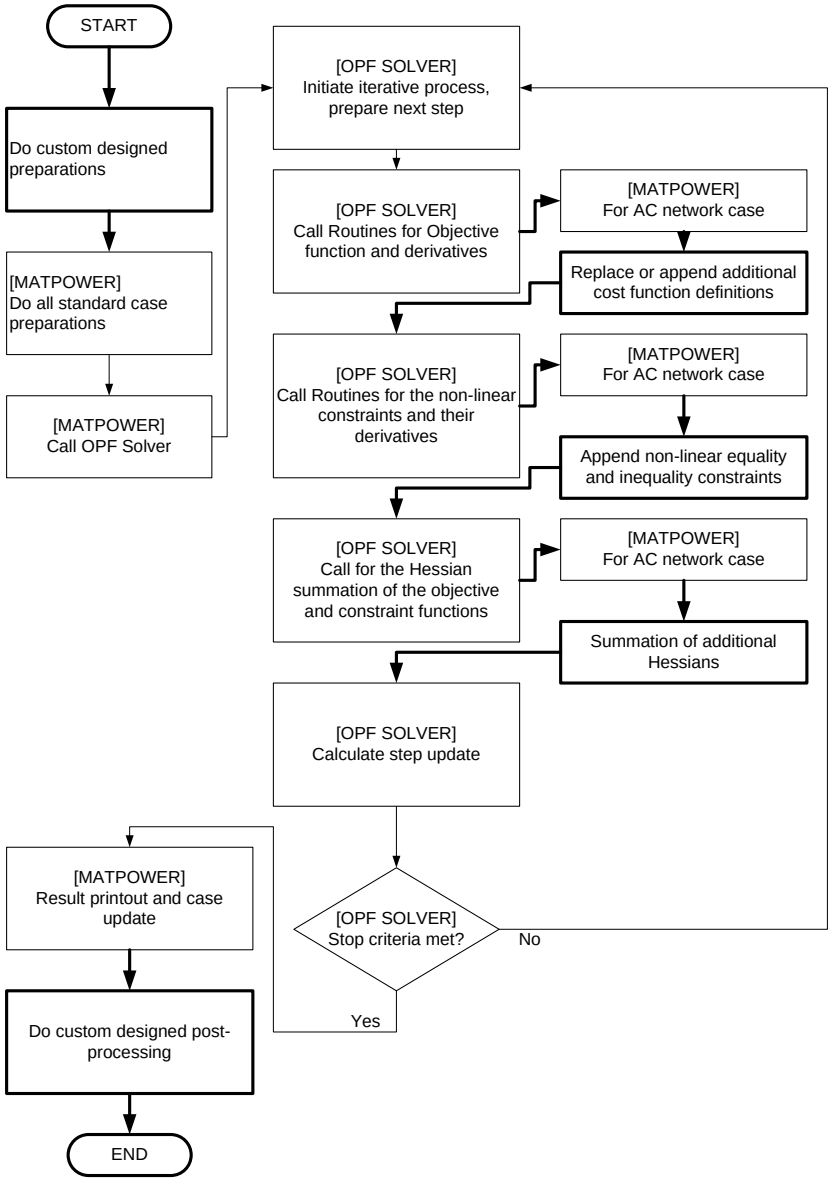

Figure 3.4: Adapted flowchart for the Optimal Power Flow with customised extensions to the non-linear cost function and constraints. **Legend**: normal line widths are used for original MATPOWER routines, bold lines for adapted adapted algorithm flow and implemented routines.

adding more functionalities, requires the intervention in almost every phase of the calculation.

Appropriate initialisation and post-processing blocks of the added functionalities are called before and after the original MatPower functions.

3.7 Defining the cost function

In the previous sections, the state variables and their constraints describe the complete structure and limitations of the AC network. In this section the Optimal Power Flow formulation is extended with the choice for an appropriate cost function, expressing mathematically the goal to be achieved (subsection 3.5.1). It is a scalar function of the state variables. The optimum is reached when the value of this function is at the global minimum within the boundary region of the optimisation case.

3.7.1 Cost function primitives

The table 3.1 gives an overview of the most common cost function primitives. The used symbols are explained first

- S_g: set of generators of the network taken into account
- S_b: set of branches taken in the optimisation process
- S_l: set of grid loads that can take part in the load shedding optimisation
- S_n: set of grid nodes that can take part in the optimisation
- S_c: set of capacitor banks to be taken into account
- S_x: set of state variables that can take part in the optimisation
- P_i: active power output of the individual generators
- $P_{bk,i}$ and $P_{bl,i}$: active power going into the branch i from bus k and l. Their sum is always positive and gives the power loss in the branch.
- P_l: total active power extracted from the grid by the loads
- Q_i: reactive power produced by generator i
- $Q_{b,i}$: reactive power consumed by branch i

Table 3.1: Examples for cost function primitives

Description	Formulation
Feasability	$f(x) = 0$
Min. active output power	$f(x) = \sum_{i \in S_g} P_i$
Min. power losses	$f(x) = \sum_{i \in S_b} (P_{bk,i} + P_{bl,i})$
Min. generation cost	$f(x) = \sum_{i \in S_g} C_i(P_i)$
Min. import and export costs	$f(x) = \sum_{i \in S_b} C_{b,i} \left(\frac{P_{bk,i} + P_{bl,i}}{2} \right)$
Max. active power transfer	$f(x) = -\sum_{i \in S_b} C_{b,i}(P_{b,i})$
Min. generation cost taking load shedding into account	$f(x) = w_g \sum_{i \in S_g} C_{b,i}(P_{b,i}) + w_l \sum_{i \in S_l} C_{l,i}(P_{l,i})$
Max. generator reactive power margin	$f(x) = \sum_{i \in S_b} \frac{(Q_i - Q_i^a)^2}{Q_{i,max} - Q_{i,min}}$
Max. reactive power margin	$f(x) = -\sum_{i \in S_g} Q_i$
Max. bus voltages	$f(x) = \sum_{i \in S_n} (V_{i,max} - V_i)^2$
Min. reactive power consumption	$f(x) = \sum_{i \in S_c} Q_i + \sum_{i \in S_b} Q_{b,i}$
Min. variation from beginning state	$f(x) = \sum_{i \in S_x} w_i (x_i - x_{i,0})^2$
Min. voltage difference between two nodes	$f(x) = w_V (V_1 - V_2)^2 + w_\theta (\theta_1 - \theta_2)^2$

- Q_i^a: attractor (or preset) value for the reactive power of generator i
- $Q_{i,max}$ $Q_{i,min}$: maximum and minimum reactive power of generator i
- V_i: voltage amplitude on node i
- θ_i: voltage angle at node i
- $V_{i,max}$: maximum voltage amplitude limit of node i
- C_i: generation cost for generator i (values differ for active and reactive power)
- $C_{b,i}$: load conduction cost for branch i
- $C_{l,i}$: load shedding cost of load i
- x_i: value of state variable i
- $x_{i,0}$: initial value of state variable i
- w_i: general symbol for the weighting factor of parameter i

With the present approach, other functions (e.g. environmental impact, investment cost) can be implemented as long as they can be expressed as a scalar function of the state variables.

3.7.2 Applications

Many references dealing with the choice of cost functions for different applications have been published. In [58, 32], the available transfer capability (ATC) and the minimisation of the system losses are discussed for systems with an integrated point-to-point HVDC system with Voltage Source Converters.

3.7.3 Combining cost functions

The primitives can be used as stand-alone functions, but for some applications, several functions can be combined, using a weighting factor. Several applications of the multi-objective optimisation and different solution methods have been published [59, 60, 61]. In [62, 63], the multi-objective optimisation is to maximise social benefit, loading margin of the decentralised electricity market and optimal placement of generation units taking into account security constraints. Different methods to choose and tune the weighting factors together with the advantages

and disadvantages are given in [64].

Particle swarm [65, 66, 67] and evolutionary algorithms [64, 68, 69] are one way to cope with the multi-objective optimisation and is made especially for those environments where no explicit optimisation algorithms are developed. For the optimisation of electrical systems described in this manuscript, these algorithms exist and the optimum point for every set of weighting factors can be found by calculation instead of trying out a multitude of scenarios to probe the Pareto-front (subsection 3.7.4).

The general formulation for combining the cost functions is

$$f(x) = \sum_{i=1}^{n} w_i f_i(x) \tag{3.73}$$

Here, $f_i(x)$ are the n chosen primitive cost functions and w_i their respective constant weighting factors. Care should be taken to their choice, as the individual cost functions may differ by several orders of magnitude. A scaling has to be applied in order to balance each term in (3.73).

A distinct application of combining cost functions, can be found in subsection 3.7.5, where state variables are forced to take pre-set values. It is possible to combine two or more concurring functions pushing the optimal solution in two different directions. Two intuitive examples with concurring objectives are given below.

Example 1

- Optimising minimum active grid losses would push the nodal voltage amplitudes towards their upper limits.
- By creating higher (positive) reactive power margins, lower bus voltages are favoured.

Example 2

- Optimising active grid losses are favouring the power plants closest to the load centres.
- Minimising specific exhaust gasses favours clean power plants (e.g. wind energy) which can be located further away from the load centres.

The solution is dictated by the weighting factors of the different parts of the cost function. A higher weighting factor for one, gives a higher priority to that cost. In some cases, two or more cost functions strive towards the same solution region, e.g. minimum grid losses and minimum generation cost. In general, this is not the case. In reality, combining cost functions gives a full range of optimal solutions, only by changing their relative weighting factor. The generic formulation of the multi-objective optimisation [68], fitted into the general OPF formulation is

$$\min_x F(x) = [f_1(x), f_2(x), \ldots, f_n(x)]^T \tag{3.74}$$

$$g(x) = 0 \tag{3.75}$$

$$h(x) \leq 0 \tag{3.76}$$

$$x_{min} \leq x \leq x_{max} \tag{3.77}$$

The last expression of this set is called the parameter space (symbol Ω), the space spanned by the vector function $F(x)$ is called the objective space without taking care of the constraints g and h and the subspace of the objective space that do take these constraints into account is called the feasible space.

In the rare case of $n \geq 2$ where all objective functions share the same optimal working state

$$\exists x^* \in \Omega : \forall x \in \Omega, f_i(x^*) \leq f_i(x) \tag{3.78}$$

$$i = 1 \ldots n \tag{3.79}$$

is called the utopian solution: the different objective functions are not mutually counteracting and a unique point is found. If $n = 1$, this reasoning degrades to the usual single goal optimisation problem.

A more realistic case is that an optimal point for one objective function, is not optimal for the other goals. Here, no improvement for one function can be found, without degrading the optimality of at least one of the other ones. An infinite number of solutions is possible, depending on the preferences of the user and his management of priorities.

3.7.4 Pareto front

Theoretical background and purpose

The Pareto set, named after the Italian economist Vilfredo Pareto, is the set of points in the parameter space which are not dominated by another point in that set [59]. Dominance means that improvement on one goal function degrades at least one other cost function.

Formally written, it gives the following statement:

State x_1 is Pareto dominant (for optimisations that seek to minimise the goal functions) over x_2 if and only if

$$\forall i \in (1 \dots n) : f_i(x_1) \leq f_i(x_2) \tag{3.80}$$

$$\exists i \in (1 \dots n) : f_i(x_1) < f_i(x_2) \tag{3.81}$$

The Pareto front is the collection of all Pareto dominant points of the multi-objective optimisation problem.

First the development of the two-dimensional Pareto front is treated, next the general multi-dimensional expressions are given.

The two outer points P_1 and P_2 of the 2D Pareto front (figure 3.5) are defined by the optimal solutions $x_1^\star$ and $x_2^\star$ of cost functions f_1 and f_2:

$$P_1 = (f_1(x_1^\star), f_2(x_1^\star)) \tag{3.82}$$

$$P_2 = (f_1(x_2^\star), f_2(x_2^\star)) \tag{3.83}$$

To calculate the points lying on the Pareto front from point P_1 to point P_2 with an almost equidistant distribution, the expression [48] for the weighting cost function is used:

$$f(x) = (1 - w)\frac{f_1(x) - f_{1,min}}{f_{1,max} - f_{1,min}} + w\frac{f_2(x) - f_{2,min}}{f_{2,max} - f_{2,min}} \tag{3.84}$$

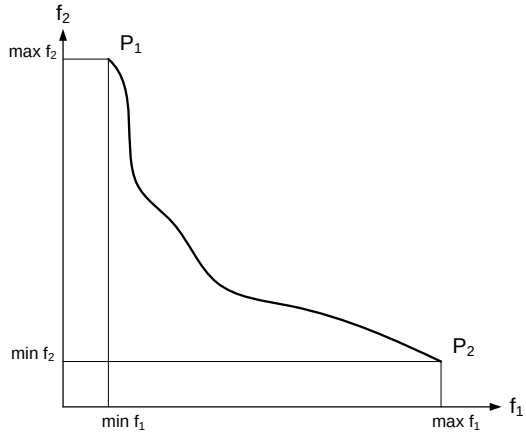

Figure 3.5: Sample of a 2D pareto front

with $w \in [0 \dots 1]$.

This approach differs fundamentally from the evolutionary Pareto front searching algorithms. For the method used here, the only varying parameter is the weighting factor w, the optimum points for each of the chosen weighting factor are calculated directly by the optimisation algorithm. The optima states that are not Pareto dominant for certain values of w, are discarded.

To extend (3.84) for more than two cost functions, the same scaling approach holds for the two-dimensional front. This results in the following formulation

$$f(x) = \sum_{i=1}^{n} w_i \frac{f_i(x) - f_{i,min}}{f_{i,max} - f_{i,min}} \tag{3.85}$$

with $\sum_{i=1}^{n} w_i = 1$ and $w_i \geq 0$.

Illustrative simulation results

For the examples (figures 3.6 and 3.7), the generator cost is assumed a polynomial function of the active generator output power:

$$C = 0.2 + 0.3P_g + 0.01P_g^2 \tag{3.86}$$

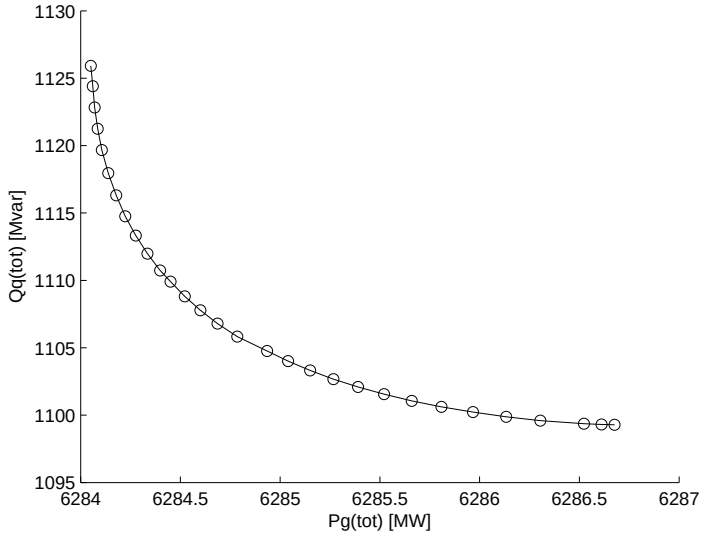

Figure 3.6: Pareto front for the 39 nodes network comparing active and reactive power. X-axis: Total generator active output power. Y-axis: Total generator reactive output power

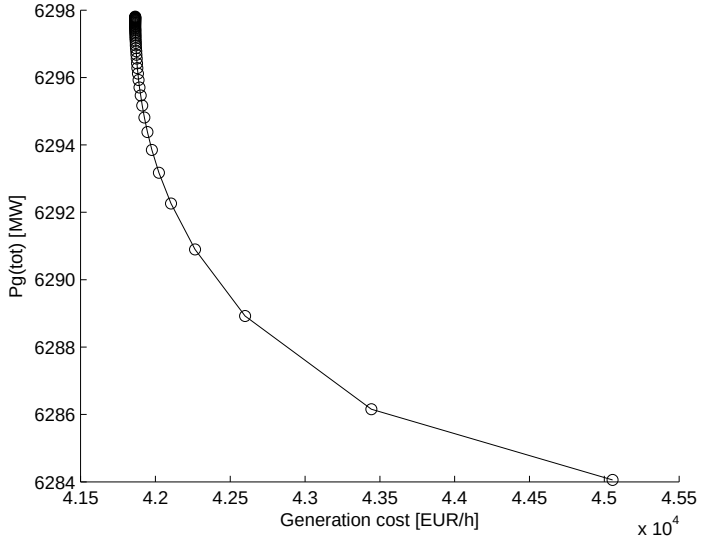

Figure 3.7: Pareto front for the 39 nodes network comparing generation cost and active power. X-axis: Generation cost. Y-axis: Total generator active output power.

3.7.5 Directly fixing state variables

In most optimal power flow definitions, the cost function only acts on a subset of elements rather than on the complete set of generators, branches, etc. For example, one wants to minimise the active output power of only the internal network whereas the generators of the outside network are treated as in a power flow calculation (PV node, where the active power and bus voltage are specified in the initial state).

Here, the approach between different software packages differ. Setting defined values to state variables

$$\forall x_i \in S : x_i = x_{i,0}, \mathrm{d}x_i = 0 \tag{3.87}$$

with S the set of state variables with preset values, means that they become constants to the case and are to be excluded from the state variable vector and to be eliminated from the constraint equations. Software packages, like MatPower, are not providing this option. This has been circumvented by using the following approach.

Directly setting the upper and lower limit of a state variable to the same value, is in theory a good option. The solver cannot converge as all value updates of that state variable are always out of their boundaries, giving the barrier function (subsection 3.3.3) an undefined value.

A solution to this problem is building an additional part on the cost function, with a high weighting for priority purposes. This method is inspired on the penalty method (subsection 3.3.3). The general mathematical expression is

$$f(x) = f_o(x) + W \sum_{i \in S_x} (x_i - x_{i,o})^2 \tag{3.88}$$

$f_o(x)$ is the desired cost function and S_x is the set of state variables that need a fixed value. This expression parabolically attracts the state variables to their setpoints. The weighting factor W is set arbitrarily. An iterative routine is implemented, adapting this factor (e.g. multiplied by 10) with each iteration when a predefined precision threshold has not been reached in order to preserve the priority nature of this part of the cost function (figure 6.4). The total residual can be compared to the threshold value

$$r = \sum_{i \in S_x} (x_i - x_{i,o})^2 \tag{3.89}$$

or the maximum value of a group of specific state variables is to be compared against the group threshold:

$$\forall i \in S_x : \max |x_i - x_{i,o}| < \Delta_{max} \tag{3.90}$$

with S_x a group of state variables.

As such, indeed, the setpoints are not imposed, but rather the optimal power flow case definition invites the variables to converge to the predefined settings. Very small allowed deviations can be defined, at the expense of calculation time.

3.7.6 Load flow case defined by OPF

Using the method of the previous subsection, one is able to set up a complete power flow case by setting

- a generator at the slack bus SB: the slack bus voltage U_{SB}, setting the angle reference is done automatically by the standard routines;
- all generators on PV buses: the active power output P_i and the corresponding reference bus voltage U_i;
- all generators on PQ nodes: their active and reactive power.

Deviations are still possible between the power flow calculations and the OPF method, as the optimiser searches a viable working point in the first place. In that case the non-linear constraints may interfere with the solution. This is normally not the case in power flow calculations. Setting the active power of all slack bus generators prevents the correct compensation of the grid losses. The corresponding state variable is thus omitted in (3.90). The same is true for the generator linked to the reference converter of the DC system (chapter 5).

3.8 Simulation results

Table 3.2 summarises the simulation results of the proper power flow routines and the use of optimal power flow routines. For every sample network, a close match is obtained. The average calculation time (based on ten consecutive runs of each algorithm) is in all cases very high for the OPF routines compared to the proper power flow calculation. In the case of the 3120 bus grid, no match has been found for the reactive power generation, as on some buses several generators are connected and only the sum of their individual reactive power outputs is taken into account by the routines.

Table 3.2: Calculation differences of the proper power flow and power flow by use of optimal power flow routines of the three sample systems

Item	Unit	5 bus	IEEE 39 bus	3120 bus
Elapsed time LF	s	0.008	0.011	0.139
Elapsed time OPF	s	0.45	0.65	77.56
Max Pg dev	MW	$1.08\ 10^{-5}$	$5.85\ 10^{-6}$	1.06
Max Qg dev	MW	$3.10\ 10^{-4}$	$2.22\ 10^{-4}$	-
Max Vm dev	%pu	$1.70\ 10^{-5}$	$1.78\ 10^{-5}$	2.39
Max Angle dev	°	$2.34\ 10^{-6}$	$4.87\ 10^{-6}$	$2.76\ 10^{-1}$

3.9 Conclusions

This chapter gives a literature overview of theories and solution methods developed for optimisation problems with non-linear objective functions and non-linear equality and inequality constraints. They are applied to AC grids where grid elements, topology and operation limits are treated.

The choice and implications of the objective functions are treated and a method was implemented when two or more concurring objectives are to be treated together. Weighting functions and the Pareto front approach were introduced. The chapter closes with two applications for the blending of the cost functions: keeping state variables at predefined setpoints and the Power Flow calculation using Optimal Power Flow techniques.

Chapter 4

Security constrained optimal power flow

4.1 Goal and importance

In the previous chapter, the Optimal Power Flow definition, inherently, assumes that the state (in service or out) of the grid elements is known and given, with the grid in its healthy, or "N" situation. To improve grid reliability and availability, during grid planning, operational planning and real time operation, more input is needed for the decision maker to understand how the grid would behave under more stressed conditions [70].

In this chapter, the focus lies on static stresses of the grid affected by security contingencies [71, 72, 73, 74, 75]. When a grid element trips, a redistribution of the power flow takes place. Redundancy of the grid branches, taking into account safe "N-1" operation, prevents overloading after such an event. The consecutive outaging of generators, grid links, converter stations and transformers (even whole substations, when a complete busbar system trips), could alter the topology of the grid drastically. This may lead to severe overloading and voltage instability in the vicinity, potentially followed by a partial or complete blackout of the system.

The chapter starts with a discussion on the importance of the security contingency analysis for different time frames and grid sizes. Next, the general

mathematical formulation of the Security Constrained Optimal Power Flow is given and an explanation how it is applied within this research. The chapter concludes with sample simulations.

The importance of the study of the network contingencies is given by the following facts

- Electricity consumption has been steadily increasing over time. Grid operators have not always been able to perform the necessary grid investments, hampered by insufficient flexibility in permitting, manufacturing capacity, time frame opportunities and lacking incentives for equipment replacements. Moreover, the consumer pressure and expectations for a reliable delivery of electrical power puts even higher constraints on the further development of the high voltage grid, especially in metropolitan and industrial areas where also the oldest equipment is found as a consequence.
- Generation capacity needs to follow demand growth as well. The original trans-European 400 kV grid was designed and developed for mutual support of neighbouring countries. Nowadays, the capacity of these links is used for international trade in auctioned contracts or via specialised energy exchanges as part of the power balance within the control area. This gives additional loading and reliability concerns on the mostly historically limited crossborder connections.
- The massive deployment of renewable power sources occurs throughout the grid, mostly in less populated regions. This can cause overloads when managing the sometimes variable amounts of power, both locally and due to distant balancing actions. In the latter case, loop flows throughout the system may occur. References [76, 77] are dealing with this subject and discuss methods for the optimal location of dispersed generation, taking into account (temporal) network security contingencies. In [78] the authors present a method to assess the contribution of dispersed generation on the voltage security margins of the grid.
- The installation of complex, fast-acting devices to tackle previous challenges, introduces new challenges in the network on their own.
- The market driven electricity system favours the optimal control of the network with minimum generation cost and post-contingency control rather than a suboptimal operation which takes into account predefined preventive control actions. Nevertheless, current operational procedures and rules are based on preventive measures. Market models are discussed in [79].

- In the day-to-day business of the Transmission System Operator, the possible grid security issues need to be assessed when a set of critical contingencies happens with the actual grid state. In [80], the authors discuss the artificial neural network method for the on-line identification of potential harmful states of a power system. Indices for a fast evaluation of the grid voltage stability have been discussed in [81].

The European FP7 PEGASE project [82] brought together needs, insights and experiences of utilities, university specialists and software providers to work on a common understanding towards tools to cope with a high number of contingencies applied to very large scale networks. The challenges for calculating power are enormous [83].

In the interconnected ENTSO-e network, the grids of the different participating countries become more intertwined. A global coordination of contingency handling is the only logical step forward. The operation of phase shifting transformers installed in Belgium [57] influence power flows in a wider region, up to Austria. Measures to manage the grid into a safe state may not degrade the security of the neighbours: the only possibility to achieve this, is to operate the system on a multi-zonal scale in a coordinated matter.

When treating contingency problems for a large network, the probability to deal with only single contingency states ("N-1") is low. Indeed, the larger the network, the higher the probability to suffer from multiple incidents and outages defining a "N-k" network state. On the other hand, in such large networks, several contingencies may occur without mutual interference. This problem can be reduced by only studying the contingency states per region. Nevertheless, some cases are affecting the whole system at once: when a storm passes, the probability to have multiple near simultaneous incidents in a widespread region is non-negligible.

4.2 Staged approach

Mainly two different approaches to manage contingencies for operators and grid planners are possible depending on the nature of the contingency and the time available for corrective actions to manoeuvre the grid back into a healthy state. Preventive security measures are taken in advance of a contingency which allow the system to remain secure after a possible outage. Curative security measures

are only taken after the contingency.

4.2.1 Preventive measures

Operators and planners can choose for a subset of security measures for preventive actions. For each of them, the conceptual structure of the grid together with an adequate choice of generator and converter setpoints are such that, in case of the actual event, the operator can rely on the fact that the grid remains in an healthy state. No immediate action is required, and the operator can slowly alter the grid parameters and topology to go to the next calculated optimal state including new security measures. Typical measures during the planning stage build in redundancy in the system, for instance through the duplication of lines or in some cases even by installing a multifold of parallel connections. Meshing of the grid is another alternative.

In order to rely only on preventive measures to restore the grid to a healthy state after a given credible contingency has taken place, the operator needs to take only these *first stage* decisions, as grid security is the main objective. From the point of view of generation cost, the grid might be operated suboptimal.

4.2.2 Curative measures

Curative or corrective measures are another subset of contingencies requiring immediate action of the operator right after an incident took place. In these cases, it is allowed to operate the grid in a state that cannot last indefinitely, due to overloading of grid elements for example. The operator has sufficient time and control possibilities to get the grid back into a healthy state. Before the contingency occurs, a screening of the possible contingencies and their required control actions is performed. Generally, outages of generators fall under this category.

These contingencies are not taken into account in the general cost function, and are treated as *zero cost* decisions, which might, in reality not always be the case. They are called *second stage* decisions.

More and more, the network operators experience that an ever growing part of the generator park is of a renewable energy nature. These depend on uncontrollable and fluctuating energy sources like wind or solar (biomass and hydro power plants do no fall under this category). It can put constraints on

the feasibility of the predefined curative actions as these power sources could be offline at the moment needed or on the contrary, are producing near peak capacity in the contingency zone with possible danger that the generated power cannot be absorbed by the network. The complexity rises when external factors, like market prices or forecasted weather conditions need to be taken into account to determine the possible curative measures.

4.2.3 Multistaged decisions

As pointed out before, due to the strong interconnection of the electrical grids, larger geographical regions need to be taken into consideration and single contingency surveys are no longer appropriate. The risk of cascading incidents needs to be taken into account which could lead to a partial or complete blackout. Even if such an event is not plausible for single contingency situations, it is for an unfortunate set of strategic (not even necessarily close-by) outages and incidents, combined with unexpected generation and consumption patterns.

Furthermore, in such complicated grid situations, it is possible that the grid operator cannot solve the situation with one single action. Indeed, during for example cascading events (e.g. slow voltage collapse), multiple actions are required within a very short time. Combined with generation and load uncertainties, there is a strong need for quick decision tools to steer the operation in an online fashion, to a safe network state. The operator is able to work intuitively the first seconds of the unplanned outage, he is surrounded by tools that show him the severity of the situation and help him during the whole process.

Day-ahead contingency analysis would prove unrealistic: too many uncertainties and an infinite number of “N-k” situations need to be taken into account.

4.3 Problem reduction

Given the fact that the network studies can be huge and that, as a natural consequence, the number of contingency states is quasi unlimited, solving directly for all contingency states simultaneously is infeasible and/or endless, due to limited resources.

When developing real networks, as a rule of thumb, the natural reduplication of assets leads to contingency constraints already fulfilled, thus unnecessarily enlarging the problem. These so-called "non-binding" contingencies can be neglected, as they cause no problem situations for the post-contingency grid state.

Several approaches to overcome the problems with large scale networks have been investigated.

4.3.1 Selection of binding contingencies

The goal is to search for the smallest possible subset of all possible binding contingencies. A contingency is said to be binding, when its impact on the final value of the objective function is higher than a predefined threshold, if included in the subset of outage cases. The non-binding contingencies have no impact on the outcome of the security constrained optimisation case [84].

It is an iterative search where four different functionalities interact.

- A security constrained optimal power flow (SCOPF) module capable of solving the case with at least the number of the binding contingencies (preferably even a bit larger subset). If the number of binding cases exceeds the available calculation power, the whole approach is inapplicable.
- A Steady-State Security Analysis (SSSA) which performs a scan on the solution of the SCOPF for all contingencies, but this time only as steady-state cases.
- A contingency selection criterion to filter out the most salient contingencies by a combination of a set of voltage, current and power criteria. The robustness of the whole approach depends on this module, as it requires (manual) tuning to rank the outcome of the different security constraints. Many publications deal with the search for the ideal severity index [85, 86].
- A post-contingency OPF module, as a last check that all constraints are met.

4.3.2 Post-contingency state model simplification

In the post-contingency state model simplification, also known as the Benders Decomposition approach [87], the SCOPF case is decomposed into a master

problem and many depending slave subproblems, which interact during the optimisation process with the master problem. An advantage of this partitioning, is the possible calculation speed-up by parallel computing. The technique requires in theory convexity, which is in general not the case and rendering this approach unreliable in some cases [88].

4.3.3 Linearisation of the post-contingency constraints

With the linearisation of the post-contingency constraints, only the relevant post-contingency inequality constraints are added to the base OPF case. They are linearised around the solution of the base OPF solution. All post-contingency equality constraints are dropped, checked anyhow by the base OPF case. Some approaches even linearise the base OPF case, rendering the whole into a linear optimisation problem. Very powerful and fast solvers can be used to solve them, but the result, due to these simplifications may be questionable at high load or when the network makes extensive use of reactive power controls.

4.3.4 Network compression techniques

Network reduction techniques are used to retain the original model in the direct neighbourhood of the contingency, whereas the network further away (where the impact of the incident is less) is reduced to only a few nodes. The algorithm is able to tune the reduction degree taking into account the number and location of the contingency states and the available computing power.

4.3.5 PEGASE approach

When dealing with SCOPF problems at a very large scale, and to get the results with relatively low computing power and calculation time, a combination of the aforementioned techniques can be used, as does the PEGASE approach [82]. It combines the power to reduce (compress) the networks together with the iterative process to find the set of binding contingencies.

4.3.6 Considerations using simplified approaches

The necessary precautions have to be taken with the previous approaches, as the simplifications can yield the results that still violate post-contingency constraints. They need to be checked again in the last stage of the process.

When the number of violations goes beyond an unacceptable level, the whole process has to be repeated, possibly with a new set of parameters or even a different approach.

4.4 Mathematical formulation

Consider an OPF formulation, where also n_c contingency states c are taken into account. For the simplicity of the general mathematical formulation [89], the long-term post-contingency state equals the long-term pre-contingency state. An extension of the formulation needs to be made to differentiate between them in case grid events with long-term outages are studied.

$$\min_{x_0 \ldots x_c, u_0 \ldots u_c} f_0(x_0, u_0) \tag{4.1a}$$

$$\text{with } g_0(x_0, u_0) = 0 \tag{4.1b}$$

$$h_0(x_0, u_0) \leq L_l \tag{4.1c}$$

$$g_{k,s}(x_{k,s}, u_0) = 0 \tag{4.1d}$$

$$h_{k,s}(x_{k,s}, u_0) \leq L_s \tag{4.1e}$$

$$g_k(x_k, u_k) = 0 \tag{4.1f}$$

$$h_k(x_k, u_k) \leq L_m \tag{4.1g}$$

$$|u_k - u_0| \leq \overline{\Delta u_k} \tag{4.1h}$$

with $k = 1 \ldots n_c$ the different contingencies c. The pre-contingency grid state is denoted as $k = 0$. In this formulation, as opposed to the formulation in the previous chapter, a distinction is made between the state variables x_i and the non-automatic control variables u_i (including the status of the breakers). The latter vector u can be directly manipulated by the operator, starting in the medium time frame. The vector of dependent state variables x contains all other state variables to complete the OPF formulation. x_0, $x_{k,s}$ and x_k are the dependent state variables for respectively the pre-, k^{th} short-term and the k^{th} mid-term contingency state. u_0 and u_k are the non-automatic control variables for respectively the pre- and the k^{th} mid-term contingency state. There are no short-term non-automatic control variables, as the operator is not yet able to

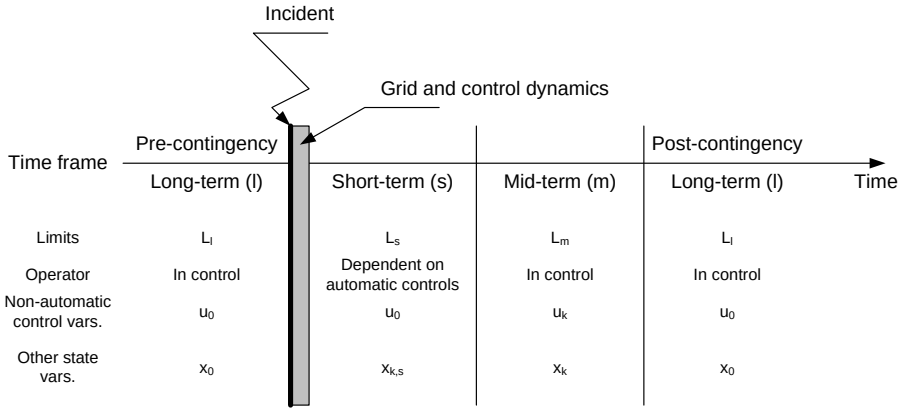

Figure 4.1: Time frames for the security constrained optimal power flow

react on the contingency.

In this system, three different time frames are introduced together with their specific limitations (figure 4.1):

- **Pre-contingency state** l, with its limits L_l (4.1b) and (4.1c). Without network changes, this situation can last indefinitely. The grid can be restored to is pre-contingency state (e.g. lightning stroke on an overhead line). For other events (e.g. transformer or underground cable failure) the operation changes for a larger period.
- **Short-term** s with limits L_s (4.1d) and (4.1e). This phase starts with the event and goes until the moment the operator is able to perform corrective actions. Only the automatic controls of the system are able to react in this time frame.
- **Mid-term** m and its limits L_m (4.1f) and (4.1g). In this time frame, the operator is able to manipulate the network. This is usually starting 20" to 1' after the grid event depending on the complexity of the incident and lasts up to all corrective actions are taken.

The (non-linear) equality constraints are again the power flow equations. Equation (4.1b) represents the pre-event configuration of the grid. The function vector $g_{k,s}$ (4.1d) gives the short-term network configuration immediately after the grid event, including (semi-) permanent outages of grid elements (permanent

line trip, internal cable fault, transformer failure, generator outage amongst others). It also takes the automatic control actions into account (for example fast load transfer schemes). The equation still uses the original pre-contingency control vector u_0, to force that the operator is still unable to intervene. Finally, (4.1f) gives the state of the grid after the intervention of the grid operator. His actions have a limited speed in real time, as changing positions of transformer tap changers and setpoints of generator takes a minimum time or rate of change. Also, the operator cannot manoeuvre outside the operation limits of grid elements. These topics are condensed in (4.1h). It expresses absolute boundaries as well as rate of change limitations. The objective function f_0 can be a function of the starting state vector of the grid, but can depend already on the outcome of one or more contingencies.

Care needs to be taken of the choice of the limits L_s, L_m and L_l. In general, for short-term actions, a higher loading of the network elements can be allowed. By nature, the spread on these limits depends on the thermal time constants of the individual group of equipment or system:

$$L_l \leq L_m \leq L_s \tag{4.1i}$$

For certain contingencies, as pointed out before, it can be desirable that no control action from the operator is required, the so-called *preventive* security constraints. Only automatic actions of the grid controls are sufficient to restore the grid to a healthy state. To convert the contingency k into a preventive security constraint, the medium term control vector u_k needs to be forced to equal the pre-contingency non-automatic control vector u_0. The previous system needs then to be extended by the following expression:

$$u_k = u_0, \forall k \in \{\text{set of preventive security constraints}\} \tag{4.1j}$$

4.5 Implemented approach

In order to integrate the security constraints into the algorithms developed, some simplifications have been made. Only the curative and preventive actions are investigated for the simplified network. No discrete control variables are chosen. The control variables in the following scenarios are the active power generator output and the voltage amplitude on the generator buses, emulating the automatic voltage control of the units. The free state variables are bus voltage angles and the reactive power output of the generators.

Outaging branches may lead to situations for which the grid is split into several subparts isolated from each other. The optimisation case becomes unsolvable if generators get isolated from the main grid or if a subgrid contains no slack bus. For the robustness of the implemented methodologies, a preliminary scan of the requested contingency states for these conditions is necessary. The bold drawn elements in figure 4.2, corresponding to the results of tables 4.2 and 4.4, are those elements in the IEEE 39 bus grid (without DC grid) that produce a grid configuration that cannot be solved by the optimisation algorithms. Outaging the generator step-up transformers isolates their generator from the grid and taking branch L27 or transformer T32 out of service, causes the creation of a subgrid without a slack bus (which is in this case node N32, associated to generator G02).

This leads to one of the main robustness issues of the security constrained OPF algorithms. When two subgrids (regardless their AC or DC nature) are connected by one single branch in the normal situation, outaging that unique branch causes their separation. Whereas in the pre-contingency system only one slack bus can be defined, that particular contingency requires a slack bus in each of the subgrids. When dealing with the preventive security constrained OPF, the algorithm needs to detect the isolated subgrids for each contingency and has to redefine a generator node as slack bus for those subgrids which have been separated from the subgrid containing the original slack bus. The automatic subgrid detection and slack bus conversion has not been developed in this work. The same discussion is applicable for a DC system with isolated subsystems in contingency states.

4.5.1 Control possibilities

Here again, the same discussion as in subsection 3.5.3 about the control constraints of the grid operator in different circumstances, is valid.

4.5.2 General approach

Before launching the preventive security constrained case, first the results of the corresponding curative case are considered. If the curative optimisation does not provide a valid solution, the preventive actions (imposing even more severe constrains on the state variable set, including the constraints of the curative case) would not do either.

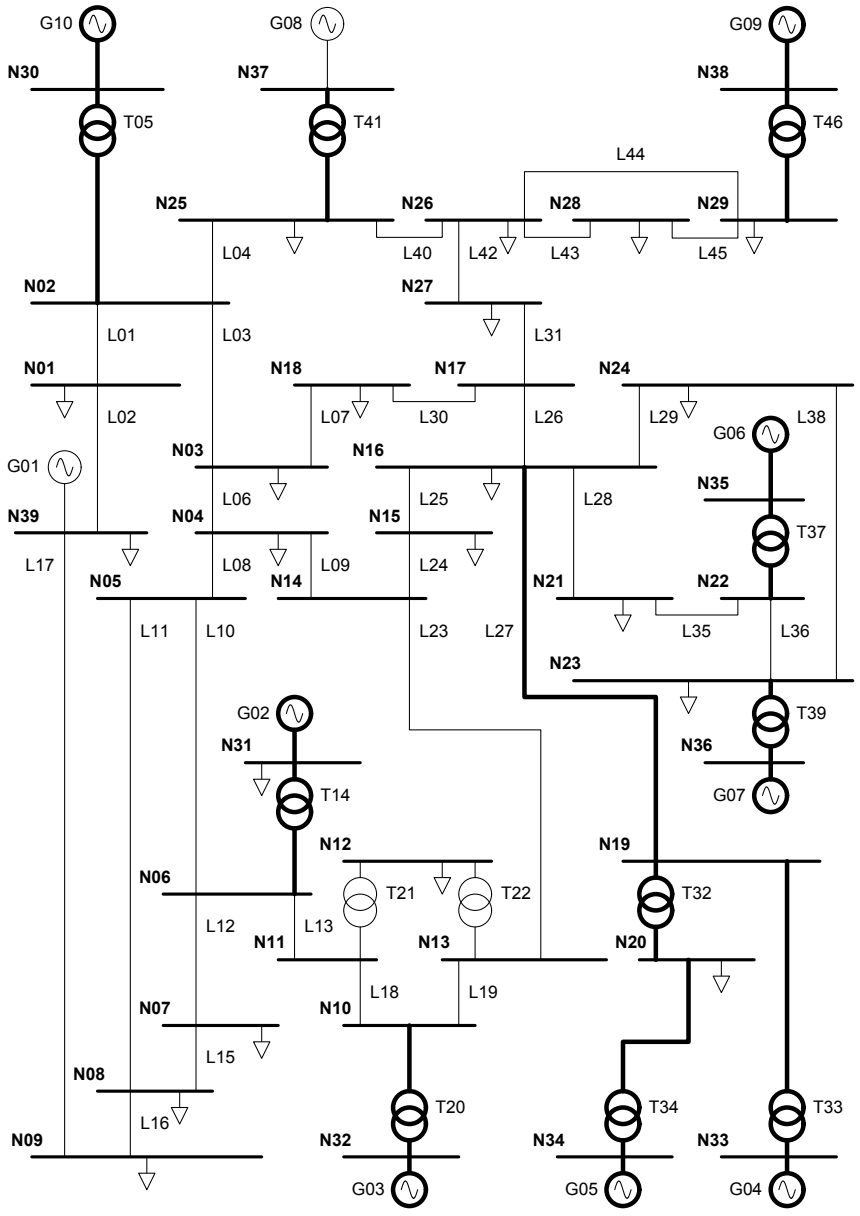

Figure 4.2: AC system of the IEEE 39-bus network with AC/DC converters. Bold drawn branches and generators cannot be safely outaged.

Furthermore, when the constraints of (4.1h) are neglected (assuming an almost unlimited time and flexibility for the operator to get the system back into a desired safe state), the curative case falls apart into k independent subproblems, which can be calculated one after the other.

For the preventive security constraints, indeed, all different cases need to be optimised together. This is a challenging task for the optimisation algorithm, as it is in general a non-convex problem. Although, by reasoning, a solution should be feasible, the algorithm could fail to converge when bouncing on inequality constraints. The choice of the starting point near enough to the expected solution is crucial.

The mathematical formulation of the preventive SCOPF here, using the conventions of the previous chapter, becomes

$$\min_{x_0} f_0(x_0) \tag{4.2a}$$

$$g_0(x_0) = 0 \tag{4.2b}$$

$$g_k(x_k) = 0 \tag{4.2c}$$

$$h_0(x_0) \leq 0 \tag{4.2d}$$

$$h_e(x_k) \leq 0 \tag{4.2e}$$

$$x_{min} \leq x \leq x_{max} \tag{4.2f}$$

$$x_k = x_0 \tag{4.2g}$$

with $k = 1 \dots c$ and c being the number of contingency cases.

For the inequality constraints, two different network limitation sets are defined: 4.2d) gives the normal state ratings (with the subscript 0), whereas (4.2e), gives the emergency state limitation set, denoted with the subscript e.

Referring to (3.51), some adaptations need to be made to translate the previous set of equations into the desired form. The vector of state variables becomes

$$x_n = \begin{bmatrix} x \\ z \end{bmatrix} = \begin{bmatrix} x_0 \\ x_1 \\ \vdots \\ x_c \end{bmatrix} \tag{4.3}$$

where the subscript 0 stands for the base case, all others $(1 \dots c)$ denote the individual c preventive security constrained optimisation cases.

The function vector $g(x_n)$ needs to be reformulated, following (3.53):

$$g(x_n) = \begin{bmatrix} g_0(x_0) \\ g_1(x_1) \\ \vdots \\ g_c(x_c) \end{bmatrix} \tag{4.4}$$

The function vectors $g_k(x_k)$ with $k = 1 \dots c$, describe the grid situation of the contingency k and differ from the base function vector $g_0(x)$ by having put the grid element of the corresponding contingency scenario out-of-service or non-existent. This slightly modifies the grid topology locally.

Computer programs, like MATPOWER, provide the user with all necessary equality and inequality constraint vectors g and h together with all their first and second derivatives for the AC network. They can be reused to construct the mathematical description of the contingency state as well. Consider $J_{g,k}$, the Jacobian of the vector function $g_k(x_k)$, the Jacobian of the whole system can be composed of the individual elements:

$$J_g(x_n) = \begin{bmatrix} J_{g,0}(x_0) & 0 & 0 & \dots & 0 \\ 0 & J_{g,1}(x_1) & 0 & \dots & 0 \\ 0 & 0 & \ddots & & \\ \vdots & \vdots & & \ddots & \vdots \\ 0 & 0 & 0 & \dots & J_{g,c}(x_c) \end{bmatrix} \tag{4.5}$$

As these are preventive contingency cases, the control variables (active generator power output and generator bus voltage amplitudes) need to be forced equal to their initial state. An additional set of equality constraints has to be implemented.

$$g_a(x_n) = \begin{bmatrix} U_{i,k} - U_{i,0} \\ P_{j,k} - P_{j,0} \end{bmatrix} = 0 \tag{4.6}$$

with $k = 1 \dots c$, $i \in \{\text{set of generator buses}\}$ and $j \in \{\text{set of generators without the slack bus generators and the DC reference converter}\}$

In (4.6), the active power equality equations for the generators connected to the AC slack bus and the equivalent AC generator of the reference converter must be omitted to find a feasible solution. If they are still present, the optimiser has to find a solution for which the grid losses of the base and contingency cases are the same. It fails in most cases because the different topologies generate different transmission losses. Omitting the slack bus and DC reference generators, still allows different system losses in both the AC and DC subsystems of each contingency case.

It is with this set of equations that the different contingency state sub-blocks are linked mathematically to the base case. The derivatives are incorporated in the Jacobian (4.5), they are off-diagonal elements outside of the shown sub-blocks.

The same procedure needs to be applied for the inequality constraints $h(x)$:

$$h(x_n) = \begin{bmatrix} h_0(x_0) \\ h_e(x_1) \\ \vdots \\ h_e(x_c) \end{bmatrix} \tag{4.7}$$

together with its proper Jacobian

$$J_h(x_n) = \begin{bmatrix} J_{h,0}(x_0) & 0 & 0 & \dots & 0 \\ 0 & J_{h,e}(x_1) & 0 & \dots & 0 \\ 0 & 0 & \ddots & & 0 \\ \vdots & \vdots & & \ddots & \vdots \\ 0 & 0 & 0 & \dots & J_{h,e}(x_c) \end{bmatrix} \tag{4.8}$$

with the same $J_{h,e}$ repeated c times, the number of preventive contingency cases. The calculation of the Hessian of the function vectors $g(x_n)$ and $h(x_n)$ is given by (3.60).

In the routine implementation, fixed overload factors can be specified for the transformer branches and the linear branches to be taken into account for the contingency cases. For the base case, the rating values remain unaltered (appendix E).

Table 4.1: Cost function differences (%) of the curative security constrained OPF outaging the generators of the 5 bus network without and with the DC system

Generator outage	w/o DC system	with DC system
1	0.051	0.029
2	-	-
max	0.051	0.029

4.5.3 Security constraints combined with DC networks

All methods described in this chapter are entirely applicable when a DC grid and AC/DC converters (chapter 5) are modelled. In (4.3), the vector x contains now the state variables of both AC and DC grid. Equations (4.4), (4.5), (4.7) and (4.8) assume that the DC grid equality and inequality constraints are incorporated.

For (4.6), linking the security cases to the pre-contingency state, different approaches apply. The fast automatic controls of the converters take immediate action after the grid incident and are able to find a new stable working state (e.g. using a droop control mechanism). In this case, it it not necessary to impose the same power and voltage constraints as in the initial state. Instead the converter control actions need to be modelled. In this work, the AC bus voltage and the converter active power are taken over from the initial state. Equation (4.3) is expanded in the same way with these converter parameters.

4.6 Simulation results for the security constrained optimal power flow

In this section, security constrained optimal power flow calculations are presented for the 5 bus and the IEEE 39 bus network. The results are presented without and with taking the associated DC system into account. Care should be taken when comparing the results: they cannot be treated as equivalent cases. The focus of the simulations lies on their robustness and correctness. The cost function for all the simulation in this section is the minimisation of the active

Table 4.2: Cost function differences (%) of the curative security constrained OPF outaging the generators of the IEEE 39 bus network without and with the DC system

Generator outage	w/o DC system	with DC system
1	0.24	0.24
2	-	0.52
3	-	0.50
4	-	0.23
5	-	0.17
6	-	0.30
7	-	0.14
8	0.12	0.11
9	-	0.28
10	-	-
max	0.24	0.52

power generation.

Tables 4.1 and 4.2 show the results of the 5 bus network and the IEEE 39 bus network when all respective generators are outaged one by one, the curative security contingency case for generators with and without DC grid. A dash (-) means that no convergence has been reached. For the 5 bus system, it is only feasible to take generator G01 out of service, generator G02 needs to be connected. For the 39 bus network, the DC system clearly improves the overall grid security for this case. Only for the outage of generator G10, no feasible working point has been found. The bottom line in the tables indicates the highest deviation of the cost function (chosen as minimum active generator output).

The next set of two tables, 4.3 and 4.4, gives for the respective systems, the curative and preventive security constrained cases with one network branch outaged. From these tables, it is clear which contingency cases are binding and which not. Again, the maximum value at the bottom helps to assess the worst case. In the IEEE 39 bus case, some branches have been deliberately omitted, following the discussion at the beginning of section 4.5. An observation of the results of table 4.4 is that the relative percentage differences are small and that in some cases, the curative security constrained OPF produces higher results

Table 4.3: Relative difference (%) of the curative and preventive security constrained OPF to the unconstrained cases of the 5 bus network

	w/o DC system		with DC system	
Outaged branch	curative	preventive	curative	preventive
1	0.001	0	0	0.007
2	0.360	0	0.168	0.007
3	0.519	0.097	0.221	0.005
4	0.583	0.101	0.289	0.005
5	3.097	0.093	0.519	0
6	0.057	0.011	0.064	0
7	0.031	0.102	0.006	0.005
max.	3.097	0.102	0.519	0.007

than the corresponding preventive SCOPF case. The opposite should always be the case, if the preventive SCOPF imposes more restrictions, demonstrating the influence of the stopping criteria of the optimisation algorithm: once reached, the iterative process is stopped. Lowering the stopping tolerances (section B.3.4) is a possible solution.

Finally, tables 4.5 and 4.6 state the optimisation routine results and elapsed calculation times for the base case and with 1, 2, 3 and 4 preventive contingency constraints (without and with the DC network). For the 5 bus network, the preventive security constraints are the outage of the branches L01, L03, L05 and L07. For the IEEE 39 bus system, they are the outage of branches L03, L06, L08 and L10. The calculation times are the average of ten consecutive runs of each scenario. For the 5 bus system, the calculation time is with each case slightly higher, the number of iteration steps being constant. The change of the objective function value is negligible. The negative values are explained by the fact that the optimisation algorithm immediately stops when its stopping criteria are reached (section B.3.4). It is possible that the algorithm stops at a slightly better cost function value, when the optimisation routine calculated a different state vector trajectory or when more constraints are added to the problem. In that case, the iterative algorithm needs more steps to find a solution complying to all constraints, giving the cost function also more steps to find even lower values than the less constrained problem. In practice, the cost function differences are so small that they can be treated as equal.

The same conclusions are valid for the IEEE 39 bus calculations.

4.7 Conclusions

In this chapter, the importance, the state-of-the-art calculations techniques and the involved time frames of the security constrained optimal power flow are discussed. In this research methodologies and algorithms for two distinct approaches have been developed. With the curative (or corrective) approach for a specific set of contingencies, the operator acts after the incident has occurred. The preventive security constrained OPF optimises the system already taking into account a parallel set of outages: the system remains secure after the occurrence of one of the contingencies in the set.

The discussed methodologies have been implemented and successfully tested on the sample networks. Specific attention is paid to the robustness of the algorithms when unsolvable grid topologies are present in the contingency set. The methodology is compatible with the inclusion of the meshed DC grids into the system model, described in chapter 5.

Table 4.4: Relative difference (%) of the curative and preventive security constrained OPF to the unconstrained cases of the IEEE 39 bus network

	w/o DC system		with DC system	
Outaged branch	curative	preventive	curative	preventive
1	0.050	0.021	0.038	0.135
2	0.013	0.004	0.005	0.079
3	0.181	0.001	0.165	0.055
4	0	0.001	0.009	0.051
6	0.012	0	0.011	0.051
7	0.018	0	0.023	0.052
8	0.036	0.006	0.028	0.058
9	0.023	0.003	0.019	0.104
10	0.063	0.002	0.067	0.057
11	0.025	0	0.026	0.060
12	0.059	0.001	0.065	0.059
13	0.055	0.008	0.050	0.106
15	0.011	0	0.012	0.054
16	0.011	0.003	0.013	0.055
17	0.004	0.004	0.001	0.058
18	0.045	0.014	0.041	0.075
19	0.059	0.019	0.054	0.086
21	0.001	0	0.001	0.052
22	0.001	0	0.001	0.051
23	0.080	0.042	0.072	0.107
24	0.027	0	0.026	0.050
25	0.044	0.002	0.028	0.059
26	0.012	0	0.004	0.061
28	0.047	0	0.046	0.081
29	0.014	0.001	0.007	0.049
30	0	0.002	0	0.054
31	0.010	0	0.011	0.050
35	0.196	0.076	0.164	0.311
36	0.009	0.001	0.009	0.058
38	0.049	0.001	0.045	0.079
40	0.034	0.029	0.030	0.058
42	0.035	0.026	0.034	0.053
43	0	0	0.002	0.052
44	0.005	0	0.004	0.052
45	0.058	0	0.058	0.052
max.	0.196	0.076	0.165	0.331

Table 4.5: Computation characteristics of the multiple preventive security constrained OPF of the 5 bus network without and with the DC system

	Item	base	1 SC	2 SC	3 SC	4 SC
w/o DC	Elapsed time (s)	0.46	0.77	1.10	1.45	1.83
	Iterations	11	10	10	10	10
	Cost fcn [MW]	167.6	167.6	167.6	167.6	167.6
	Cost diff (%)		0	0.001	0.005	0.004
with DC	Elapsed time (s)	0.53	0.78	1.12	1.65	4.06
	Iterations	12	10	10	11	23
	Cost fcn [MW]	170.3	170.4	170.4	170.3	170.3
	Cost diff (%)		0.007	0.015	-0.005	-0.005

Table 4.6: Computation characteristics of the multiple preventive security constrained OPF of the IEEE 39 bus network without and with the DC system

	Item	base	1 SC	2 SC	3 SC	4 SC
w/o DC	Elapsed time (s)	0.52	1.26	1.77	2.41	3.35
	Iterations	12	15	15	14	16
	Cost fcn [MW]	6284.2	6284.4	6284.4	6284.9	6284.6
	Cost diff (%)		0.003	0.004	0.010	0.006
with DC	Elapsed time (s)	0.57	1.32	2.10	3.14	3.94
	Iterations	11	14	15	17	17
	Cost fcn [MW]	6295.0	6298.6	6298.2	6298.2	6298.7
	Cost diff (%)		0.056	0.050	0.051	0.058

Chapter 5

Optimal Power Flow with meshed DC networks

5.1 Goal

The general approach and the detailed development are given for the modelling of the meshed DC grid parallel to the AC grid through the AC/DC converter interface points. In the first section 5.2 the general approach, basic assumptions and state-of-the-art are given. The development of the Voltage Source Converter model is found in section 5.3. For the DC grid branches and topology, two different methods have been implemented. The first one, section 5.4, uses the analogy of the admittance matrix of the AC grids. With the alternative mode, section 5.5, a different set of state variables and constraint functions are defined. The implementation of the power flow limitations of the converters and the DC branches, together with the DC bus voltage limits, is stated in 5.6. The chapter concludes with simulation results, section 5.7, and a benchmarking of both grid modelling methods. The results of the 5+3 AC/DC hybrid system have also been successfully compared with an independently developed tool [90].

5.2 General approach and state-of-the-art

The general approach to model the DC system and the AC/DC converters, whether it is a mere point-to-point link [32, 91], a radial grid or a complex meshed grid with a multitude of AC/DC converters, remains the same. The

implementation flexibility comes from the systematic approach of how the different components (converters and other grid elements) are linked to get the right DC grid structure.

Both the main and the alternative approach separate the equality constraints into two parts. The first common part states the power loss model of the converters followed by the equations for the DC system.

In the following, the coupling between the AC and DC systems is exclusively made by Voltage Sourced Converter (VSC) HVDC technology (section 2.4) as it is the technology enabling to construct generic DC networks.

The number of VSC converters in the complete network is n_v, the number of DC branches n_c and the number of DC nodes n_N. A DC node in this context is defined as the location in the electrical DC network where two or more DC elements (converters and/or branches) are connected. A point-to-point link contains $n_N = 2$ DC nodes. Furthermore, it is assumed that all VSC converters in the same DC bus, are emulated as one. Separate auxiliary DC buses need to be defined if this manipulation cannot be done (e.g. the converters are not connected to the same AC bus).

The DC system uses the same power base as the AC grid. The reference voltage, expressed in *pu*, may differ. The model assumes that the rated voltage of the DC system is well-chosen so that all converters can operate in the given DC voltage ranges.

The optimal power flow for hybrid AC/DC meshed grids is situated within a wider range of system analysis tools for multi-terminal HVDC grids operated in parallel with AC systems. Other exponents of these tools are the power flow and dynamic calculations ([92, 93]), modelling the same AC and DC systems and work towards different calculation goals. Both the power flow and OPF methodologies obtain a steady-state solution: the first finds solutions for which specific output of generators is given; the latter searches the global optimum of an objective function within the feasibility region by varying power setpoints.

In [94, 32], the authors propose a unified optimal power flow algorithm as presented in this manuscript, however only point-to-point HVDC systems have been developed and more emphasis is placed on the choice of control system parameters and market consequences. The method described in [95] follows the same outline as this research; it is able to do an optimisation of the hybrid

AC/DC meshed network in a unified way. The authors of [19] propose the optimisation of control scheme parameters, in this case the droop control voltage-power on the DC side of the VSC converters. Their application to minimise the losses of the intermediate DC grid connecting several large wind power plants to the main AC grid on several interface substations.

The optimisation problem can be extended to the time domain, where a high number of controller gains and other parameters needs to be chosen [96].

The unified method, as developed here, has also been applied to the Power Flow calculations [97].

Sequential solving of the decoupled AC and DC subsystems [58] is another method to combine both systems into a single algorithm. These subsystems are optimised separately and the solution of one is used as starting point for the other. The common state variables of the AC and DC system are matched iteratively. This sequential method is also extensively used for the classic power flow of the hybrid meshed AC/DC systems [98, 99, 100].

Not only HVDC but also FACTS applications have been incorporated into optimal power flow calculations [101].

5.3 Modelling VSC HVDC converters

The n_c converters are mathematically described as a set of non-linear equality constraints. For each converter, the equation of the power balance between the AC and DC is used, differing by a loss term P_{loss} i.e. the converter losses. On the AC side, the HVDC installation is emulated as a normal AC generator. On the DC side, an equivalent controlled DC source is chosen.

The notation and direction convention of active and reactive powers and the voltages are shown in figure 5.1. Positive values of power on the AC side are injections into that grid (same convention as for the other generators), positive values on the DC side are always directed towards the converter.

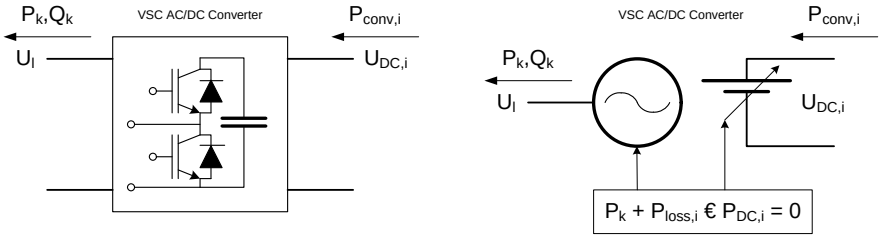

Figure 5.1: Converter model equivalents. Left: AC/DC VSC converter, Right: OPF equivalent

The loss equation for converter with index i, connected on the AC side to bus l modelled by the AC generator with index k, is

$$P_k + P_{loss,i} - P_{DC,i} = 0 \tag{5.1}$$

Regardless the operation mode, the converter losses are always positive, implying that more active power enters from one side than leaves to the other. In inverter mode, P_k and $P_{DC,i}$ are positive and $P_k < P_{DC,i}$. In rectifier mode, they are negative and again the expression $P_k < P_{DC,i}$ holds. From (5.1), the loss term $P_{loss,i}$ is always positive:

$$P_{loss,i} = P_{DC,i} - P_k > 0 \tag{5.2}$$

The general formulation of the converter i is (5.3) [32].

$$g_i(x) = P_k + P_{loss,i}(U_{m,l}, P_k, Q_k) - P_{DC,i} = 0 \tag{5.3}$$

with $i = 1 \dots n_v$.

Depending on the nature of the $P_{loss,i}$, (5.3) is either linear or non-linear. In the general case and thus for the remainder of the manuscript, a non-linear function is used, rendering the whole power balance equation for the converters non-linear. Any model of the loss term can be used for the developed methodologies, as long as their first and second derivatives to all the parameters are defined.

Table 5.1: Per unit converter loss coefficients

	a ($\times 10^3$)	b ($\times 10^3$)	c ($\times 10^3$)	r ($\times 10^3$)
rectifier	11.033	3.464	4.400	1.0
inverter	11.033	3.464	6.667	1.0

The fact that the AC side of the converter is a normal generator for the AC network, independent control of active and reactive power is possible. As a consequence, the AC node (index l) where the converter is connected, should automatically be converted to a PV node for the power flow calculations. This, however, is not relevant for the optimal power flow (section 3.2). All simulations in this work use the same loss function

$$P_{loss,i} = a_i + b_i I_k + (c_i + r_i) I_k^2 \tag{5.4}$$

with

$$I_k = \frac{\sqrt{P_k^2 + Q_k^2}}{U_{m,l}} \tag{5.5}$$

the current of the generator on the AC side of the corresponding converter.

The factors a_i, b_i and c_i stand for the individual loss factors of converter i. The content of the individual factors is:

- no-load loss factor a_i: no-load losses of transformers, averaged auxiliary equipment losses (i.e. lightning, heating, cooling, control systems);
- linear current factor b_i: switching losses of the valves, more in particular the turn-off losses of the IGBTs and free-wheeling diodes;
- square current factor c_i: conduction losses of the valves. If significant differences exist between them for the rectifier and inverter mode, they should be parameterised separately;
- square current factor r_i: load losses of transformers, series reactances and other AC equipment.

Typical values (Table 5.1) for a 600 MW ±300 kV VSC converter installation, have been used in this research [32, 100]. The content of the different terms of (5.4) are discussed in [32].

Combining (5.3), (5.4) and (5.5) gives the complete expression (5.6) of one HVDC converter:

$$g_{conv,i}(x) = P_{k,i} - P_{conv,i} + a_i + b_i \frac{\sqrt{P_k^2 + Q_k^2}}{U_{m,l}} + (c_i + r_i) \frac{P_k^2 + Q_k^2}{U_{m,l}^2} = 0 \quad (5.6)$$

Obviously, in order to avoid impossible solutions, the AC voltage amplitude must be strictly higher than zero. In a realistic OPF case, minimum positive voltage limits are specified, solving this issue in a natural way. Note that (5.6) does not depend on the DC bus voltage. This fact is important for the development in section 5.5, when writing the DC network topology into equality constraints.

Section 3.4 describes the methodology to extend the optimisation case with additional state variables and constraint equations. For the n_v converters, the same number of extra variables, $\mathbf{P}_{conv} = [P_{conv,i}]$ are added and n_v constraint functions (5.6) are appended to the function vector $g(x)$. Appendix D gives the first and second derivatives of these equality constraints in order to construct the Jacobian and the Hessian matrices.

$$\mathbf{J}_{conv,i}(\mathbf{x}) = \left[\frac{\partial g_i}{\partial x_j}\right] \quad (5.7a)$$

$$\mathbf{H}_{conv,i}(\mathbf{x}) = \left[\frac{\partial^2 g_i}{\partial x_j \partial x_k}\right] \quad (5.7b)$$

The standard initial point when not starting from a previous calculation, is constructed by taking the average of the respective upper and lower bounds of the state variables. For symmetric bidirectional grid devices (e.g. VSC converters), the initial power setpoints $P_{k,0} = Q_{k,0} = 0$. For this particular situation, some of the first and second derivatives in the Jacobian and Hessian are undefined (appendix D). The implemented solution is altering the initial converter setpoints to other values within their bounds. As all converters present no-load losses, it is practically excluded that the optimal setpoint for a converter $P_k = Q_k = 0$.

Equation (5.6) does is not depend on DC side voltage. As mentioned in section 5.2, correct operation of the VSC converters are assumed for any value of the DC bus voltage lying between the defined limits (section 5.6).

5.4 Modelling DC branches and grid topology

The same approach as for the AC network branches and structure (Appendix C), using the admittance matrix, is applied. The equations turn out to be much simpler than in the AC case as only the DC bus voltage magnitudes need to be taken into account and phase angles are irrelevant. Shunt elements are omitted as well (i.e. there is no steady-state reactive charging of the system branches nor iron losses in transformers).

A number of new state variables $\mathbf{U}_{DC}$, equal to the number of DC buses (n_N) in the system, is defined.

The admittance of the branch between the arbitrary nodes i and j is

$$y_{ij} = \begin{cases} 0 \text{ , when no branch exists between nodes } i \text{ and } j \\ 0 \text{ , when } i = j \\ \sum_k \frac{1}{r_{ij,k}} \end{cases} \tag{5.8}$$

Here, $r_{ij,k}$ is the series resistance of the k-th branch ($k \geq 1$) between nodes i and j. The resistance is expressed in pu, using the voltage base of the DC network and the same power reference as in the AC network. For convenience, the individual admittances are already summed at the setup of the OPF DC case, should there be more than one branch in parallel between these nodes. Also for the DC case $y_{ij} = y_{ji}$.

For the (equivalent) branch between nodes i and j ($i \neq j$), with admittance y_{ij} from (5.8), the relation between currents (positive direction is inward towards the branch) and voltages becomes

$$I_{DC,i} = y_{ij} \left(U_{DC,i} - U_{DC,j} \right) \tag{5.9a}$$

$$I_{DC,j} = y_{ij} \left(-U_{DC,i} + U_{DC,j} \right) \tag{5.9b}$$

or in matrix notation

$$\begin{bmatrix} I_{DC,i} \\ I_{DC,j} \end{bmatrix} = \begin{bmatrix} y_{ij} & -y_{ij} \\ -y_{ij} & y_{ij} \end{bmatrix} \cdot \begin{bmatrix} U_{DC,i} \\ U_{DC,j} \end{bmatrix} \tag{5.9c}$$

Using (5.9c), similarly to the summing method for the AC grid, the matrix of the current going out of the node i into the connected DC branches on that node is

$$[I_{br,i}] = [Y_{br,ij}] \cdot [U_{DC,j}] \tag{5.10}$$

with

$$\begin{cases} Y_{br,ii} & = \sum_{j=1}^{n_N} y_{ij} \\ Y_{br,ij} & = -y_{ij} \ , \ i \neq j \end{cases} \tag{5.11}$$

The active power flowing out of the node i towards the connected DC branches is

$$\begin{aligned} P_{br,i} &= U_{DC,i} I_{br,i} \\ &= U_{DC,i} \sum_j Y_{br,ij} U_{DC,j} \\ &= U_{DC,i}^2 Y_{br,ii} + U_{DC,i} \sum_{j \neq i} Y_{br,ij} U_{DC,j} \end{aligned} \tag{5.12}$$

The power balance for the DC bus i is

$$\begin{aligned} g_{br,i}(\mathbf{x}) &= P_{br,i} + \sum_k P_{conv,k} \\ &= U_{DC,i}^2 Y_{br,ii} + U_{DC,i} \sum_{j \neq i} Y_{br,ij} U_{DC,j} + \sum_k P_{conv,k} \end{aligned} \tag{5.13}$$

with $j = 1 \dots n_N$ and $k \in \{\text{set of converters connected to bus } i\}$. The previous set (5.13) defines n_N non-linear equality constraints describing the DC branches and topology. Together with the n_v equations of the converters themselves, the DC grid is connected to the AC grid and all are optimised together.

To calculate the Jacobian, all different non-zero derivatives need to be calculated to the state variables. Consider again the arbitrary bus i. The derivative of the DC power of the converter k connected to that node is

$$\frac{\partial g_{br,i}(\mathbf{x})}{\partial P_{conv,k}} = 1 \tag{5.14}$$

again with $k \in \{\text{set of converters connected to bus } i\}$. The derivatives of these constraint functions g_i to the bus voltages differ in nature: for the DC voltage on the same bus i the derivatives (5.15a) are obtained

$$\frac{\partial g_{br,i}(\mathbf{x})}{\partial U_{DC,i}} = 2Y_{br,ii}U_{DC,i} + \sum_{j \neq i} Y_{br,ij}U_{DC,j} \tag{5.15a}$$

and (5.15b) for all other voltages

$$\frac{\partial g_{br,i}(\mathbf{x})}{\partial U_{DC,j}} = Y_{br,ij}U_{DC,i} \text{ with } j \neq i \tag{5.15b}$$

The non-zero elements of the Hessian are easily calculated by

$$\frac{\partial^2 g_{br,i}(\mathbf{x})}{\partial U_{DC,i}^2} = 2Y_{br,ii} \tag{5.16a}$$

$$\frac{\partial g_{br,i}(\mathbf{x})}{\partial U_{DC,i}\partial U_{DC,j}} = Y_{br,ij} \text{ with } j \neq i \tag{5.16b}$$

Using this method to implement the DC system in the optimisation case, n_v+n_N new state variables are defined, using notation convention (3.51):

$$\mathbf{z} = \begin{bmatrix} \mathbf{P}_{conv} \\ \mathbf{U}_{DC} \end{bmatrix} \tag{5.17}$$

with

- $\mathbf{P}_{conv} = [P_{conv,i}]$ with $i = 1 \dots n_v$, the DC power going into converter i
- $\mathbf{U}_{DC} = [U_{DC,j}]$ with $j = 1 \dots n_N$, the DC voltage of the node j

The additional set of n_v+n_N equality constraints, using the notation convention (3.53), for this method is

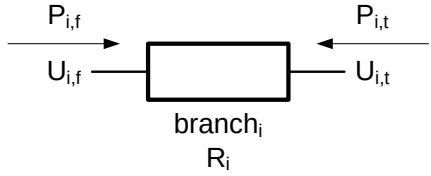

Figure 5.2: Conventions for an arbitrary DC branch i

$$\mathbf{g}_n(x,z) = \begin{bmatrix} \mathbf{g}_{conv,i} \\ \mathbf{g}_{br,i}(z) \end{bmatrix} \tag{5.18}$$

with the n_v constraints $\mathbf{g}_{conv,i}$ (5.6) for the converters and n_N constraints $\mathbf{g}_{br,i}$ (5.13) for the DC system topology.

5.5 Alternative approach to the DC grid

To benchmark the simulation results of the previous method for the DC system topology, an alternative method is developed [102]. The formulation is less compact and uses a multitude of state variables. Due to the higher number of state variables and constraint equations, it is less memory efficient for complex DC systems.

Unlike the previous method, where the grid topology is expressed in one single admittance matrix (5.11), the alternative method divides its process in two distinct steps. The first step gives the equations for the individual branches and the second links them together to construct the desired topology. The branch equations are non-linear while the topology equations are linear.

5.5.1 Branch equations

Disregarding the DC grid topology, the first step takes each individual branch and constructs two non-linear constraint equations. They are written in the format $g_n(z) = 0$ (3.53). The first expression imposes the current balance of both ends of the branch and the second one gives the power loss due to the resistivity of that branch. Power and current are positive when directed into

the branch (figure 5.2).

The current balance for the arbitrary branch i (with resistance R_i, expressed in pu) between its $from-$ and $to-$bus sides, is

$$I_{i,f} = I_{i,t} \tag{5.19}$$

Rewriting in terms of power and voltages, as required by the choice of state variables, gives

$$\frac{P_{i,f}}{U_{i,f}} = \frac{P_{i,t}}{U_{i,t}} \tag{5.20}$$

To avoid possible singularities with the division or with the first and second derivatives of the corresponding equality constraint functions, the previous equation is multiplied by the term $U_{i,f} \cdot U_{i,t}$. The first of the two branch constraint equations is obtained:

$$g_{br,2i-1}(x) = P_{i,f}U_{i,t} - P_{i,t}U_{i,f} = 0 \tag{5.21}$$

The second equation of the DC branch describes the losses in the resistance R_i (expressed in pu) of that link. Starting from the voltage drop equation

$$U_{i,f} - R_i I_{i,f} - U_{i,t} = 0 \tag{5.22}$$

and expressing it with the same choice of variables as in (5.21) and again avoiding the division, finally gives the second branch constraint

$$U_{i,f} - R_i \frac{P_{i,f}}{U_{i,f}} - U_{i,t} = 0$$

$$\Rightarrow g_{br,2i}(x) = U_{i,f}^2 - R_i P_{i,f} - U_{i,f}U_{i,t} = 0 \tag{5.23}$$

The non-linear function vector for each DC branch to be added to the set of equality constraints (3.53) is

$$\mathbf{g}_{br}(\mathbf{z}) = \begin{bmatrix} g_{br,2i-1}(x) \\ g_{br,2i}(x) \end{bmatrix} = \begin{bmatrix} P_{i,f}U_{i,t} - P_{i,t}U_{i,f} \\ U_{i,f}^2 - R_i P_{i,f} - U_{i,f}U_{i,t} \end{bmatrix} = 0 \tag{5.24}$$

with $i = 1 \dots n_c$, the number of DC branches in the network.

Setting up new equations, requires also the definition of new state variables for the DC system. Whereas the main method only requires one state variable per DC node (5.17), the alternative takes four additional state variables per DC

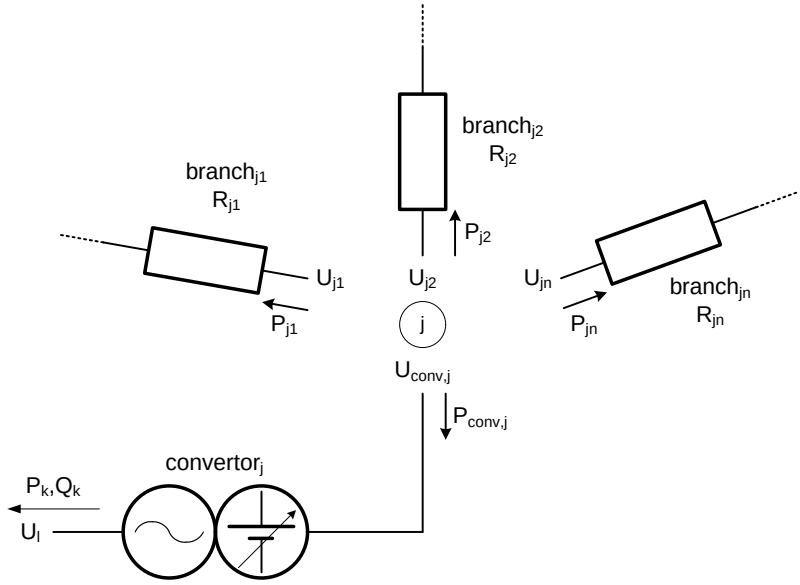

Figure 5.3: Sample DC grid, drawn for node j with voltage and active power nomenclature

branch:

$$z = \begin{bmatrix} P_{conv} \\ P_{br,f} \\ P_{br,t} \\ U_{br,f} \\ U_{br,t} \end{bmatrix} \tag{5.25}$$

In (5.25), the subvectors are for n_v converters and n_c DC branches (figure 5.3):

- $P_{conv} = [P_{conv,i}]$, vector of DC power going into converters $i = 1 \dots n_v$
- $P_{br,f} = [P_{i,f}]$, vector of DC power going into the $from-$bus side of DC branches $i = 1 \dots n_c$
- $P_{br,t} = [P_{i,t}]$, vector of DC power going into the $to-$bus side of DC branches $i = 1 \dots n_c$
- $U_{br,f} = [U_{i,f}]$, vector of DC bus voltage of the $from-$bus side of DC branches $i = 1 \dots n_c$

- $U_{br,t} = [U_{i,t}]$, vector of DC bus voltage of $to-$bus side of DC branches $i = 1 \dots n_c$

The length of the vector z is $n_v + 4n_c$.

The first and second derivatives of (5.24) enable to construct the Jacobian (3.58) and the Hessian (3.59).

5.5.2 DC system topology

So far in this alternative method, the equations for the converters (section 5.3) and individual branches (subsection 5.5.1) were set up, without explicitly defining how they are linked. For each of the n_N DC nodes, the power balance and voltage equality is represented by a set of linear constraints. Figure 5.3 shows the power direction and notation conventions.

It is assumed that each converter is linked to a DC bus and that the branches are connected to two different DC buses. However, it is possible to specify more than one DC branch between the same two end buses. Any grid configuration can be made, including system meshes.

The nature of the DC buses is divided in two categories: nodes exchanging power with a converter station and the others connecting only to branches. This distinction plays only a role when setting up the topology equations.

First, the power balance per DC node is written by setting the sum of the power of the connected converter and branches to zero, giving n_N additional linear equality constraints:

$$g_{topo,j}(z) = \sum_i P_i = 0 \tag{5.26}$$

with $i \in$ {set of converters, $from-$ and $to-$bus power of branches connected to DC bus j}.

Secondly, the voltage of the corresponding branch ends need to be matched per node. In section 5.3, it is noted that the DC side voltage of the VSC converters is not playing a role in their loss equation. The equations are a set of subtractions:

$$g_{topo,jk}(z) = U_{j,k} - U_{j,1} = 0 \tag{5.27}$$

with $k \in C_j =$ {set of $from-$ and $to-$bus sides of the DC branches connected to bus j} and $k \neq$ the first member of C_j.

The number of equations generated by (5.27) for bus j is one less than the number of DC branches connected to that bus. Only the voltage at bus j of the first branch in the set C_j is taken as a reference for the rest of the branches connected to bus j for numbering purposes.

With tools making a clear distinction between linear and non-linear constraints, like MatPower, the linear equations obtained in this subsection need only to be specified once per optimisation and not for each iteration step as is the case for non-linear constraint functions.

5.6 Inequality constraints for the DC network

Converter and DC branch loading limitations are treated in this section. The same reasoning as for the AC networks (section 3.6) is followed. The development in this section is only valid for the main DC topology method (section 5.4). For the alternative method, a more direct approach is applied.

5.6.1 Main topology method

The limitations for the active and reactive power exchange of the AC/DC converters with the AC network are specified by directly imposing the limits on the respective generator state variables (3.62). The limits of the DC power exchange and the DC bus voltages are set directly to the lower and upper limits of the corresponding state variables (5.17).

The branch loading limits need to be explicitly written, and are appended to the matrix of non-linear inequality constraints (3.54).

For each DC branch, a set of two inequality constraints is defined, one for the maximum loading of the "from-" (subscript f) and the other for the "to-" (subscript t) bus side of that branch. For DC branch i, they are

$$h_{i,f}(\mathbf{z}) = P_{i,f}^2 - P_{i,max}^2 \tag{5.28a}$$

$$h_{i,t}(\mathbf{z}) = P_{i,t}^2 - P_{i,max}^2 \tag{5.28b}$$

These equations cannot be integrated directly into the optimisation case as they need to be written as functions of the defined state variables $\mathbf{z}$ (5.17). All expressions for the to-bus are the same, with the indices f and t interchanged. Only the state variables of the DC bus voltages are used:

$$\begin{aligned} h_{i,f}(\mathbf{x}) &= P_{i,f}^2 - P_{i,max}^2 \\ &= (U_{i,f} \cdot I_{i,f})^2 - P_{i,max}^2 \\ &= \left(U_{i,f}\left(\frac{U_{i,f} - U_{i,t}}{R_i}\right)\right)^2 - P_{i,max}^2 \\ &= \frac{1}{R_i^2}\left(U_{i,f}^4 - 2 \cdot U_{i,f}^3 \cdot U_{i,t} + U_{i,f}^2 \cdot U_{i,t}^2\right) - P_{i,max}^2 \end{aligned} \tag{5.29}$$

In these expressions the voltages $U_{i,f}$ and $U_{i,t}$ are the corresponding DC bus voltages of the *from-* and the *to-* bus of the DC branch i.

The non-zero equations of the first and second derivatives for the from-bus are

$$\frac{\partial h_{i,f}(\mathbf{x})}{\partial U_{i,f}} = \frac{1}{R_i^2}\left(4 \cdot U_{i,f}^3 - 6 \cdot U_{i,f}^2 \cdot U_{i,t} + 2 \cdot U_{i,f} \cdot U_{i,t}^2\right) \tag{5.30}$$

$$\frac{\partial h_{i,f}(\mathbf{x})}{\partial U_{i,t}} = \frac{1}{R_i^2}\left(2 \cdot U_{i,f}^2 \cdot U_{i,t} - 2 \cdot U_{i,f}^3\right)$$

$$\frac{\partial^2 h_{i,f}(\mathbf{x})}{\partial U_{i,f}^2} = \frac{1}{R_i^2}\left(12 \cdot U_{i,f}^2 - 12 \cdot U_{i,f} \cdot U_{i,t} + 2 \cdot U_{i,t}^2\right) \tag{5.31}$$

$$\frac{\partial^2 h_{i,f}(\mathbf{x})}{\partial U_{i,t}^2} = \frac{2}{R_i^2} \cdot U_{i,f}^2$$

$$\frac{\partial^2 h_{i,f}(\mathbf{x})}{\partial U_{i,f} \partial U_{i,t}} = \frac{1}{R_i^2}\left(4 \cdot U_{i,f} \cdot U_{i,t} - 6 \cdot U_{i,f}^2\right)$$

5.6.2 Alternative topology method

As the branch power of the *from-* and the *to-* bus of the DC branches are state variables themselves (5.25), their limits are set directly using

$$-\mathbf{P}_{max} \leq \mathbf{P}_{br,f} \leq \mathbf{P}_{max} \tag{5.32a}$$

$$-\mathbf{P}_{max} \leq \mathbf{P}_{br,t} \leq \mathbf{P}_{max} \tag{5.32b}$$

The branch end voltages in (5.25) get the limits of the corresponding DC node.

5.7 Simulation results

Several scenarios have been simulated in order to test the features of the developed algorithms and methodologies. For each of the simulations, the chosen cost function is minimum system losses.

The following convention has been used in the table headers to denote the calculation variants:

- AC: reference case, the AC network without the associated DC system;
- AC+DC: simulation of the AC together with the DC system, using the main method (section 5.4);
- AC+DC (alt): simulation of the AC together with the DC system, using the alternative method (section 5.5);
- AC+DC (lim): simulation of the AC together with the DC system with limitations on converter and DC branch flows, using the main method.

To express voltage differences (tables 5.4, 5.7 and 5.10), the symbol "%pu" stands for $\frac{1}{100}pu$.

5.7.1 5 nodes network

This section starts with the results of the OPF calculation of the 5 bus grid without DC system as a reference case (figure 5.4). Next, figures 5.5 and 5.6 show the optimal power flow results for the same grid, but this time with the DC grid. The ratings of the converters and the DC branches have been chosen

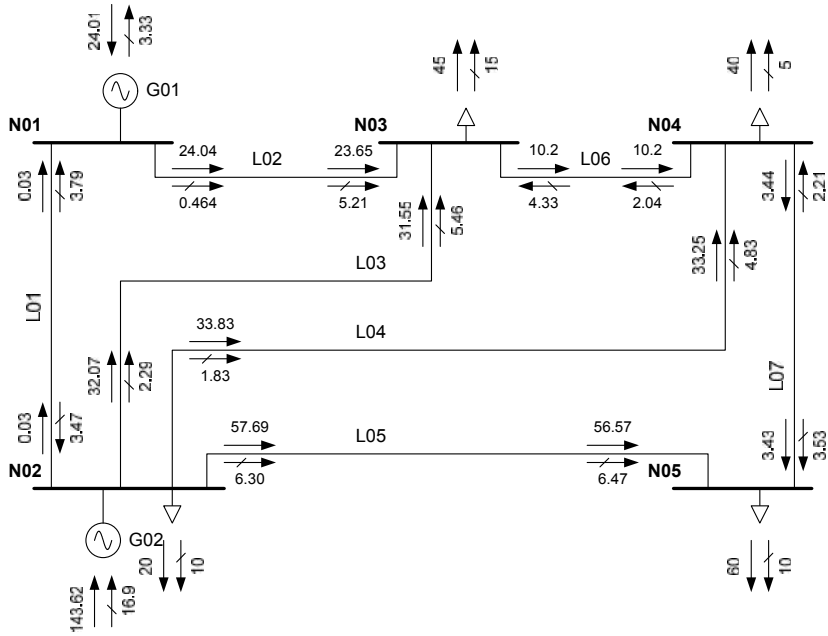

Figure 5.4: Optimal power flow of the AC system of the 5-bus network without AC/DC converters. **Legend**: $\rightarrow$ Active power [MW] and $\nrightarrow$ Reactive power [MVar]

Table 5.2: Calculation comparison of 5 bus network based on 10 consecutive runs

	AC	AC+DC	AC+DC (alt)	AC+DC (lim)
Elapsed time $[s]$	0.49	0.54	0.67	0.57
Nbr iterations	11	12	16	13
Cost $[MW]$	167.63	170.34	170.34	170.53

sufficiently high in order not to constrain the flows in the DC system. Figures 5.7 and 5.8 show the results for the same AC+DC network with converters ratings limited to 20 MW and 20 MVar and the flow through the DC branches is limited to 10 MW. In each of the three calculation cases, convergence is reached and the solutions correctly take the predefined limitations into account.

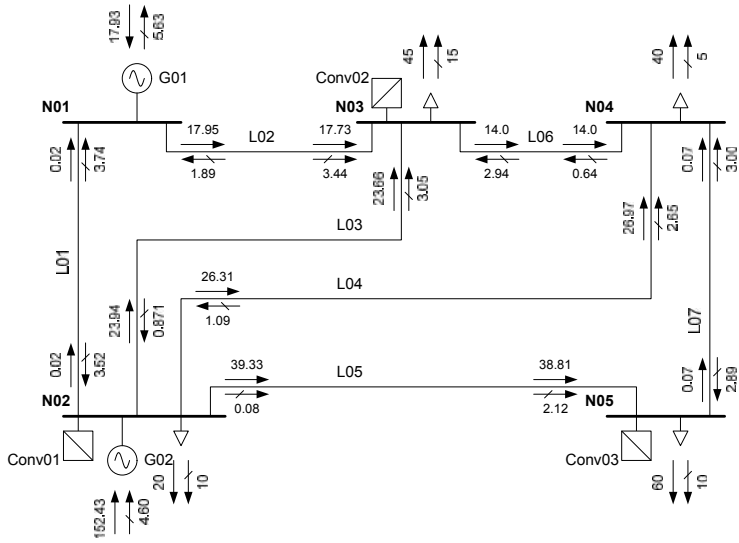

Figure 5.5: Power flow in the AC system of the optimised 5-bus network. **Legend**: → Active power [MW] and ↛ Reactive power [MVar]

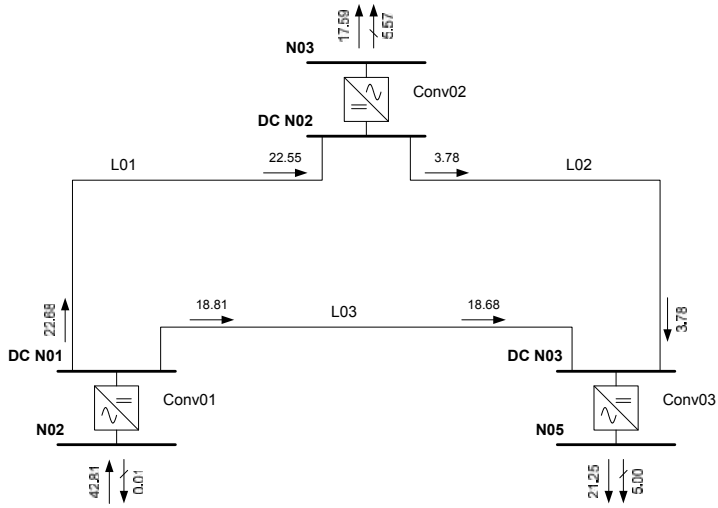

Figure 5.6: Power flow in the DC system of the optimised 5-bus network with DC branch and converter limits. **Legend**: → Active power [MW] and ↛ Reactive power [MVar]

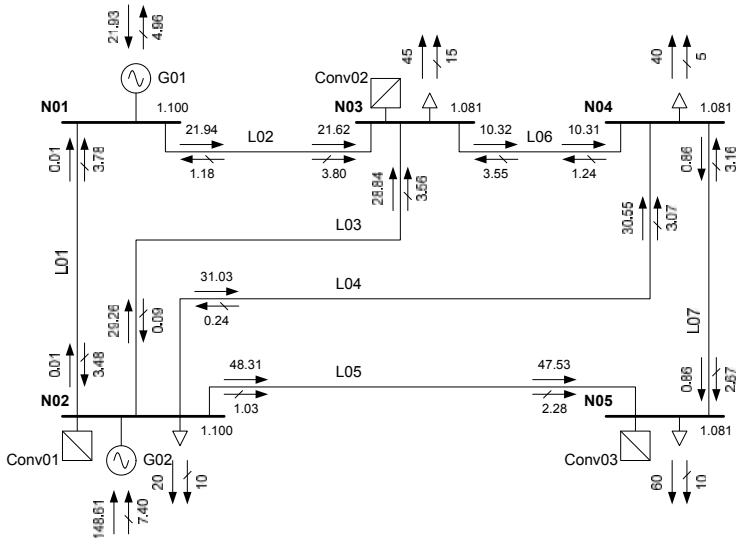

Figure 5.7: Power flow in the AC system of the optimised 5-bus network with DC branch and converter limits. **Legend**: → Active power [MW] and ⇝ Reactive power [MVar]

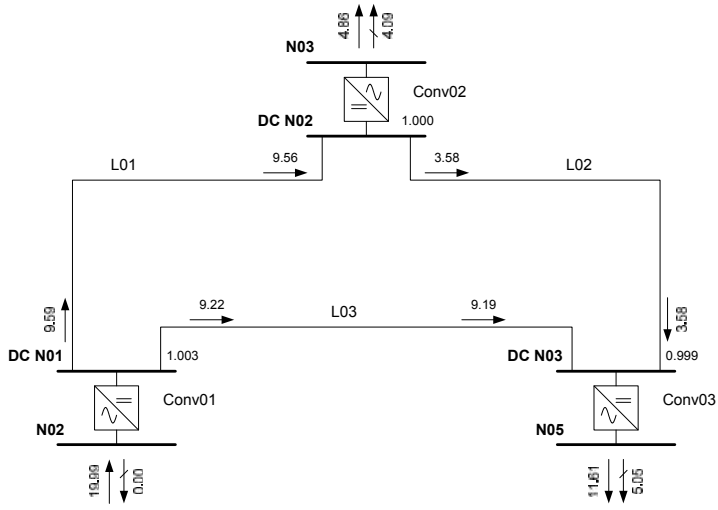

Figure 5.8: Power flow in the DC system of the optimised 5-bus network with DC branch and converter limits. **Legend**: → Active power [MW] and ⇝ Reactive power [MVar]

Table 5.3: Cost function differences of 5 bus network

Cost Diff $[MW]$	AC	AC+DC	AC+DC (alt)	AC+DC (lim)
AC	0	2.71	2.71	2.91
AC+DC		0	0.00057	0.19
AC+DC (alt)			0	0.19
AC+DC (lim)				0

Table 5.4: Maximum convergence differences between base and alternative AC+DC optimisation method for 5 bus network

System	Maximum difference	Unit	Value
AC system	P_g	MW	0.0709
	Q_g	MVar	0.0712
	V_m	%pu	0.0064
	V_a	°	0.0011
Converters	P_{vsc}	MW	0.0044
DC Branches	P_{br}	MW	0.0025
	V_{dc}	%pu	0.0142

Finally, for the calculation results of this sample network, a set of three tables is presented. Table 5.2 states for ten consecutive runs the average elapsed time, number of iterations and cost function results. They remain in close proximity. Table 5.3 gives the cost function result differences of the base AC case, the main hybrid OPF method, the alternative hybrid OPF method and the calculation with the component limitations as described above. The difference without and with the DC grid is explained by the no-load offset of the converters. They are considerable for small networks without high power flows through the branches. The difference between the main and alternative hybrid method is negligible. The limitations on the DC components drives the cost function even higher. Table 5.4 compares the results of the unlimited main and alternative hybrid method. The differences are negligible.

In [90], the authors have made a successful benchmark using this hybrid system with an independently developed calculation tool.

Table 5.5: Calculation comparison of IEEE 39 bus network based on 10 consecutive runs

	AC	AC+DC	AC+DC (alt)	AC+DC (lim)
Elapsed time $[s]$	0.66	0.63	0.72	0.68
Nbr iterations	17	15	17	16
Cost $[MW]$	6284.1	6294.8	6294.9	6295.0

Table 5.6: Cost function differences of IEEE 39 bus network

Cost Diff $[MW]$	AC	AC+DC	AC+DC (alt)	AC+DC (lim)
AC	0	10.63	10.73	10.84
AC+DC		0	0.10	0.21
AC+DC (alt)			0	0.12
AC+DC (lim)				0

5.7.2 39 nodes network

For the IEEE 39 bus system, figure 5.9 shows the optimal power flow results in the DC system and figure 5.10 in the case when the same limitations as for the 5 bus network are activated. In both cases, convergence is reached as well and the algorithm has correctly taken care of the component limitations.

The same result tables as for the 5 bus system are repeated in tables 5.5, 5.6 and 5.7. The same conclusions hold.

5.7.3 3120 nodes network

Exactly the same exercise is done for the 3120 bus network: figure 5.11 for the DC results without the DC component limitations activated and figure 5.12 when the same limitations are set. Also for this network, convergence is reached and limitations are correctly taken into account.

Tables 5.8, 5.9 and 5.10 repeat the calculation scenarios. The same conclusions as for the other sample networks hold. In absolute values, the differences

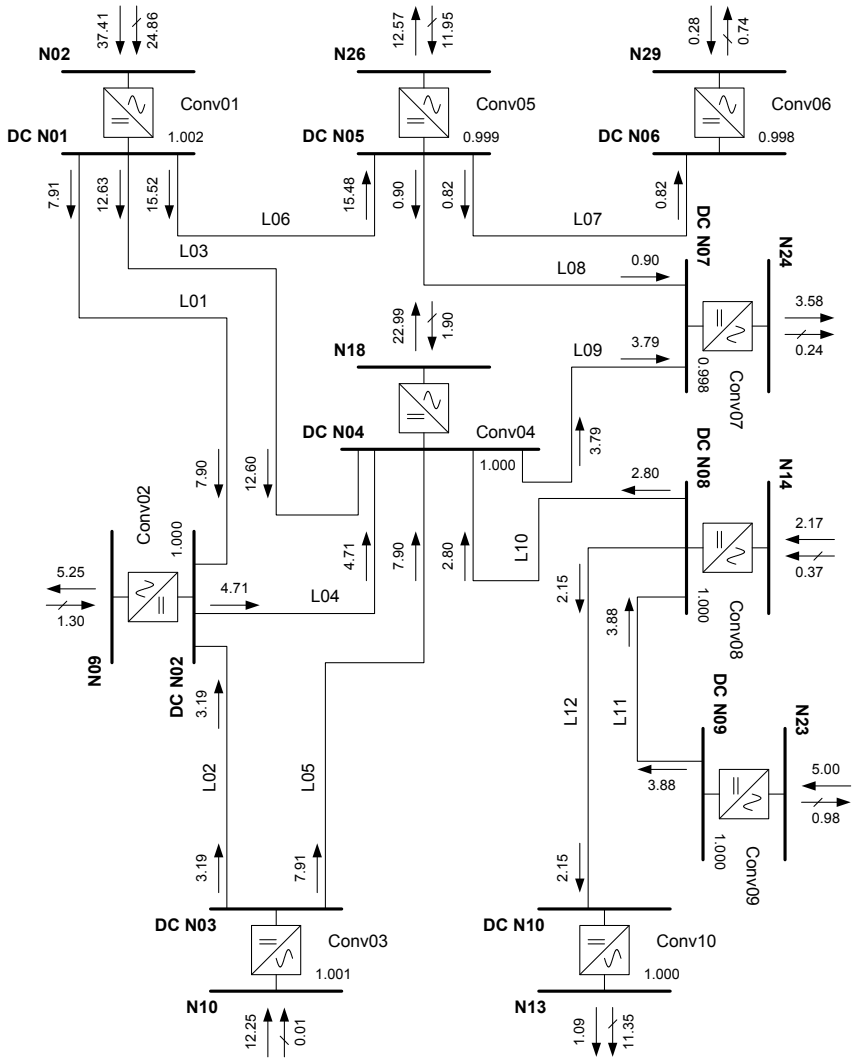

Figure 5.9: Power flow in the DC system of the optimised IEEE 39-bus network.
Legend: $\rightarrow$ Active power [MW] and $\nrightarrow$ Reactive power [MVar]

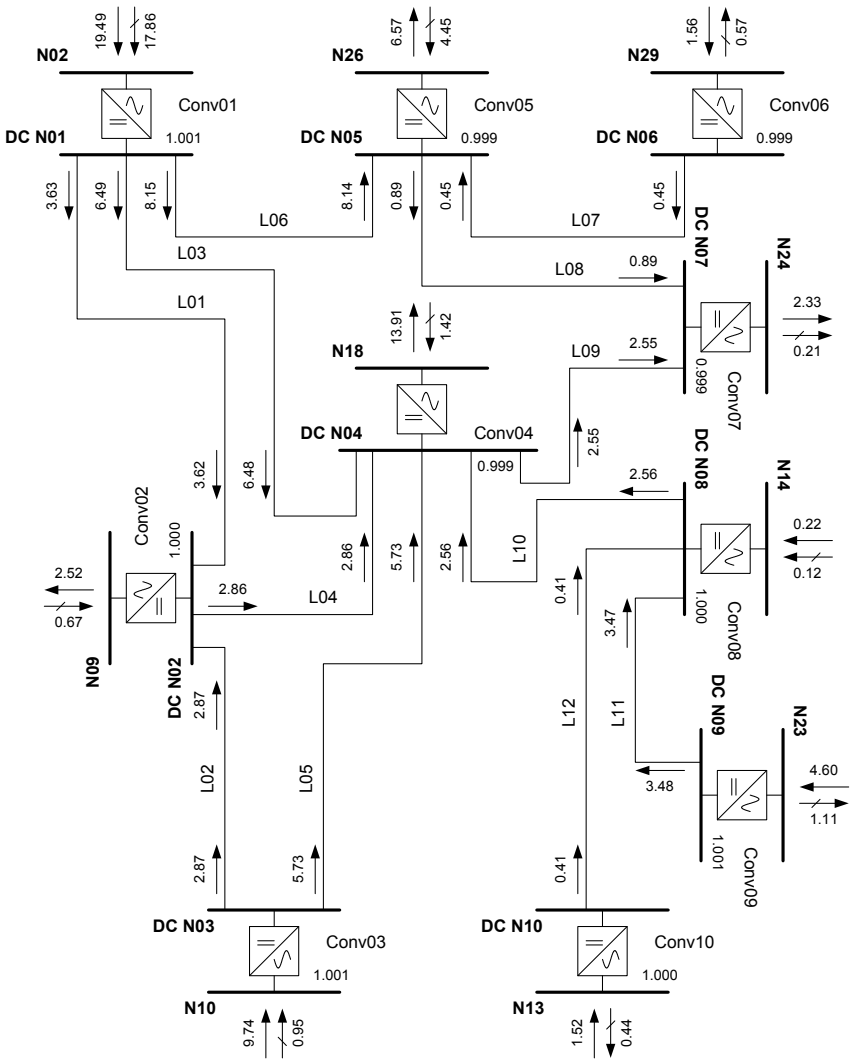

Figure 5.10: Power flow in the DC system of the optimised IEEE 39-bus network with DC branch and converter limits. **Legend**: $\rightarrow$ Active power [MW] and $\dashrightarrow$ Reactive power [MVar]

Table 5.7: Maximum convergence differences between base and alternative AC+DC optimisation method for IEEE 39 bus network

System	Maximum difference	Unit	Value
AC system	P_g	MW	2.04
	Q_g	MVar	1.87
	V_m	%pu	0.10
	V_a	°	0.03
Converters	P_{vsc}	MW	2.06
DC Branches	P_{br}	MW	2.08
	V_{dc}	%pu	4.81

Table 5.8: Calculation comparison of 3120 bus network based on 10 consecutive runs

	AC	AC+DC	AC+DC (alt)	AC+DC (lim)
Elapsed time $[s]$	27.66	27.97	27.43	28.01
Nbr iterations	32	32	31	32
Cost $[MW]$	21513.9	21517.9	21518.2	21519.0

between the main and alternative hybrid method are higher, but still negligible compared to the active power output.

Table 5.9: Cost function differences of 3120 bus network

Cost Diff $[MW]$	AC	AC+DC	AC+DC (alt)	AC+DC (lim)
AC	0	4.04	4.27	5.07
AC+DC		0	0.23	1.03
AC+DC (alt)			0	0.80
AC+DC (lim)				0

Table 5.10: Maximum convergence differences between base and alternative AC+DC optimisation method for 3120 bus network

System	Maximum difference	Unit	Value
AC system	P_g	MW	2.36
	Q_g	MVar	9.14
	V_m	%pu	0.22
	V_a	°	0.04
Converters	P_{vsc}	MW	0.06
DC Branches	P_{br}	MW	0.04
	V_{dc}	%pu	0.04

5.8 Conclusions

This chapter discusses the methodologies to include meshed DC systems into the classic AC optimal power flow case. The AC/DC converters are modelled by their loss model and two different methodologies for the DC grid have been proposed and implemented. For both variants, the algorithms also include the limitations on the converter and DC branch flows.

The calculation results show that both methods converge systematically to the same optimum. The implementation of the limitations of the converters and DC branches also proves valid. The simulations are a proof of concept, while not being exhaustive. Nevertheless, it is shown that the methodology is applicable for different power systems, even large ones, and this with reasonable convergence characteristics and computation time.

For the 5+3 bus AC/DC hybrid system, a successful result comparison has been obtained.

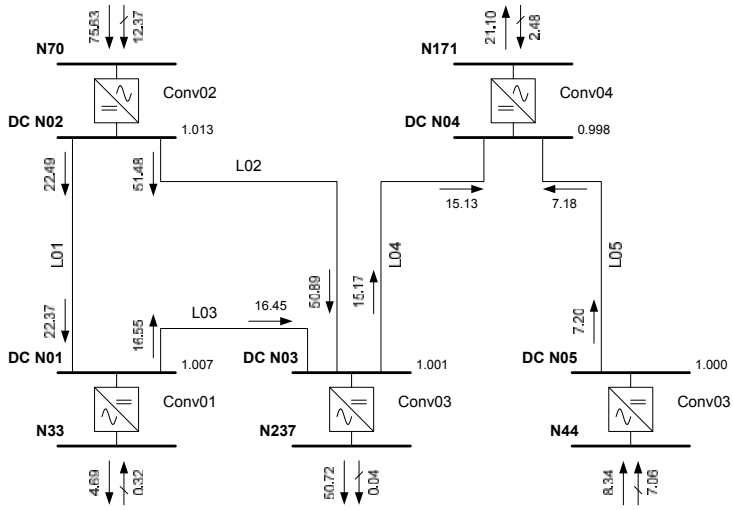

Figure 5.11: Power flow in the DC system of the optimised 3120-bus network. **Legend**: → Active power [MW] and ↛ Reactive power [MVar]

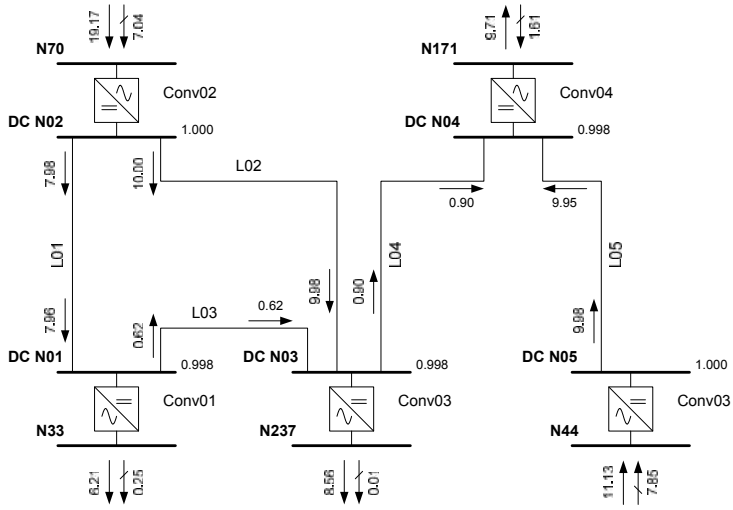

Figure 5.12: Power flow in the DC system of the optimised 3120-bus network with DC branch and converter limits. **Legend**: → Active power [MW] and ↛ Reactive power [MVar]

Chapter 6

Methodology overview and application: incident recovery

6.1 Goal

All previous methods and algorithms describe a module which can be tested and used in a separate way. However, the principal idea of the routines set up is such that they can interact and be combined into one joint functionality, using meshed DC networks, contingency states, a customised objective function and fixed state variables. The first part describes the general outline of the extended OPF routines with these features.

As a demonstration application combining all additional functionalities, inspiration was found from the daily work of grid operators. As an aid to their decision making process when handling grid incidents, the basic idea of the algorithm is to propose the outcome of several possible actions to restore the grid from its emergency state back to a safe state.

A step-by-step procedure is calculated to form a series of phases, comparable with the results of a quasi steady-state calculation. The resulting grid transients are not included.

The coordination of multiple HVDC links in alert and emergency grid states has also been discussed in [103].

The implementation overview figures are placed at the end of this chapter.

6.2 Routine overview

The routines developed in this research to implement and test all previously described methodologies are reusing the routines for the AC network model and general program flow coming with and tested by MatPower. They involve case preparation, launching the OPF solver, writing out the results and calculating all AC network related constraints equations including their first and second derivatives. All additional routines act as a wrapper around the base AC routines. They intervene in all stages of the program flow: case preparation, OPF solver routines and post-processing (figure 6.2).

In this and all following figures showing the algorithm flow, the bold arrows indicate where the original program flow has been altered. The bold functional blocks are the implemented algorithms for this research. Intervention in almost all phases of the algorithm flow is needed for proper functioning and integration of the developed methodologies. Only a small portion of the original MatPower program flow is maintained.

The remainder of this section describes in detail how the different processes are linked.

6.2.1 Case preparation

In order to achieve robust programming, it is assumed that no additional user-defined linear equality nor inequality constraints are defined (figure 6.3).

First, the expanded preparation routine checks if the OPF case contains a proper definition of the DC network. In this case, the following actions are performed

- Add converter generators to the AC network, one for each specified VSC converter. The nature of the corresponding PQ nodes is converted to PV nodes.
- A number of additional state variables needs to be defined: one variable per AC/DC converter and per DC node.
- The upper and lower limits of these variables need to be specified.

- The DC admittance matrix, which remains constant throughout the remainder of the algorithm, is calculated.
- A scan for impossible configurations (section 4.5) for the base case and the requested contingency cases is performed. The detected impossible cases are discarded.

Next, the requested contingency states are treated. For the preventive security constrained case, only the outages on AC branches are taken into account, as the outages of the AC generators are treated as separate optimisation cases (section 4.5). With the current version of the routines, no contingency state can be defined in DC branches and VSC converters. The routine expands the vector of state variables (4.3) to accommodate the variables for each of the contingency cases. Furthermore, as MatPower requires linear constraints to be specified in the beginning of the optimisation, the linear equations (4.6) are added to express the AC node voltage and active generator output equality amongst the different contingency states.

Then the original cost function is copied and replaced by its zero equivalent, in order to preserve all predefined fields for proper functioning of the MatPower routines and to avoid interference with the custom made version called by the OPF solver.

After these preparatory steps, MatPower is requested to perform its actions. The size of the optimisation problem is reduced by making a second simplified AC network, discarding AC generators and out-of-service branches. The standard initial state vector as entry point for the optimiser is constructed.

Finally, the appropriate initial point (the standard one, or the solution of a previous calculation) is selected. After this, the case definition is handed over to the user-selected optimisation solver.

6.2.2 Solver routines

Figure 6.4 shows the implementation outline of the main algorithm. It consists of two nested iterative loops.

The first is selected when there are state variables that have to remain at a predefined value (subsection 3.7.5). This iteration is successfully stopped when

the residual r (3.89) or the maximum deviation of the individual fixed state variable (3.90) is lower than their threshold value. The iteration is also stopped when compared to the previous run of the iteration, no change of the residual or the fixed state variables is found. This implies that within the current system definition, even if convergence of the individual optimal power flow algorithm is obtained, no feasible working point can be found. This is due to active element limitations. In all other cases, a next iteration of this loop is taken when the algorithm estimates that with a higher weighting factor W, the residual can result in a lower value. The implemented methodology starts with $W = 10^4$ and subsequent iterations multiply this factor with 10 with a maximum of $W = 10^{10}$ for which the iteration loop is halted and the optimisation case is considered infeasible.

The inner iteration loop is the actual interior point optimisation solver. It requires the calculation of the objective function, its first and second derivatives (figure 6.5), the function vectors, the first derivatives of the equality and inequality constraints (figure 6.6) and their second derivatives (figure 6.7). The last two routines need to be run once for the base case and for each of the contingency cases. The respective vectors and matrices then need to be compiled according to (4.4)-(4.8).

6.2.3 Post-processing

During this step, the results are cast into the appropriate data structures and, upon request, printed on screen (figure 6.8).

6.3 Application: incident recovery

Several parameters, on top of choosing the system to work with, need to be specified in order to properly initialise the algorithm:

- all relevant preventive and curative contingency states;
- control possibilities of the operator can use to get the grid back into a safe state; other control parameters are then forbidden to use;
- incident or outage to take place;
- cost function describing the operator objective; it only plays a role for choosing the best suited control action proposed to the operator.

The incident recovery starts with preliminary checks and defining the initial state of the network, taking into account all predefined contingency states and assuming that the initial state is independent from the control possibilities. As such, with a first run of the program, ignoring the predefined control restrictions and the incident to be played, the optimal initial state is determined. Should the optimisation problem not converge, the user is warned and further calculation is halted.

Next, the predefined outage is applied to the initial state. This can either be a generator, AC or DC branch or a AC/DC converter. At this point, the control restrictions of the operator apply (figure 6.9).

Next, the final target state is determined. One of the following three possibilities occurs (figure 6.10):

1. The algorithm is able to find a target state which takes into account all necessary contingency states. This state is automatically selected.
2. The calculation did not find a viable solution for the security constrained optimal power flow, however, neglecting the contingency state a solution is found. For the sake of demonstration, the user is warned, but the search function carries on. The user may want to redefine the calculation case, taking into account this information.
3. The optimisation algorithm did not find a viable solution for the case without security constraints. Further calculation is halted and the user is warned.

As the target state (with or without taking into account the requested contingency conditions) is defined, the algorithm tries to reach this step by step.

Before actually starting the search function, the set of control possibilities is determined. This set is based on the assumption that the operator is restricted to alter one or two converter setpoints per step. This assumption is justified as the system needs time for the transients to damp out. The AC slack bus generator and the DC reference converter always try to balance the active power flow in the AC and DC systems. They are always implied in any control action of the operator and their reaction is automatic.

The system state right after the incident cannot be calculated by means of an optimal power flow. It requires a classic Power Flow calculation, taking into

account the automatic controls of the converters and generators (e.g. droop control effects).

For each step, the search algorithm performs the same actions (figure 6.11):

1. For each control combination separately, a security constrained OPF is performed and the result saved.
2. Should the security constrained OPF not have converged, an OPF without contingencies is done.
3. All results are distributed amongst three categories: 1) contingency safe states, 2) safe, but not contingency safe states and 3) unsafe states.
4. In the case that no safe grid state for any control combination has been found in step 3, the optimisation problem needs to be relaxed, i.e. voltage ranges are to be widened where possible or power flow limitations be set higher. Time limitations must then be set for the corrective actions as well. The whole searching process must be repeated starting from step 1.
5. Each group of results, set up in step 3, is sorted individually, giving the highest ranking to the solutions with the lowest cost function result.
6. Giving priority to the contingency safe group, then to the mere safe state group, the highest ranked state, and its associated control combination setpoints are proposed to the grid operator and are taken as the new starting point for the next round.
7. When the contingency safe group contains at least one solution, the whole process is stopped. The operator has now sufficient time to steer the grid to the desired optimum state.
8. When relaxation is applied in step 4, undo this by setting back the original limitations;
9. Repeat another round by going back to step 1.

Figure 6.1 shows the graphical interpretation of the previous discussion. On the left side, the initial situation is depicted. With the actual (optimal) control parameters, the grid state resides well within the “N” and “N-1” safe regions. After the incident, these safety regions could shift as shown in the right side figure (b) as the grid topology has changed implying e.g. overloading of branches. The grid, still with the initial control parameters, comes out of the safe regions

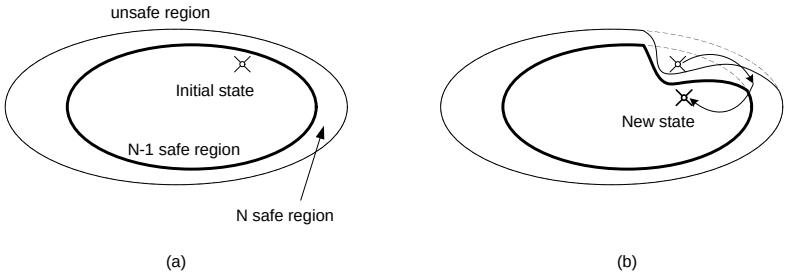

Figure 6.1: Schematic overview of the recovery actions after incident. (a) situation before incident, (b) safe region evolution and grid state changes.

and is now situated in a position that can only be sustained for a certain time span. The operator needs to alter the control parameters (e.g. setpoints for converters, generators (if possible), tap positions of transformers) in order to get the system back to the "N-1" safe regions. As he is able to perform very few actions at a time, it can be that several consecutive manipulations are needed (in the figure, two are needed: one to get into the "N" and the next to the "N-1" safe state). After the system has been put into the "N-1" safe state, the operator has sufficient time to find and steer to a new optimum in the altered topology.

6.4 Simulation results

A simulation has been run to demonstrate this methodology. It starts from the IEEE 39 bus network with its associated DC system. The chosen preventive contingency state is the outage of branches L03, L06, L08 and L10 (4.6). This system has a feasible solution for each of the four contingency cases. Branch L07 is duplicated for this demonstration. The starting position of the algorithm is the converged security constrained OPF solution of this configuration. The chosen cost function is minimum system losses.

The system is constructed that when the branch L07 is taken out of service after an incident has occurred, the optimisation algorithm is able to find a feasible point taking the security constraints into account. However, the system state right after the incident is not "N-1" secure.

The chosen control possibilities for this case are the adjustment of one generator or converter setpoints per iteration. These adjustments are compensated by the AC slack bus generator and the DC reference converter.

At the **first iteration**, the search algorithm is not able, given the control restrictions, to find a feasible point complying with the security constraints. The algorithm proposes, as the best choice for this iteration, to lower the active power output of converter C04 (connected to node N18) by 12.3 MW, pushing that power difference to the reference converter C02 (connected to node N09).

Starting from this new state, with the **second run** of the iteration, the algorithm is now able to find feasible secure system states for all control possibilities. The operator needs, given this search method, two control steps acting on the converter setpoints to get the system back in a secure state.

The initial DC power flow was hindering the secure operation of the post-contingency state. With search methods implying more generator or converter setpoint changes per iteration, it is possible to recover the system in just one control step. It should be noted that many fast OPF calculations are necessary for this tool to be efficient for the operator.

6.5 Conclusions

In this chapter, the algorithm outline is given and it is explained how all the developed methodologies from the previous chapters are linked into one unique optimisation routine. All calculations related the AC network are handled by the original MatPower routines. The development reuses them for the implementation of the functions created in this research to verify the correctness of the proposed methodologies.

To activate all developed functions, an incident recovering tool has been proposed introducing an iterative search pattern, proposed to the system operator, to find safe system states with the least number of control actions after an arbitrary incident has occurred. It combines the hybrid AC/DC optimisation algorithm with security constraints and control restrictions modelled as fixing the state variable values of generators and converters.

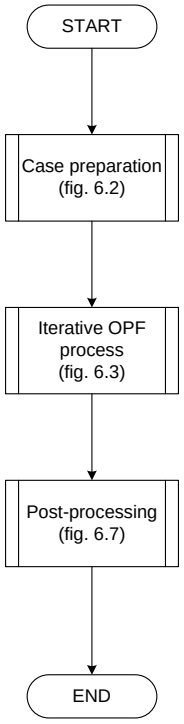

Figure 6.2: Overview flowchart for the extended Optimal Power Flow Routine. **Legend**: normal line widths are used for original MATPOWER routines, bold lines for adapted adapted algorithm flow and implemented routines.

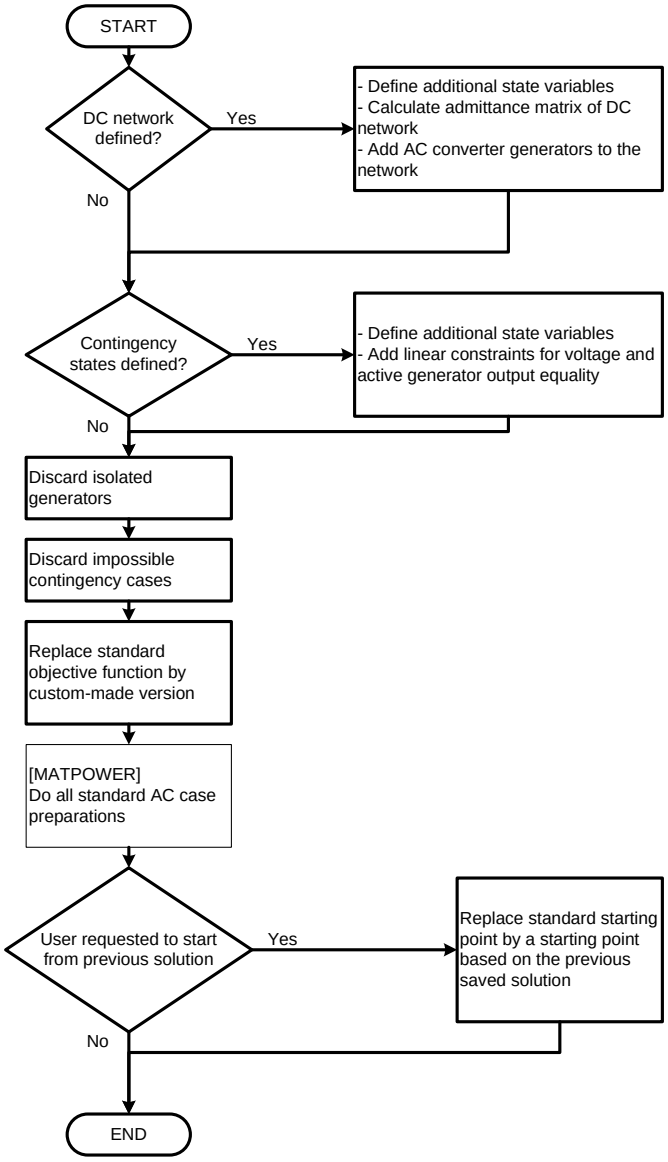

Figure 6.3: Flowchart for the extended Optimal Power Flow Routine: preparation step. **Legend**: normal line widths are used for original MATPOWER routines, bold lines for adapted adapted algorithm flow and implemented routines.

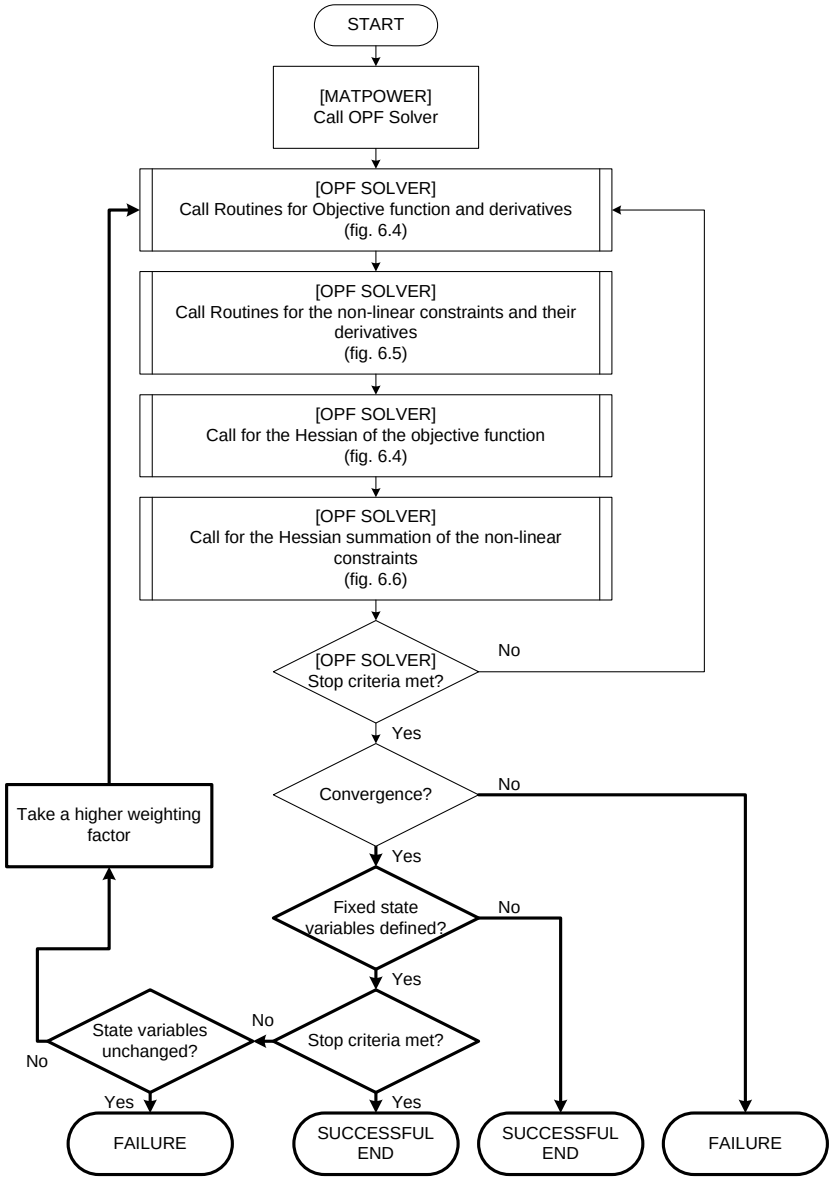

Figure 6.4: Flowchart for the extended Optimal Power Flow Routine: iteration loop for the solver. **Legend**: normal line widths are used for original MatPower routines, bold lines for adapted adapted algorithm flow and implemented routines.

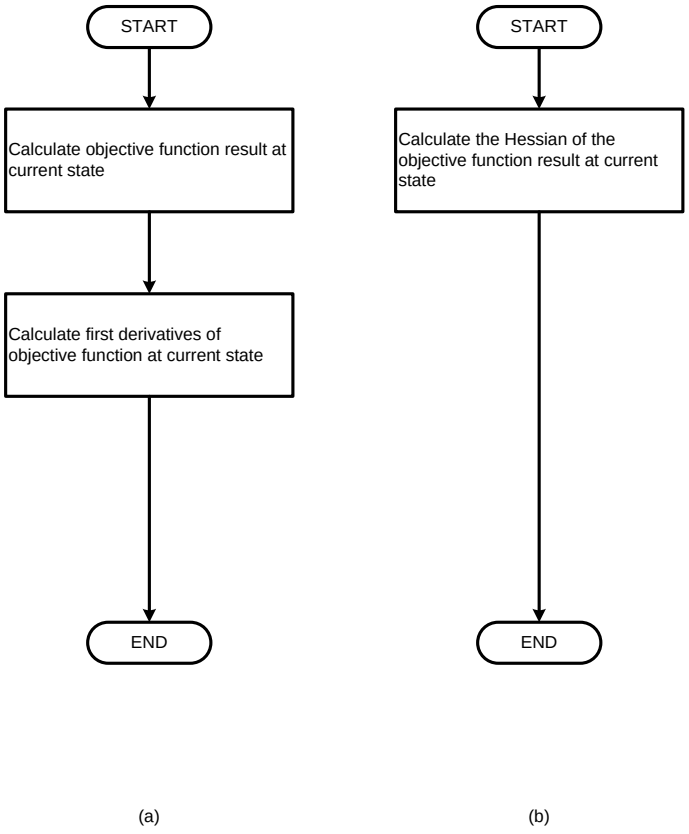

Figure 6.5: Flowchart for the extended Optimal Power Flow Routine: treatment of the objective function. Left (a): Calculation of the function result and first derivatives. Right (b): Calculation of the Hessian. **Legend**: normal line widths are used for original MATPOWER routines, bold lines for adapted adapted algorithm flow and implemented routines.

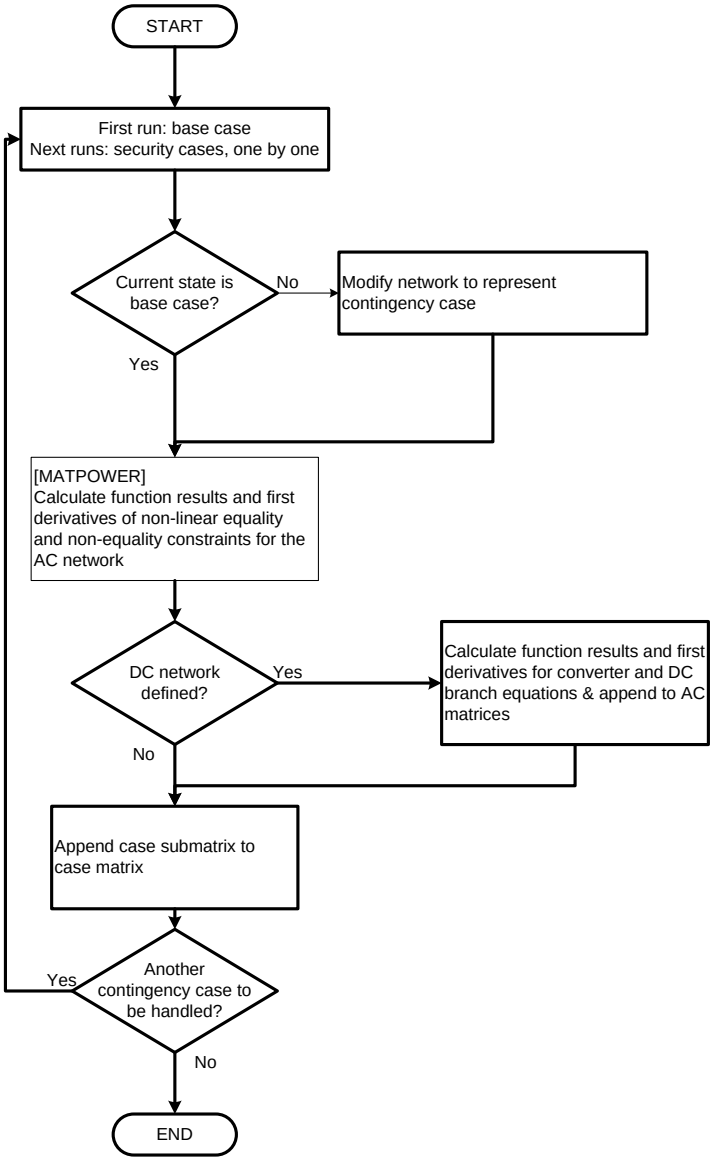

Figure 6.6: Flowchart for the extended Optimal Power Flow Routine: calculation of the function result and first derivatives for the non-linear constraints. **Legend**: normal line widths are used for original MATPOWER routines, bold lines for adapted adapted algorithm flow and implemented routines.

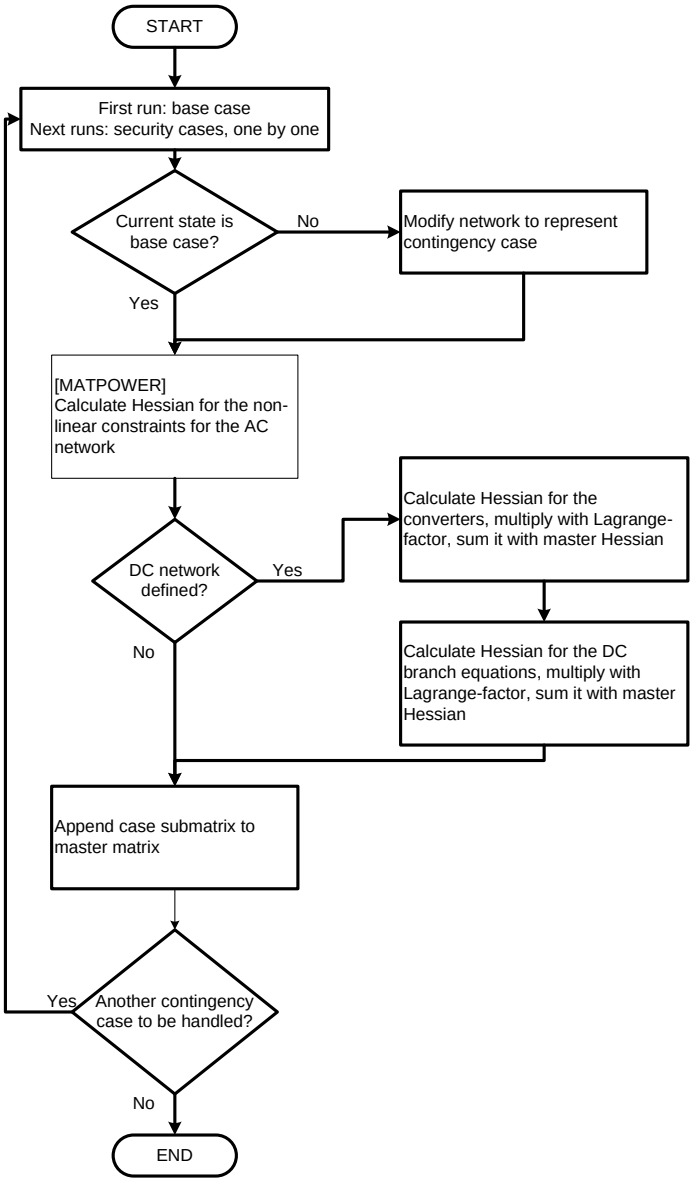

Figure 6.7: Flowchart for the extended Optimal Power Flow Routine: calculation and summation of the Hessians for the non-linear constraints. **Legend**: normal line widths are used for original MATPOWER routines, bold lines for adapted adapted algorithm flow and implemented routines.

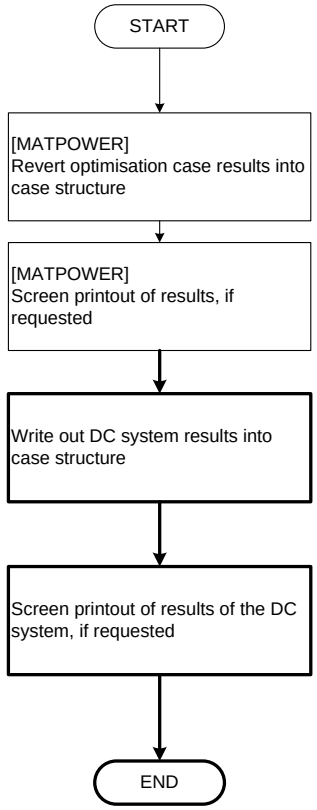

Figure 6.8: Flowchart for the extended Optimal Power Flow Routine: post-processing. **Legend**: normal line widths are used for original MatPower routines, bold lines for adapted adapted algorithm flow and implemented routines.

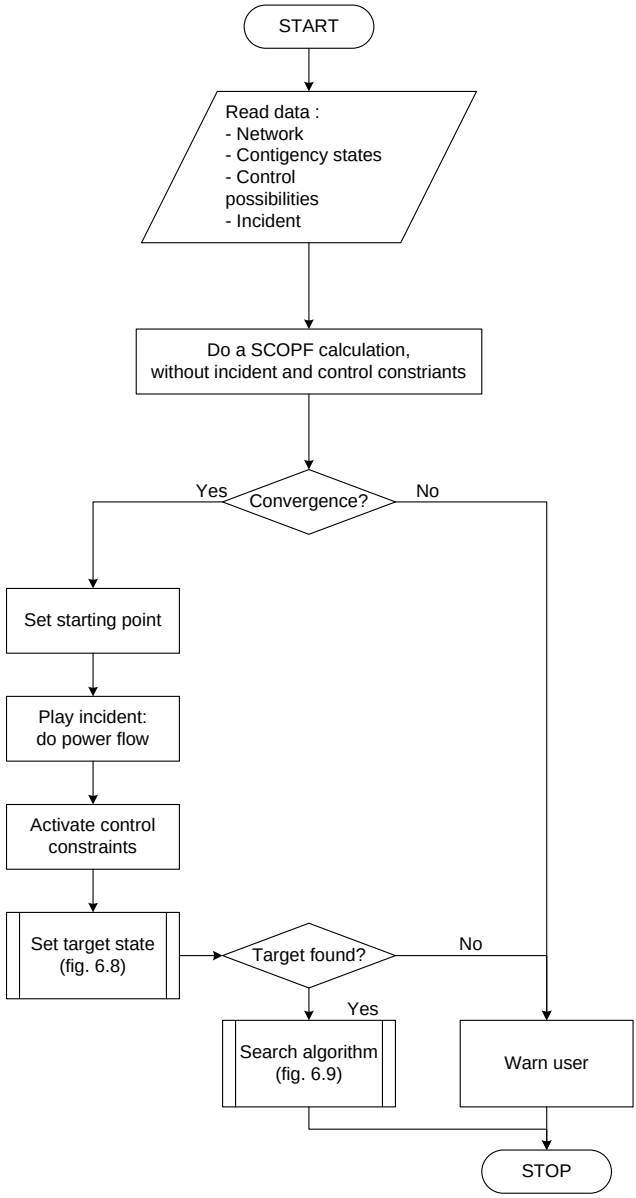

Figure 6.9: Main routine for the incident recovery algorithm

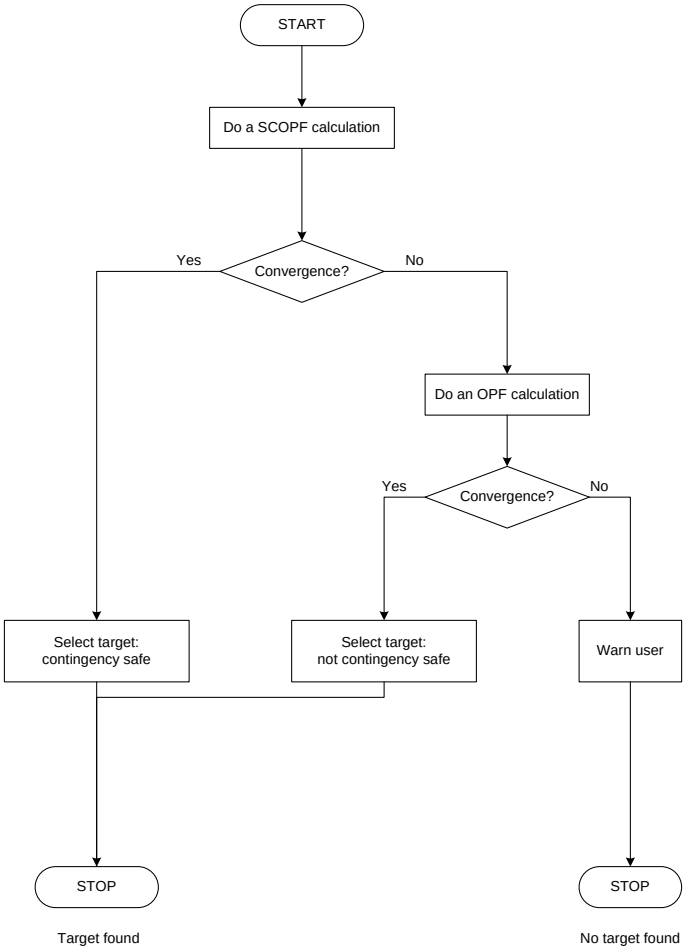

Figure 6.10: Subroutine for the incident recovery algorithm: selecting the target grid state

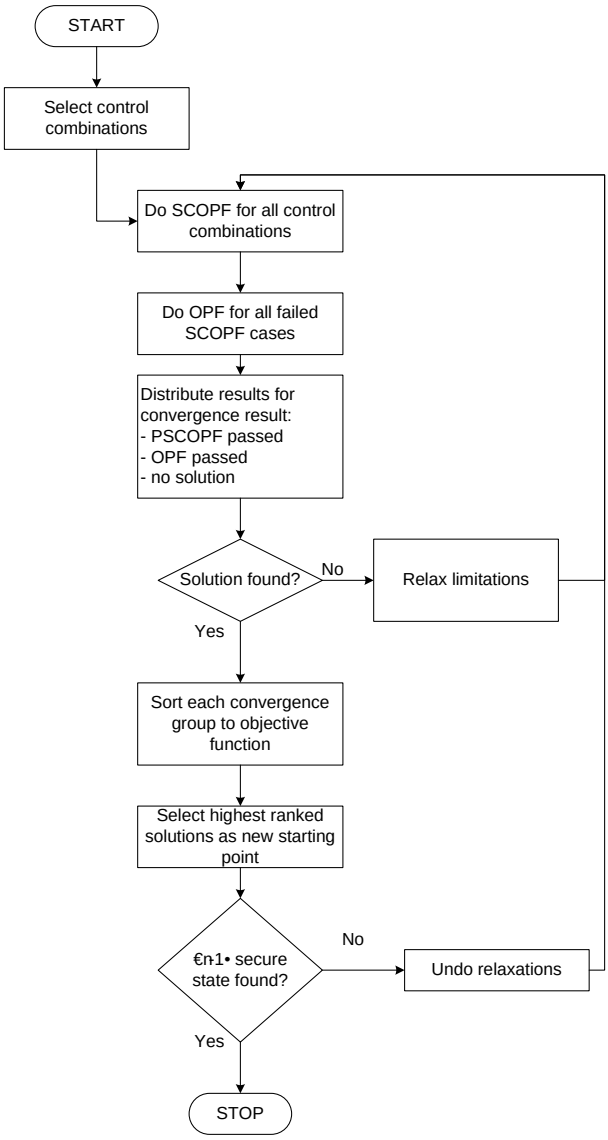

Figure 6.11: Subroutine for the incident recovery algorithm: iterative routine for determining the largest possible step

Chapter 7

Conclusions and further developments

In this final chapter, an overview of the major accomplishments of the previous chapters is given and general conclusions and main contributions of research are discussed. Further developments building on this work conclude this chapter.

7.1 Summary and conclusions

High Voltage Direct Current solutions have become available for ever more elaborated configurations, as discussed in chapter 2. Starting from point-to-point or back-to-back connections between isolated or asynchronous grids, going over applications integrated in meshed AC networks and eventually evolving into multi-vendor multi-infeed systems and finally meshed DC networks, the DC technology comes to a point where it coexists and is intertwined with its AC counterpart.

Two different technologies exist: the Line Commutated Converter, based on thyristor elements, and the Voltage Source Converter, using fast switching transistor technology. The latter, especially in the form of the multi-level modular converter topology is ready to be built in complex DC grid topologies.

Mathematical models and methodologies are important for planning, development, installation and operation of the hybrid meshed AC and DC networks. Chapter 3 goes deeper into the optimal power flow theory and mathematical methodologies. First it discusses the general optimisation theory for the case where a non-linear cost function is combined with non-linear equality and inequality constraints. Theorems for global convergence and solution methods are given.

The non-linear optimisation case is then applied to AC power systems and their implication on planning and operation is discussed. Preparatory methodologies for the later chapters have been introduced: the extension of the optimisation case with additional constraints and user-defined cost function primitives. Derived applications have been developed: multi-objective optimisation, keeping state-variables at a defined initial value and a method to solve a power flow case by means of optimal power flow algorithms.

Chapter 4 discusses the extension of the classic optimal power flow definition from the previous chapter to take into account security constraints in the form of generator and grid branch outages. A general introduction of the state-of-the art and the general calculation approach in this field is given together with various methods to solve them for very large networks.

The methodologies implemented in this research and simulation results are given and focus on the static preventive and curative security contingency cases. The algorithms developed are applicable to use in meshed DC grids and the AC/DC converters discussed in the next chapter. Simulation results of this hybrid combination are stated as well.

In chapter 5, modelling the AC/DC converters and the DC system topology for optimal power flow calculations is the central topic. The voltage source converters link the AC and DC grids, using non-linear equality constraints giving the converter loss model. The independent models have been used for the DC grid topology. The first is developed in an analogous way as the AC system. The second method uses non-linear constraint functions stating the current conservation and resistive voltage drop of the individual DC branches. Converter and branch power limitations for both alternatives are added to the optimisation case. Simulation comparisons have been performed for both methods.

The last technical chapter 6 explains how all of the previously discussed methodologies and algorithms link and form a consistent optimisation algorithm. As an application to combine all developments, an iterative tool for the system operator is described which proposes the best control actions after a grid incident has occurred.

This work exceeds current studies by integrating state-of-the-art research of AC optimisation with the integration of state-of-the-art VSC HVDC systems.

The main contributions of this thesis are

- Two different methodologies for the modelling of hybrid AC/DC meshed networks have been established: the main method using an admittance matrix and the alternative method with separate branch and topology equations. Both methodologies are capable to work with a wide range of different DC grid topologies. The innovative part of this work is correctly setting up the system equations for the DC grid and AC/DC converters and linking them to the AC network. The same problem reduction philosophies (discarding outaged generators, branches and buses) as for the AC grid had to be followed.
- The extension of classic AC and hybrid AC/DC optimisation cases for the security constrained OPF taking into account both corrective and preventive actions. The number of parallel optimisation cases is only limited by the robustness and efficiency of the optimisation algorithm. The methodology used compiles the different cases into one global optimisation, which calls the individual cases using the traditional OPF routines.
- More flexibility has been given to the objective functions, user-defined cost function primitives can be combined, rendering a set of new research possibilities: multi-objective optimisation, creation of Pareto-fronts and setting state variables to predefined values.
- Several applications for these new tools have been developed and tested.
- All methodologies and algorithms have been tested and combined into a unique and robust easy-to-configure open-source tool, to be used together with the MatPower simulation package. This tool can be the starting point for further research in the field of applications for the optimisation of hybrid meshed AC/DC grids.

7.2 Future work and developments

The following list discusses different areas where improvements lead to the modelling and optimisation of large and realistic hybrid power systems. The demonstration of the methodologies has been successful on small and larger demonstration systems. With this research, the basis is laid for a multifunctional tool, able to robustly optimise large networks with detailed modelling.

- No calculation optimisation has been done for the security constrained optimal power flow for large networks and many different parallel cases.
- Up till now, only contingency constraints involving AC generators and branches have been implemented. For operational purposes, the modelling must be extended to also correctly take outages of DC elements (nodes, branches and converters) into account.
- For the robustness of the preventive security constrained OPF, an automated detection of isolated AC and DC subgrids for the contingency states and the creation of additional slack or reference buses has to be developed.
- When appropriate, models for DC/DC converters need to be modelled and implemented. Similar to the AC/DC converters, they are modelled using their loss equation for the active power flowing through the device. The voltages on both buses are not correlated and thus optimised independently.
- No attempt is made for droop-control optimisation of the individual AC/DC converters.
- To model under more realistic circumstances and to enable the use of switchable elements and discrete transformer tap changer positions, techniques for integrating on/off and discrete state variables need to be implemented.
- Extension of the incident handling tool: adding the power flow algorithms for the situation calculation right after the incident and more suitable patterns are to be researched and developed.
- Implementation of dynamics of the hybrid grids starting from optimised system states.
- Optimising the ancillary services and the total transfer capacity of trans-border connections.

- Search algorithms for the optimal location and configurations of the converters and DC system.
- Data structure alignment with the other grid calculation tools developed by the KULeuven.

Appendix A

Algorithm overview and sample networks

A.1 Functionality overview of Matpower and added routines

The base functionalities of MatPower for the Optimal Power Flow calculations are:

- Integrated optimising routine: Matlab Interior Point Solver (MIPS). The routines are also fit to use the KNITRO for Matlab solver.
- Meshed AC network topology.
- Limits on generator output powers, bus voltages and branch flows.
- Piece-wise linear and polynomial generation cost functions for active and reactive power.
- Definition of additional custom state variables.
- Possibility to incorporate additional linear (equality and inequality) constraints using the original and custom defined state variables.
- It is assumed that all generators are free to control. No selection can be made to distinguish between free and fixed setpoints.
- No use of discrete state variables.

Table A.1: Characteristics of the sample networks

Name	5 nodes	IEEE 39	3120 nodes
Number of buses	5	39	3120
Number of generators	2	10	505
Number of branches	7	46	3693
Number of loads	4	21	2277

The following functionalities are added through this research to the optimal power flow calculations

- Further customisation of cost function (chapter 3);
- Multi-objective optimisation and generation of Pareto front curves (chapter 3);
- Confining state variables to defined values (chapter 3);
- Modelling of a meshed DC grid and definition of AC/DC converters connecting AC and DC network (chapter 5);
- Limiting the converter power flows, DC bus voltages and DC branch flows (chapter 5);
- Extension for parallel optimisation of different subnetworks for the security constrained OPF (chapter 4).

A.2 Sample grids

This section introduces the different sample grids used for demonstration purposes throughout this manuscript. Table A.1 gives an overview of the grid characteristics. The next subsections give some more details.

A.2.1 5 Node network

The first network is a very simple one with only 5 nodes, initially introduced in [104], figure A.1. The proposed DC network has three connections with the AC network through AC/DC converters and the DC branches form a single

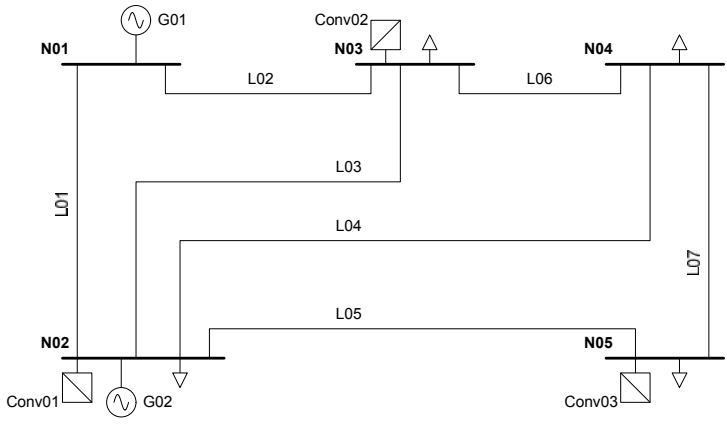

Figure A.1: AC system of the 5-bus network with AC/DC converters

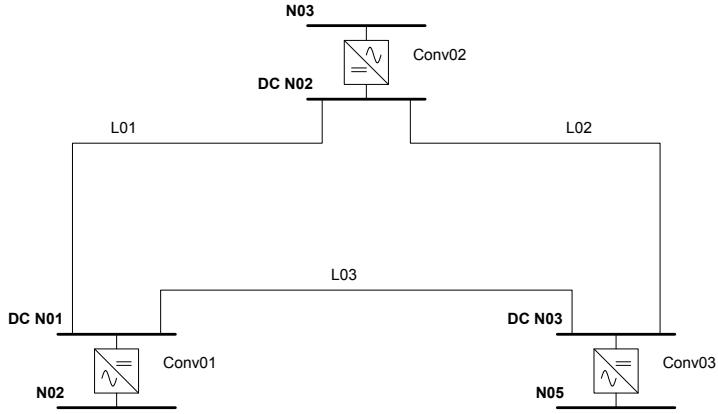

Figure A.2: DC system of the 5-bus network with the AC nodes of the AC/DC converters

Table A.2: Lower and upper element limits of the 5 node sample network

Element type	Characteristic	Minimum	Maximum
AC Nodes	Voltage amplitude [pu]	0.9	1.1
Generator 1	Active power [MW] Reactive power [MVar]	10 -500	250 500
Generator 2	Active power [MW] Reactive power [MVar]	10 -300	300 300
AC branches	Branch loading [MVA]		100
DC nodes	Voltage amplitude [pu]	0.7	1.05
AC/DC converters	Active AC power [MW] Reactive AC power [MVar] DC power [MW]	-100 -100 -100	100 100 100
DC branches	Branch loading [MW]		100

mesh (figure A.2). Table A.2 gives the overview of minimum and maximum voltage and power limits of these scheme's elements.

A.2.2 IEEE 39 node network

The second network used is the IEEE 39 bus network (figure A.3). It generally represents the 345 kV New England system (but is not the exact model of it). This 39 bus, 10 generator network [105] is available in the standard MatPower package. Figure A.4 gives the associated sample DC system.

A.2.3 3120 bus network

In order to test the applicability and the stability of the algorithms, another MatPower case file is used, using 3120 AC buses. It generally represents the Polish 400, 220 and 110 kV grids during 2008 summer morning peak conditions. As the exercise here is to monitor the behaviour of the algorithms using large networks, special attention goes to calculation time as well. The associated DC system is shown in figure A.5.

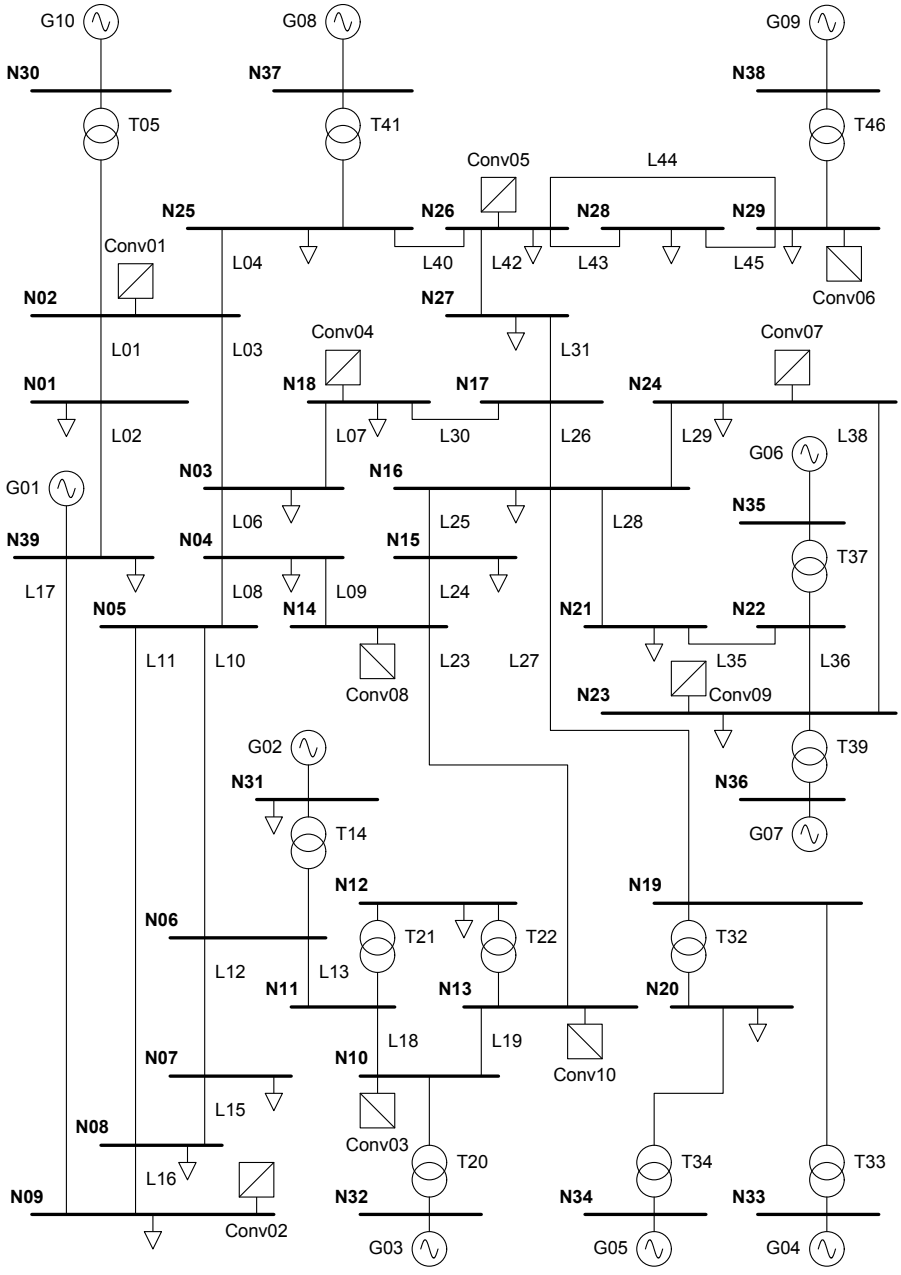

Figure A.3: AC system of the IEEE 39-bus network with AC/DC converters

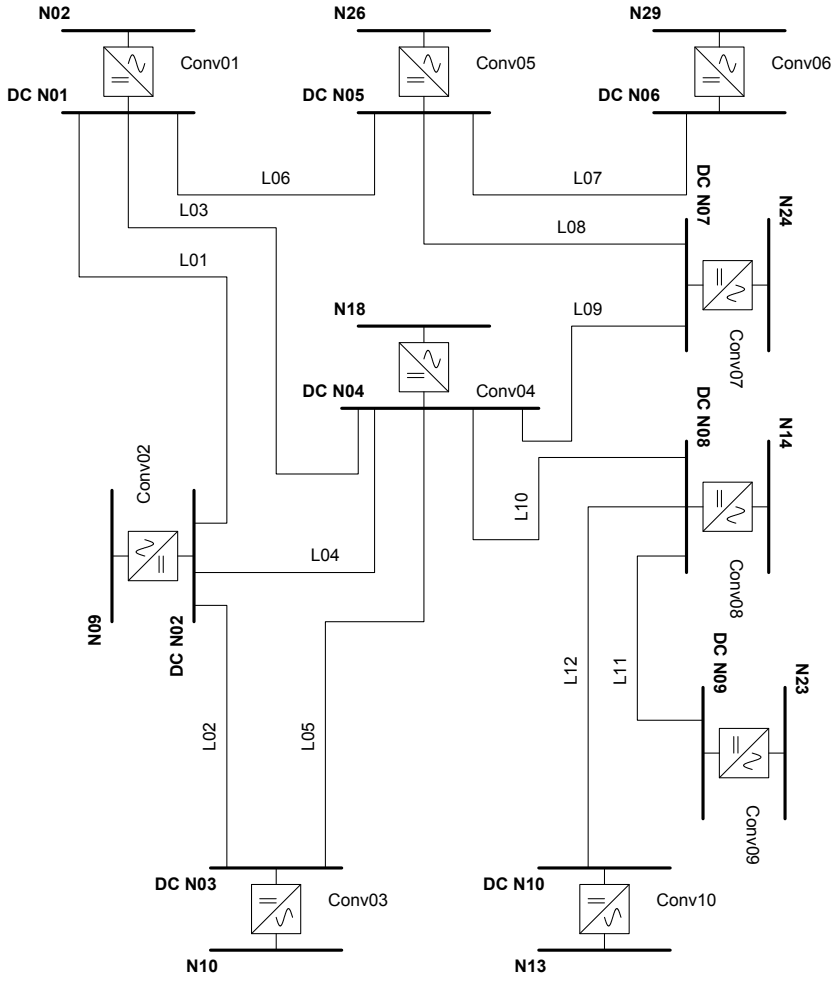

Figure A.4: DC system of the IEEE 39-bus network with the AC nodes of the AC/DC converters

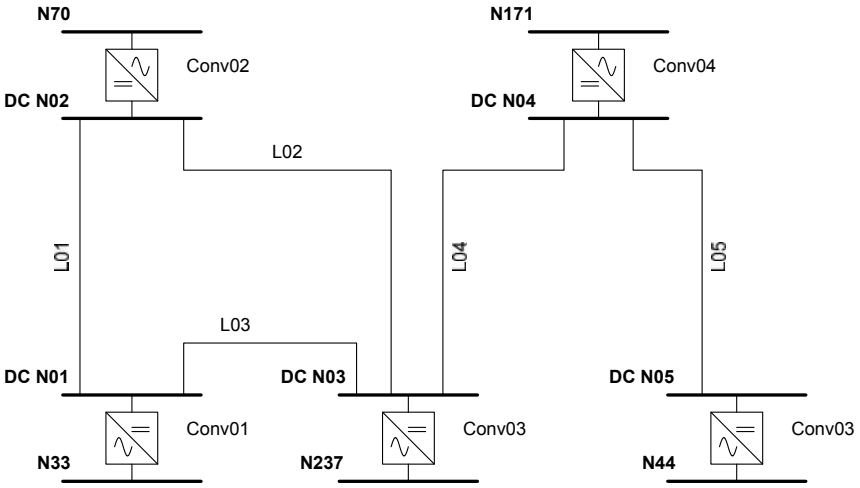

Figure A.5: DC system of the 3120-bus network with the AC nodes of the AC/DC converters

Appendix B

Barrier method optimisation routine

In order to give the reader a feeling on how a complete optimisation routine is set up, this appendix introduces the barrier method (section 3.3) for solving optimisation problems with non-linear cost, equality and inequality functions. This appendix is completely based on [40], p. 241-248.

B.1 Theoretical development for the step increments

The reference formulation of the non-linear programming problem is

$$\min_x f(x) \tag{B.1a}$$

$$\text{with } g(x) = 0 \tag{B.1b}$$

$$L_l \leq h(x) \leq L_u \tag{B.1c}$$

The constant vectors L_l and L_u represent the lower and upper bounds of the (non-linear) inequality functions $h(x)$.

Assume that the cost function f is a scalar function, the state variable vector x has n elements, the number of equality constraints is p and the number of inequality constraints is m. m may be higher than n but p cannot. All bounds imposed directly on the state variables x are included into the vector function $h(x)$.

The formulation is solved using the Karush-Kuhn-Tucker (KKT) necessary conditions (subsection 3.3.2) and the barrier penalty functions. The recursive Newton method (subsection 3.3.4) is applied to calculate the step updates.

The first step in the approach is to transform the inequality into equality constraints using non-negative buffering or slack variables r for the lower and s for the upper bound:

$$h(x) - r = L_l \tag{B.2a}$$

$$h(x) + s = L_u \tag{B.2b}$$

Applying the logarithmic barrier functions to deal with the non-negativity of the slack variables, the augmented scalar cost function is constructed.

$$f_a(x) = f(x) - \sum_{j=1}^{m} u_j \ln s_j - \sum_{j=1}^{m} v_j \ln r_j \tag{B.3}$$

The variables u_i and v_i are also non-negative. When these variables approach zero, optimising $f_a(x)$ or $f(x)$ leads to the same result when subjected to the same constraints. As such, the non-negativity of the slack variables may be ignored.

The Lagrangian function of the optimisation problem is (B.4), the corresponding Lagrange multipliers being μ, λ and γ, the KKT conditions require them to be non-negative.

$$\mathfrak{L} = f_a + \mu^T g + \lambda^T (h + s) - \gamma^T (h - r) \tag{B.4}$$

Differentiation of the Lagrangian function (B.4) to its parameters x, r and s and setting them to zero, leads to the necessary optimality conditions of the problem. For the state variable vector, this yields

$$\nabla_x \mathfrak{L} = \nabla f + \nabla g \cdot \mu + \nabla h \cdot (\lambda - \gamma) \tag{B.5}$$

Differentiating (B.4) to the slack variables r and s yields respectively:

$$\nabla_r \mathfrak{L} = -R^{-1} \cdot v + \gamma = 0 \tag{B.6a}$$

$$\nabla_s \mathfrak{L} = -S^{-1} \cdot u + \lambda = 0 \tag{B.6b}$$

where the R and S are the associated diagonal matrices of the vector r and s. Rewriting the previous equations gives

$$\begin{aligned} R \cdot \gamma &= v \\ S \cdot \lambda &= u \end{aligned} \tag{B.7}$$

The increment equations of (B.7) are

$$\begin{aligned} (R + \Delta R) \cdot (\gamma + \Delta\gamma) &= v \\ (S + \Delta S) \cdot (\lambda + \Delta\lambda) &= u \end{aligned} \tag{B.8}$$

By neglecting the double increment terms and solving (B.8) for the Lagrange multiplier increments yields

$$\begin{aligned} \Delta\gamma &= R^{-1}v - \gamma - R^{-1}\Delta R\gamma \\ \Delta\lambda &= S^{-1}u - \lambda - S^{-1}\Delta S\lambda \end{aligned} \tag{B.9}$$

or

$$\begin{aligned} \Delta\gamma &= R^{-1}v - \gamma - R^{-1}\Gamma\Delta r \\ \Delta\lambda &= S^{-1}u - \lambda - S^{-1}\Lambda\Delta s \end{aligned} \tag{B.10}$$

where Γ and Λ are diagonal matrices of the vectors γ and λ and by using $\Delta R \cdot \gamma = \Gamma \cdot \Delta r$ and $\Delta S \cdot \lambda = \Lambda \cdot \Delta s$.

The penalty vectors u and v may vary with each iteration step, but remain constant within each step. Writing out the increment expressions of the equations (B.2a) and (B.2b) and neglecting the higher order terms of Δx yields the linear expressions B.11 and B.12

$$\begin{aligned} \nabla_x h^T \Delta x - \Delta r &= L_l - h + r = d_2 \\ \nabla_x h^T \Delta x + \Delta s &= L_u - h - s = d_1 \end{aligned} \tag{B.11}$$

or

$$\begin{aligned} \Delta r &= -d_2 + \nabla_x h^T \Delta x \\ \Delta s &= d_1 - \nabla_x h^T \Delta x \end{aligned} \tag{B.12}$$

Substitution of (B.12) into (B.10) yields (B.13)

$$\begin{aligned} \Delta\gamma &= R^{-1}(v + \Gamma d_2) - \gamma - R^{-1}\Gamma\nabla_x h^T \Delta x \\ \Delta\lambda &= S^{-1}(u - \Lambda d_1) - \lambda + S^{-1}\Lambda\nabla_x h^T \Delta x \end{aligned} \tag{B.13}$$

The increment equation of the Lagrangian function (B.4), after neglecting the higher order terms of Δx and $\Delta\mu$ as well, gives (B.14). Here, all the variables are augmented.

$$\nabla_x \mathfrak{L}_a = \nabla\mathfrak{L} + H\Delta x + \nabla g \cdot \Delta\mu + \nabla h \cdot (\Delta\lambda - \Delta\gamma) \tag{B.14}$$

with

$$H = \nabla^2 f + \sum_{j=1}^{p} \mu_j \nabla^2 g_j + \sum_{j=1}^{m} (\lambda_i - \gamma_i)\nabla^2 h_i \tag{B.15}$$

The expression (B.14) is written into the form

$$\nabla_x \mathfrak{L}_a = A\Delta x + \nabla g \Delta\mu + b = 0 \tag{B.16}$$

Then, by identifying the terms and using (B.13), the expressions of the parameters A and b are obtained

$$A = H + \nabla H(S^{-1}\Lambda + R^{-1}\Gamma)\nabla h^T \tag{B.17a}$$

$$b = \nabla L + \nabla h \left(S^{-1}(u - \Lambda d_1) - R^{-1}(v + \Gamma d_2) - (\lambda - \gamma)\right) \tag{B.17b}$$

Linearisation of the equality constraints gives

$$g + \nabla g^T \Delta x = 0 \tag{B.18}$$

Combining (B.16) and (B.18) finally yields the system of equations for the increments Δx and $\Delta\mu$

$$\begin{bmatrix} A & \nabla g \\ \nabla g^T & 0 \end{bmatrix} \cdot \begin{bmatrix} \Delta x \\ \Delta\mu \end{bmatrix} = - \begin{bmatrix} b \\ g \end{bmatrix} \tag{B.19}$$

The square $(n+p)$ matrix on the left hand side is symmetrical and thus invertible. (B.19) together with (B.12) and (B.13) define all step increments Δx, $\Delta\mu$, Δr, Δs, $\Delta\lambda$ and $\Delta\gamma$.

B.2 Penalty vectors

Each element of the u and v vector needs to approach zero when the recursive method advances and the solution approaches the optimum. There is no strict obligation for each of the elements to be equal. The equipenalty scheme, on its turn, provides a method for selecting the same value for all elements of both vectors:

$$u = v = \rho\sigma E_m \tag{B.20}$$

with $0 \leq \rho \leq 1$, E_m is a m-element column vector with all elements equal to 1. The penalty factor σ needs to steadily approach zero during the iteration process. A possible choice for this factor is

$$\sigma = \frac{1}{2m}(\lambda^T s + \gamma^T r) \tag{B.21}$$

At the optimum, following the KKT conditions, $\sigma = 0$.

B.3 Iterative process

B.3.1 Process start-up

For the **state variable vector** x_0 a starting position needs to be chosen using a trained guess (e.g. from a previous solution, by satisfying $\nabla f(x_0) = 0$ or choosing the average of the state variable bounds).

The **Lagrange multiplier vectors** can be initialised using $\mu = 0$ and $\lambda = \gamma = (1 + \|\nabla f(x_0)\|)$.[1]

For the **slack variables**, $r = s = \frac{1}{2}(L_u - L_l) < 0$ is chosen as an initial guess.

For the **penalty parameter**, $0.1 \leq \rho \leq 0.5$ may be chosen. A larger number may slow down the iteration process, a lower can cause instability or divergence. The small numbers ϵ_1 and ϵ_2 are chosen as **numerical tolerance value for zero** for the computer implementation. They can be different and are dependent on the number precision of the computer.

B.3.2 Calculate step increments

Calculate the parameters in this order for the k^{th} iteration step

- penalty vectors σ, u and v using (B.21) and (B.20)
- auxiliary parameters $d_1 = L_u - h - s$ and $d_2 = L_l - h + r$ from (B.11)
- equation system parameters A and b using (B.17a) and (B.17b)
- step increments Δx_k, $\Delta \mu_k$, Δr_k, Δs_k, $\Delta \lambda_k$ and $\Delta \gamma_k$ following (B.19), (B.12) and (B.13)

[1] $\|\nabla f(x_0)\| = \sum_{i=1}^{n} \left|\frac{\partial f}{\partial x_i}\right|$, the L_1 *Manhattan* vector norm.

B.3.3 Increment size and step update

In order to calculate the next iteration point, the step size needs to be calculated. For this, two numbers, giving indication of the step size are calculated

$$N_{1,k} = \min\left(\frac{\Delta s_{i,k}}{s_{i,k}}, \frac{\Delta r_{i,k}}{r_{i,k}}\right) \text{ with } i \in [1 \dots m] \tag{B.22a}$$

$$N_{2,k} = \min\left(\frac{\Delta \lambda_{i,k}}{\lambda_{i,k}}, \frac{\Delta \gamma_{i,k}}{\gamma_{i,k}}\right) \text{ with } i \in [1 \dots m] \tag{B.22b}$$

Then the parameters $\beta_{1,k}$ and $\beta_{2,k}$ are calculated, using (B.22a) and (B.22b)

$$\beta_{1,k} = \begin{cases} 1 \text{ if } N_{1,k} \geq -1 \\ \frac{-1}{N_{1,k}} \text{ if } N_{1,k} < -1 \end{cases} \tag{B.23a}$$

$$\beta_{2,k} = \begin{cases} 1 \text{ if } N_{2,k} \geq -1 \\ \frac{-1}{N_{2,k}} \text{ if } N_{2,k} < -1 \end{cases} \tag{B.23b}$$

And finally, set the step update. Assume that the current step number is k and the next step number is $k+1$.

$$\begin{aligned} x_{k+1} &= x_k + \beta_{1,k}\Delta x_k \\ r_{k+1} &= r_k + \beta_{1,k}\Delta r_k \\ s_{k+1} &= s_k + \beta_{1,k}\Delta s_k \\ \mu_{k+1} &= \mu_k + \beta_{2,k}\Delta \mu_k \\ \gamma_{k+1} &= \gamma_k + \beta_{2,k}\Delta \gamma_k \\ \lambda_{k+1} &= \lambda_k + \beta_{2,k}\Delta \lambda_k \end{aligned} \tag{B.24}$$

B.3.4 Termination test

Calculate the following two parameters

$$\sigma = \frac{1}{2m}(\lambda^T s + \gamma^T r) \tag{B.25}$$

$$\nabla \mathfrak{L} = \nabla f + \nabla g \cdot \mu + \nabla h \cdot (\lambda - \gamma) \tag{B.26}$$

Stop the iteration when both conditions $\sigma \leq \epsilon_1$ and the L_1 norm $\|\nabla \mathfrak{L}\| \leq \epsilon_2$ are met. In the other case, continue with subsection B.3.5.

B.3.5 Step adjustment

Start a new iteration step by repeating the calculation from subsection B.3.2 if both $N_1 \geq -0.995$ and $N_2 \geq -0.995$. Otherwise, first adjust all variables with the following set of expression before going back to subsection B.3.2.

$$\begin{aligned}
x_{k+1} &= x_k - 0.005 \cdot \Delta x_k \\
r_{k+1} &= r_k - 0.005 \cdot \Delta r_k \\
s_{k+1} &= s_k - 0.005 \cdot \Delta s_k \\
\mu_{k+1} &= \mu_k - 0.005 \cdot \Delta \mu_k \\
\gamma_{k+1} &= \gamma_k - 0.005 \cdot \Delta \gamma_k \\
\lambda_{k+1} &= \lambda_k - 0.005 \cdot \Delta \lambda_k
\end{aligned} \tag{B.27}$$

Appendix C

Admittance matrix and branch powers

The expressions of the active and reactive power flowing out of the arbitrary AC node to the (passive) grid branches (overhead lines, underground cables, power transformers, phase shifting transformers) are developed.

The generic AC grid has a total of n_b buses, n_l branches between two buses and n_s shunt elements.

This appendix, contrarily to all other chapters in this manuscript, extensively uses complex numbers, their rms values and phase angles, using the chosen notation convention.

$$\overline{z} = \Re(z) + \jmath\Im(z) = z \cdot e^{\jmath\varphi} = z\cos(\varphi) + \jmath z\sin(\varphi) \tag{C.1}$$

The complex conjugate of a number is written with a star ($z^\star$).

C.1 General scheme

A distinction is made between 2-bus branches, connecting two different buses of the AC network to exchange electrical power, and passive shunt elements (e.g.

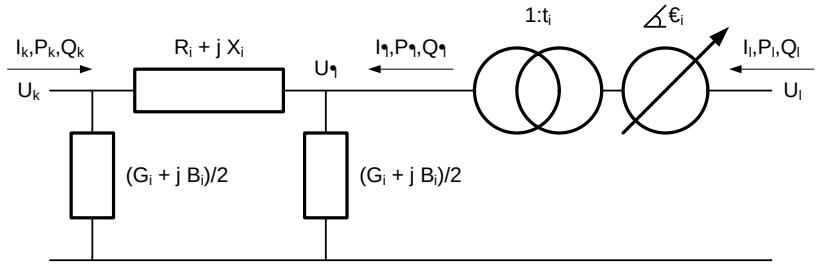

Figure C.1: Generic AC branch used for the Power Flow equations

capacitor banks, shunt reactors) usually installed with the purpose to absorb or generate reactive power or to energise long overhead lines.

C.1.1 2-bus branch

Figure C.1 shows the operating scheme for the 2-bus branch. The general scheme for a passive AC branch with index i, connected between buses k and l, is based on a Π-model for the shunt and series impedances of the branch. The model is completed with an ideal transformer (in-phase transformation of voltages and currents) and an ideal phase-shifting transformer introducing an angle shift but no amplitude change of voltage and current. In practice, physical phase shifting transformers of the asymmetrical type have usually a regulation in quadrature, consequently, voltage amplitudes vary when changing angles.

This general model, used in most textbooks, is asymmetrical, i.e. except for linear assets, the bus indices to which this branch is connected, cannot be swapped although in general, power transformers and some types of phase shifting transformers show, in per unit, a symmetrical impedance.

The complex transformation ratio k_i is used to combine the transformation ratio t_i and the phase shift α_i and is introduced for easy reading:

$$\overline{k}_i = t_i \cdot e^{\jmath\alpha_i} \tag{C.2a}$$

$$\overline{k}_i^{\star} = t_i \cdot e^{-\jmath\alpha_i} \tag{C.2b}$$

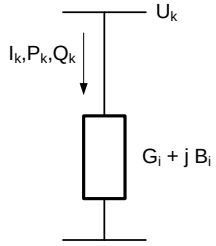

Figure C.2: Generic shunt branch

The ideal transformation of current and voltage between node l and the auxiliary node $l^{'}$ is

$$\begin{cases} \overline{U}_l = \overline{k} \cdot \overline{U}_l^{'} \\ \overline{I}_l = \frac{1}{\overline{k}^*} \overline{I}_l^{'} \end{cases} \tag{C.3}$$

To reduce the size of the equations, the half shunt admittance $\overline{Y}_{sh,i}$ and series admittance $\overline{Y}_{se,i}$ of the branch i are defined:

$$\overline{Y}_{sh,i} = \frac{1}{2}\left(G_i + \jmath B_i\right) \tag{C.4a}$$

$$\overline{Y}_{se,i} = \frac{1}{R_i + \jmath X_i} \tag{C.4b}$$

When dealing with an overhead line or underground cable, the transformation ratio is set $t_i = 1$ and the angle $\alpha_i = 0$. Normal power transformers used in an off-nominal tap position have a ratio $t_i \neq 1$ and $\alpha_i = 0$. There is no need to specify the fixed angle shift (e.g. the $-30°$ for an YNd11 vector group transformer in a pure per-unit environment). Usually for power and phase shifting transformers, the magnetising branch can be omitted. In most power flow and optimal power flow cases, their admittance is relatively small compared to the other admittances.

C.1.2 Shunt branches

Passive shunt elements are treated in a similar (but simpler) way as the 2-bus branches. Figure C.2 gives the notation and flow conventions. The admittance $\overline{Y}_{s,i}$ is

$$\overline{Y}_{s,i} = G_{s,i} + \jmath B_{s,i} \tag{C.5}$$

C.2 Implementation

In order to develop the expressions for active and reactive power flowing to other buses and into the connected shunts of the arbitrary bus k, first the expressions for the current going into each individual branch and shunt element are written. With these equations, the so-called admittance matrix is constructed by adding all contributions in a structured way. Finally, the desired active and reactive powers are calculated.

C.2.1 Connection matrix

An interesting form to express the connection of shunt branches, but also generators and loads, to the corresponding AC nodes, is the construction of a so-called connection matrix. In the most general way, consider a vector of n_x variables (e.g. shunt admittances or active generator output). The (complex) variable x_j belongs to the j^{th} element in that series. Each element is connected to a particular node in the network i (e.g. in the vector of bus voltages or active power injections), with n_y elements.

The connection matrix, with size $(n_y \times n_x)$, contains n_x columns. All elements are zero, except for the one in the column corresponding to the node where the element is connected, being 1.

$$\left[\overline{Y}\right] = \begin{bmatrix} \vdots \\ \overline{y}_i \\ \vdots \end{bmatrix} = \begin{matrix} \\ i^{th} \end{matrix} \begin{matrix} \overset{j^{th}}{\begin{bmatrix} \vdots \\ 1 \\ \vdots \end{bmatrix}} \end{matrix} \cdot \begin{bmatrix} \vdots \\ \overline{x}_j \\ \vdots \end{bmatrix}$$

$$= [C] \cdot \left[\overline{X}\right] \tag{C.6}$$

This expression is a compact method to transfer the values in the dedicated column vector to the right node in the grid. This manuscript uses several instances for this connection vector: C_g for the generator values, C_s for the shunt branches and finally C_l for the network loads.

When writing the equation for one node i, it is obvious that all elements connected to that node are summed.

$$\begin{aligned} [\overline{y}_i] &= [C_{ij}] \cdot [\overline{x}_j] \\ &= \sum_{j=1}^{n_x} C_{ij} \overline{x}_j \end{aligned} \tag{C.7}$$

There is no clear way to invert this operation. One cannot calculate the contributions of the different elements on the same node once the calculation is completed and the total result for that node is determined. The inverse of these connection matrices C does not exists.

C.2.2 2-bus branch

The currents going from the nodes k and l into the branch i are, after rewriting to ease the transcription into a matrix:

$$\begin{aligned} \overline{I}_k &= \overline{Y}_{sh,i}\overline{U}_k + \overline{Y}_{se,i}\left(\overline{U}_k - \overline{U}_l^{'}\right) \\ &= \left(\overline{Y}_{sh,i} + \overline{Y}_{se,i}\right)\overline{U}_k - \overline{Y}_{se,i}\overline{U}_l^{'} \\ &= \left(\overline{Y}_{sh,i} + \overline{Y}_{se,i}\right)\overline{U}_k - \frac{\overline{Y}_{se,i}}{\overline{k}_i}\overline{U}_l \end{aligned} \tag{C.8a}$$

$$\begin{aligned}\overline{I}_l &= \frac{1}{\overline{k}_i^\star}\left(\overline{Y}_{sh,i}\overline{U}_l^{'} + \overline{Y}_{se,i}\left(\overline{U}_l^{'} - \overline{U}_k\right)\right)\\ &= \frac{1}{\overline{k}_i^\star}\left(-\overline{Y}_{se,i}\overline{U}_k + \frac{\overline{Y}_{sh,i}+\overline{Y}_{se,i}}{k_i}\overline{U}_l\right)\\ &= -\frac{\overline{Y}_{se,i}}{\overline{k}_i^\star}\overline{U}_k + \frac{\overline{Y}_{sh,i}+\overline{Y}_{se,i}}{t_i^2}\overline{U}_l \end{aligned} \tag{C.8b}$$

or are expressed in matrix notation

$$\begin{bmatrix} \overline{I}_k \\ \overline{I}_l \end{bmatrix} = \begin{bmatrix} \overline{Y}_{sh,i}+\overline{Y}_{se,i} & -\frac{\overline{Y}_{se,i}}{k_i} \\ -\frac{\overline{Y}_{se,i}}{\overline{k}_i^\star} & \frac{\overline{Y}_{sh,i}+\overline{Y}_{se,i}}{t_i^2} \end{bmatrix} \cdot \begin{bmatrix} \overline{U}_k \\ \overline{U}_l \end{bmatrix} \tag{C.9}$$

From (C.9) a new equation is derived where the column vectors (still complex numbers) have a length n_b.

$$\begin{bmatrix} \vdots \\ \overline{I}_k \\ \vdots \\ \overline{I}_l \\ \vdots \end{bmatrix} = \begin{array}{c} \\ k^{th} \\ \\ l^{th} \\ \\ \end{array} \begin{bmatrix} & k^{th} & & l^{th} & \\ \vdots & \vdots & & \vdots & \\ \cdots & \overline{Y}_{sh,i}+\overline{Y}_{se,i} & \cdots & -\frac{\overline{Y}_{se,i}}{\overline{k}_i} & \cdots \\ \vdots & \vdots & & \vdots & \\ \cdots & -\frac{\overline{Y}_{se,i}}{\overline{k}_i^\star} & \cdots & \frac{\overline{Y}_{sh,i}+\overline{Y}_{se,i}}{t_i^2} & \cdots \\ \vdots & \vdots & & \vdots & \end{bmatrix} \cdot \begin{bmatrix} \vdots \\ \overline{U}_k \\ \vdots \\ \overline{U}_l \\ \vdots \end{bmatrix}$$

$$= \overline{\mathbf{Y}}_i \cdot \begin{bmatrix} \vdots \\ \overline{U}_k \\ \vdots \\ \overline{U}_l \\ \vdots \end{bmatrix} \tag{C.10}$$

The admittance matrix $\overline{\mathbf{Y}}_i$ is a square $(n_b \times n_b)$ asymmetrical matrix. All elements are zero, except for the elements shown in the equation. For both vectors, the values on the k^{th} and l^{th} rows are currents coming out and voltages of the corresponding buses k and l into the branch i.

C.2.3 Shunt branches

A similar procedure is followed for the shunt elements. First, all shunt admittances that are connected to the same node k (for the case should there be more than one), are summed to emulate in one single unit for each node of the AC network:

$$\overline{I}_{s,k} = \sum_i \overline{Y}_{s,ki} \overline{U}_k \tag{C.11}$$

with $i \in \{\text{index subset of AC shunt branches connected to node } k\}$.

Secondly, a similar matrix construction as for the 2-bus branches is made where again, all elements except for those shown are zero.

$$\begin{bmatrix} \vdots \\ \overline{I}_k \\ \vdots \end{bmatrix} = {}^{k^{th}} \begin{bmatrix} & \overset{k^{th}}{\vdots} & \\ \dots & \overline{Y}_{s,k} & \dots \\ & \vdots & \end{bmatrix} \cdot \begin{bmatrix} \vdots \\ \overline{U}_k \\ \vdots \end{bmatrix}$$

$$= \overline{\mathbf{Y}}_{s,k} \cdot \begin{bmatrix} \vdots \\ \overline{U}_k \\ \vdots \end{bmatrix} \tag{C.12}$$

For each node k, the shunt admittance matrix $\overline{\mathbf{Y}}_{s,k}$ (of size $(n_b \times n_b)$) is formed and contains one non-zero element of the diagonal.

C.2.4 Combining everything

The admittance matrices from (C.10) and (C.12) are still only for one particular branch or shunt element. They represent one 'layer' of the complete admittance matrix, which is the sum of all these individual layers . The vector $\overline{\mathbf{I}}_{br}$ gives, for each node k, the current flowing out of the node in the connected branches and shunts. $\overline{\mathbf{U}}$ is the vector of (complex) bus voltages.

$$\begin{aligned}\overline{\mathbf{I}}_{br} &= \left[\sum_{i=1}^{n_l} \overline{\mathbf{Y}}_i + \sum_{k=1}^{n_s} \overline{\mathbf{Y}}_{s,k}\right] \overline{\mathbf{U}} \\ &= \overline{\mathbf{Y}}_{br} \cdot \overline{\mathbf{U}} \end{aligned} \tag{C.13}$$

A transcription of (C.13) using amplitudes and argument angle for the admittance matrix and the bus voltage vectors yields:

$$\begin{aligned}\left[\overline{I}_{br,k}\right] &= \left[Y_{kl} e^{\jmath\varphi_{kl}}\right] \cdot \left[U_l e^{\jmath\theta_l}\right] \\ \overline{I}_{br,k} &= \sum_{l=1}^{n_b} Y_{kl} e^{\jmath\varphi_{kl}} U_l e^{\jmath\theta_l} \end{aligned} \tag{C.14}$$

The worked-out matrix sum for the branch current of node k is

$$\overline{I}_{br,k} = \sum_{l=1}^{n_b} Y_{kl} U_l e^{\jmath(\varphi_{kl}+\theta_l)} \tag{C.15}$$

Finally, the apparent branch powers are calculated (C.16) and by splitting this expression into its real and imaginary parts, the desired result is obtained:

$$\begin{aligned}\overline{S}_{br,k} &= \overline{U}_k \overline{I}^{\star}_{br,k} \\ &= U_k e^{\jmath\theta_k} \sum_{l=1}^{n_b} Y_{kl} U_l e^{-\jmath(\varphi_{kl}+\theta_l)} \\ &= \sum_{l=1}^{n_b} Y_{kl} U_k U_l e^{\jmath(\theta_k-\theta_l-\varphi_{kl})} \end{aligned} \tag{C.16}$$

$$P_{br,k} = \sum_{l=1}^{n_b} Y_{kl} U_k U_l \cos\left(\theta_k - \theta_l - \varphi_{kl}\right) \tag{C.17a}$$

$$Q_{br,k} = \sum_{l=1}^{n_b} Y_{kl} U_k U_l \sin\left(\theta_k - \theta_l - \varphi_{kl}\right) \tag{C.17b}$$

Appendix D

Converter loss model

In this appendix, the converter loss model, (5.6) is derived to its state variable parameters to be implemented in the Jacobian and the Hessian matrices.

The non-linear equality constraint for converter i, connected to the AC bus l and with AC generator index k is

$$g_i(x) = P_k - P_{conv,i} + a_i + b_i \frac{\sqrt{P_k^2 + Q_k^2}}{V_{m,l}} + (c_i + r_i) \frac{P_k^2 + Q_k^2}{V_{m,l}^2} = 0 \tag{D.1}$$

The first derivatives of equation (D.1) to all its parameters are

$$\frac{\partial g_i(\mathbf{x})}{\partial P_{conv,i}} = -1 \tag{D.2a}$$

$$\frac{\partial g_i(\mathbf{x})}{\partial P_k} = -1 + b_i \frac{P_k}{V_{m,l}\sqrt{P_k^2 + Q_k^2}} + (c_i + r_i) \frac{2P_k}{V_{m,l}^2} \tag{D.2b}$$

$$\frac{\partial g_i(\mathbf{x})}{\partial Q_k} = b_i \frac{Q_k}{V_{m,l}\sqrt{P_k^2 + Q_k^2}} + (c_i + r_i) \frac{2Q_k}{V_{m,l}^2} \tag{D.2c}$$

$$\frac{\partial g_i(\mathbf{x})}{\partial V_{m,l}} = -b_i \frac{\sqrt{P_k^2 + Q_k^2}}{V_{m,l}^2} - 2\,(c_i + r_i) \frac{P_k^2 + Q_k^2}{V_{m,l}^3} \tag{D.2d}$$

With these expressions, the Jacobian matrix for the converter loss models $\mathbf{J}_{conv}(\mathbf{x}) = \left[\frac{\partial g_i}{\partial x_j}\right]$ is constructed. All the other derivatives are zero.

Finally, the matrix $\mathbf{H}_{conv,i}(\mathbf{x}) = \left[\frac{\partial^2 g_i}{\partial x_j \partial x_k}\right]$ of all second derivatives of the function vector $\mathbf{g}_{conv}(\mathbf{x})$ is constructed for each converter i with the following non-zero elements

$$\frac{\partial^2 g_i(\mathbf{x})}{\partial P_k^2} = \frac{b_i}{V_{m,l}} \frac{Q_k^2}{\sqrt{\left(P_k^2 + Q_k^2\right)^3}} + 2\left(c_i + r_i\right) \frac{1}{V_{m,l}^2} \tag{D.3a}$$

$$\frac{\partial^2 g_i(\mathbf{x})}{\partial Q_k^2} = \frac{b_i}{V_{m,l}} \frac{P_k^2}{\sqrt{\left(P_k^2 + Q_k^2\right)^3}} + 2\left(c_i + r_i\right) \frac{1}{V_{m,l}^2} \tag{D.3b}$$

$$\frac{\partial^2 g_i(\mathbf{x})}{\partial P_k \partial Q_k} = -\frac{b_i}{V_{m,l}} \frac{P_k Q_k}{\sqrt{\left(P_k^2 + Q_k^2\right)^3}} \tag{D.3c}$$

$$\frac{\partial^2 g_i(\mathbf{x})}{\partial V_{m,l}^2} = 2 b_i \frac{\sqrt{P_k^2 + Q_k^2}}{V_{m,l}^3} + 6\left(c_i + r_i\right) \frac{P_k^2 + Q_k^2}{V_{m,l}^4} \tag{D.3d}$$

$$\frac{\partial^2 g_i(\mathbf{x})}{\partial P_k \partial V_{m,l}} = -b_i \frac{P_k}{V_{m,l}^2 \sqrt{P_k^2 + Q_k^2}} - 4\left(c_i + r_i\right) \frac{P_k}{V_{m,l}^3} \tag{D.3e}$$

$$\frac{\partial^2 g_i(\mathbf{x})}{\partial Q_k \partial V_{m,l}} = -b_i \frac{Q_k}{V_{m,l}^2 \sqrt{P_k^2 + Q_k^2}} - 4\left(c_i + r_i\right) \frac{Q_k}{V_{m,l}^3} \tag{D.3f}$$

Appendix E

OPF Model structure and functions

The extended optimal power flow structure and the developed functions are explained, as a guide for the user of the routines. Table E.1 gives an overview of the different field names and indicates MatPower fields and which data fields parameterise new functionalities. The reader is referred to the MatPower documentation [44] for the use of these fields. These fields are indicated with a star (*) in the MP column. The meaning and use of each field is explained in alphabetical order. The last section gives an overview of the routines developed for this research.

E.1 Cost function definition

The cost function routine automatically sums all required cost functions. The user can add as much cost functions as desired. Table E.2 gives the overview of the different fields (columns in the `.cost` matrix).

Field 1, the cost function primitive, is an ordinal number taken from table E.3. When n_c is the number of cost functions specified in the `.cost` matrix, then, following the symbol conventions of table E.2, the resulting cost function is constructed:

$$f = \sum_{i=1}^{n_c} w_i \cdot f_{s,i} \left(f_i(\mathbf{x}) - f_{o,i} \right) \tag{E.1}$$

Table E.1: OPF case structure

Field	MP	Description
`.baseMVA`	*	Reference power base. Default = 100MVA
`.branch`	*	AC branch specifications and OPF results
`.bus`	*	AC bus specifications and OPF results
`.gen`	*	AC generator specifications and OPF results
`.gencost`	*	AC generator cost functions
`.version`	*	MATPOWER versioning parameter
`.x`	*	Resulting state variable vector of the OPF calculation. This field can be used to start the OPF algorithm. See field `.start`
`.cost`		Cost function parameters
`.inc`		(Incident Recovery Tool) Grid incident to investigate
`.reg`		(Incident Recovery Tool) Control possibilities of the OPF solver for generators and converters
`.secopf`		Definition of the requested contingency states
`.set`		Generators and converters where active power output is unaltered from previous saved solution
`.start`		Start from previous solution saved in this structure as field `.x`
`.vsc`		DC network and AC/DC converter definitions and OPF results

E.2 Grid incident to investigate

The `.inc` field is only treated by the reliability improvement routine, described in section 6.3. It may specify only one incident on the AC grid: outage of a branch or an AC generator. The routine for the incident recovery warns the user when multiple incidents have been selected, when the incident corresponds to a contingency state or when DC branches or converters are specified.

To specify an AC generator to be outaged, the field `.inc.gen` must contain the ordinal number of that generator. When playing the incident on an AC branch, the field `.inc.branch` gets its ordinal number.

Table E.2: Cost parameter field

Field number	Symbol	Description
1		Serial number of the cost function primitive
2	w_i	Weighting factor for the cost function
3	$f_{s,i}$	Scaling factor for the cost function
4	$f_{o,i}$	Linear offset of the cost function
5		(Result) unweighted cost function result for the found solution

Table E.3: Ordinal number of the cost function primitives

Ordinal	Description
00	Feasibility
01	Active AC power generation cost of all generators, as defined by MatPower
02	Sum of all AC generator active power output
11	Sum of all AC generator reactive power output
12	Squared sum of the AC bus voltage deviations from their upper limit
31	Automatically added when fixed generator active power output and bus voltage are requested by the `.fix` field
32	Automatically added when fixed converter active power output and bus voltage are requested by the `.fix` field

E.3 Operator control possibilities

As the `.inc`, described in previous section, the `.reg` field is also only treated by the incident recovery tool. This field is structured in the following way:

- Field `.reg.gen` needs to contain a linear list with the ordinal numbers of the generators which may be varied in active power and bus voltage amplitude by the OPF solver, emulating the control possibilities of the network operator.
- Field `.reg.vsc` contains a linear list with the ordinal numbers of the AC/DC converters, likewise the AC generators.

A careful choice of the controllable AC generators and converters needs to made, as the algorithm considers that the AC slack bus generators and the AC/DC reference converter are always controllable.

E.4 Contingency states

Only AC generators and AC branches can be specified as being a contingency state in the current version of the program. These states can be given in the `.secopf` field:

- `.secopf.gen` contains a linear list of the ordinal numbers of those AC generators to be taken into consideration for the security constrained OPF calculation. Outaging generators are treated using curative security constraints.
- `.secopf.branch` holds a linear list of the ordinal numbers of those AC branches for the curative and preventive security constraints.
- `.secopf.ohl`: overload factor for overhead lines and underground cables in contingency states. Default value = 1.5
- `.secopf.tfo`: overload factor for transformers in contingency states. Default value = 1.2

E.5 Setpoints for generators and converters

With the field `.set`, the user can specify those AC generators and converters, with settings for AC active power output and bus voltage amplitude not to be changed by the OPF solver (section 6.3). For both generators and converters, the routine takes the values for active power and bus voltage amplitude from the `.gen` and `.vsc.gen` fields from the columns where the OPF results for these fields are stored. It is however not necessary to start from a previous converged state: the user may already fill out these fields before any other calculation.

- `.set.gen`, the list with the ordinal numbers of the AC generators
- `.set.vsc`, the list with the ordinal numbers of the AC/DC converters

Table E.4: DC network data structure

Field	Description
`.active`	Control field to indicate that the DC network has been correctly read in
`.conn`	Structure for the topology and branch specifications of the DC network
`.gen`	Structure for the AC/DC converter specifications
`.model`	Field to specify the modeling method of the DC network
`.ref`	Field to specify the DC reference bus and its reference voltage
`.Umin`	Field to specify the minimum voltage of the DC nodes
`.Umax`	Field to specify the maximum voltage of the DC nodes

E.6 Starting from a previous converged state

The presence of the `.start` field in the OPF case, regardless of its value, triggers the routine to compile a starting position for the actual case and take that as the initial position. The starting position is taken from the `.x` field directly. A warning is issued when this `.x` field is not present or if it corresponds to a non-converged solution.

E.7 Topology of the DC grid and AC/DC converters

The complete DC network and the AC/DC converters are specified in the `.vsc` structure. Table E.4 gives the overview of all fields and their functions. Hereunder, a detailed description of each field and variable is given.
The `vsc.active` field is used for internal coordination. The presence of this field, no matter the value, indicates to the algorithm that the equivalent AC generators have been added to the `.gen` and the `.gencost` fields and that, when applicable, their bus type conversion (from PQ node to PV node) has already been done.

All information about the VSC converter present in the network is assembled in the `.vsc.gen` field. It has a matrix structure, each row representing a distinct

Table E.5: Column structure of the `.vsc.gen` field

Column	Result	Description
1		Ordinal number of the AC to which the converter is connected to
2		Factor a of the converter loss model
3		Factor b of the converter loss model
4		Factor $c+r$ of the converter loss model in **rectifier** mode
5		Factor $c+r$ of the converter loss model in **inverter** mode
6		Maximum active AC converter power in MW
7		Maximum reactive AC converter power in $MVar$
8		Maximum DC converter power in MW
9	*	Ordinal number of the converter AC equivalent generator
10	*	Active AC power output
11	*	Reactive AC power output
12	*	DC power extracted from the DC grid
13	*	AC bus voltage amplitude
14	*	DC bus voltage

converter. The column overview for data and results are given by the table E.5.

The DC grid topology, together with the resistive components of the branches and OPF results are stored in the `.vsc.conn` field. The column overview is given in table E.6.

The `.vsc.model` specifies the DC network model to be used by the optimisation algorithm. It is an optional field. When `.vsc.model = 1` or when this field is not present in the structure, the model described in section 5.4 is used. Only when this field is present and its value is `.vsc.model = 2` the alternative method described in section 5.5 is used.

The `.vsc.ref` contains 2 values and is an optional field. When this field is present in the `.vsc` structure, the first value specifies the DC reference bus and the second value its reference voltage setting (in pu). When this field is not present, no reference bus is taken into account.

The `.vsc.Umin` and `.vsc.Umax` fields contain the minimum and the maximum

Table E.6: Column structure of the `.vsc.conn` field

Column	Result	Description
1		DC *from*-bus of the DC branch
2		DC *to*-bus of the DC branch
3		Resistive component of the DC branch, in *pu*
4		Maximum branch loading, in *MW*
5	*	DC power flowing into the *from*-side of the branch
6	*	DC power flowing into the *to*-side of the branch
7	*	DC bus voltage of the *from*-bus
8	*	DC bus voltage of the *to*-bus

voltage limit respectively for each DC node, expressed in *pu*. Their default values are 0.7 and 1.05 *pu*.

E.8 Routine overview

Tables E.7 (for part 1) and E.8 (for part 2) summarise all routines that have been developed during this research. The first column states the function name, the second specifies whether or not that routine is called within every optimisation iteration step or during the pre- or post-processing. The third gives the purpose of that routine.

Table E.7: Matlab routine overview, part 1

Routine	It.	Description
`runopf.m`		Main routine and entry point. Only this routine should be called by the user.
`opf_consfcn.m`	*	Construction of the non-linear constraint vectors and their first derivatives. Wrapper routine to mask the original.
`opf_costfcn.m`	*	Calculation of the cost function and its derivatives. Wrapper routine to mask the original.
`opf_hessfcn.m`	*	Construction of the Hessian summations. Wrapper routine to mask the original.
`cosopf.m`		Preparation the case structure for the use of user-defined cost functions.
`cos_costfcn.m`	*	Construction of the user-defined cost function and its first derivatives.
`cos_hessfcn.m`	*	Construction of the Hessian summation of the user-defined cost function.
`costeval.m`	*	Evaluates the cost for a given case and cost function.
`cost01.m`	*	Calculation of the cost function 01 and construction of its first derivatives.
`cost02.m`	*	Calculation of the cost function 02 and construction of its first derivatives.
`cost11.m`	*	Calculation of the cost function 11 and construction of its first derivatives.
`cost12.m`	*	Calculation of the cost function 12 and construction of its first derivatives.
`cost31.m`	*	Calculation of the cost function 31 and construction of its first derivatives.
`cost32.m`	*	Calculation of the cost function 32 and construction of its first derivatives.
`hess01.m`	*	Construction of the Hessian for cost function 01.
`hess02.m`	*	Construction of the Hessian for cost function 02.
`hess11.m`	*	Construction of the Hessian for cost function 11.
`hess12.m`	*	Construction of the Hessian for cost function 12.
`hess31.m`	*	Construction of the Hessian for cost function 31.
`hess32.m`	*	Construction of the Hessian for cost function 32.

Table E.8: Matlab routine overview, part 2

Routine	It.	Description
`pareto2D.m`		Routine to construct Pareto-fronts for two cost functions.
`pareto3D.m`		Routine to construct Pareto-fronts for three cost functions.
`par_front.m`		Auxiliary routine to select the Pareto-dominant points from a multi-dimensional vector.
`tri_mesh.m`		Auxiliary routine to construct a triangular mesh, used by the `pareto3D.m` routine.
`secopf.m`		Preparation of the case structure for the use of security constraints.
`ext2int.m`		Copies the bus and generator reordering of the original to each contingency case.
`sec_consfcn.m`	*	Construction of the non-linear constraint vectors and their first derivatives when using contingency cases.
`sec_hessfcn.m`	*	Construction of the Hessian summation when using contingency cases.
`sec_cura.m`	*	Routine to evaluate the curative security contingency cases.
`sec_prev.m`		Routine to evaluate the preventive security contingency cases.
`chksecopf.m`		Routine to check the AC branch loading for each contingency case solution in the case structure.
`vscopf.m`		Preparation of the case structure for the use of DC networks.
`vscprep.m`		Auxiliary preparatory routine used by `vscopf.m`
`vsc_consfcn.m`	*	Construction of the non-linear constraint vectors and their first derivatives when DC networks.
`vsc_hessfcn.m`	*	Construction of the Hessian summation when using DC networks.
`printvsc.m`		Routine for printing the DC network results on screen.
`vscaddconv.m`		Routine to add an AC/DC converter to the case structure.
`vscaddconn.m`		Routine to add an DC branch to the case structure.
`inc_rec.m`		Main routine for the incident recovery tool.

Bibliography

[1] J. Skog, H. Van Asten, T. Worzyk, and T. Andersrod, "NorNed, world's longest powercable," in *CIGRE Paris 2010 session, paper B1.106*, 2010.

[2] R. Beune, J. Van Putten, K. Barmsnes, and O. Gjerde, "Interregional market coupling, a challenge for the norned cable," in *CIGRE Paris session 2010, paper C5.103*, 2010.

[3] J. Rimez, J. Limelette, and B. Brijs, "The first Belgian HVDC Link NEMO: technical choices, obstacles and future developments," in *CIGRE Belgium Conference, Brussels*, 2014.

[4] Amprion, "Infoflyer: Ausbau der Umspannanlage Oberzier, Planung eines Konverters für die Stromverbindung ALEGrO nach Belgien," Online, www.amprion.net/sites/default/files/pdf/Flyer_Alegro_Konverter.pdf, June 2013.

[5] P. Francos, S. Verdugo, and S. Guyomarch, "New french-spanish VSC link," in *CIGRE Paris 2012 session, paper B4.110*, 2012.

[6] CIGRE Joint Working group C4/B4/C1-604, "Influence of embedded HVDC transmission on system security and AC network performance, technical brochure 536," Paris, 2013.

[7] V. C. Billon, J. Taisne, V. Arcidiacono, and F. Mazzoldi, "The Corsican tapping: from design to commissioning tests of the third terminal of the Sardinia-Corsica-Italy HVDC," *Power Delivery, IEEE Transactions on*, vol. 4, no. 1, pp. 794–799, 1989.

[8] W. Long and S. Nilsson, "HVDC transmission: yesterday and today," *Power and Energy Magazine*, vol. 5, no. 2, pp. 22–31, 2007.

[9] Svenska Kraftnet, "Kort om sydvästlänken, informationsblad," Online, www.svk.se/Global/03_Projekt/Pdf/SydVastlanken/Faktablad_sydvastlanken_20130124.pdf, January 2013.

[10] Netzentwicklungsplan STROM, "Fact sheet german grid development plan 2013," Online, www.netzentwicklungsplan.de, July 2013.

[11] ENSTO-e, "Network Code on HVDC Connections," Online, www.entsoe.eu/major-projects/network-code-development/high-voltage-direct-current/, 2011.

[12] CIGRE Working group B4-52, "HVDC grid feasibility study, technical brochure 533," Paris, 2012.

[13] P. Adam and J. Kowal, "Medgrid — An industrial initiative for the development of interconnections between the Mediterranean power grids," in *Power Electronics and Applications (EPE), 15th European Conference on.* IEEE, 2013, pp. 1–10.

[14] D. Van Hertem and M. Ghandhari, "Multi-terminal VSC HVDC for the european supergrid: Obstacles," *Renewable and Sustainable Energy Reviews*, vol. 14, no. 9, pp. 3156 – 3163, 2010. [Online]. Available: http://www.sciencedirect.com/science/article/pii/S1364032110002480

[15] A. A. van der Meer, R. T. Pinto, M. Gibescu, P. Bauer, J. T. Pierik, F. D. Nieuwenhout, R. L. Hendriks, W. L. Kling, and G. A. van Kuik, "Offshore transnational grids in europe: The north sea transnational grid research project in relation to other research initiatives," in *9th International Workshop on Large-Scale Integration of Wind Power*, 2010, pp. 18–19.

[16] G. Asplund, B. Jacobson, B. Bergren, and K. Lindén, "Continental overlay HVDC-grid," in *CIGRE Paris 2010 session, paper B4.109*, 2010.

[17] S. Cole, K. Karoui, T. Vrana, O. Fosso, J. Curis, A. Denis, and C. Liu, "A european supergrid: present state and future challenges," in *17th Power Systems Computation Conference, Stockholm*, 2011.

[18] A. Aguado, "Towards a European supergrid." PSCC, 2011.

[19] M. Aragüés-Peñalba, A. Egea-Alvarez, O. Gomis-Bellmunt, and A. Sumper, "Optimum voltage control for loss minimization in HVDC multi-terminal transmission systems for large offshore wind farms," *Electric Power Systems Research*, vol. 89, pp. 54–63, 2012.

[20] Atlantic Wind Connection, "Fact Sheet New Jersey Energy Link," Online, atlanticwindconnection.com/resources, January 2013.

[21] T. Langeland, Y. Yang, and C. Öhlen, "Risk based approach for development of offshore hvdc transmission technologies," in *European Wind Energy Association, Annual conference of.* EWEA, 2012.

[22] R. Zimmerman, C. Murillo-Sánchez, and R. Thomas, "MATPOWER: Steady-state operations, planning, and analysis tools for power systems research and education," *Power Systems, IEEE Transactions on*, vol. 26, no. 1, pp. 1–8, 2011.

[23] R. Rudervall, J. Charpentier, and R. Sharma, "High voltage direct current (HVDC) transmission systems technology review paper," *Energy Week*, vol. 2000, 2000.

[24] A. Nekrasov and A. Posse, "Work done in the soviet union on high-voltage long-distance dc power transmission," *Transaction of the AIEE: Power Apparatus and Systems, part III*, vol. 78, no. 3, pp. 515–521, 1959.

[25] P. Kundur, N. Balu, and M. Lauby, *Power System Stability and Control*, ser. EPRI: Power Systems Engineering. New York: McGraw-Hill, 1994, no. ISBN: 0-07-035958-X.

[26] U. Axelsson, A. Holm, C. Liljegren, K. Eriksson, and L. Weimers, "Gotland HVDC light transmission-world's first commercial small scale DC transmission," in *CIRED Conference, Nice, France*, vol. 32, 1999.

[27] S. Teeuwsen and R. Rossel, "Dynamic performance of the 1000 MW BritNed HVDC interconnector project," in *Power Engineering Society General Meeting*. IEEE, 2010, pp. 1–8.

[28] P. Jones and L. Stendius, "The challenges of offshore power system construction – Troll A, electrical power delivered successfully to an oil and gas platform in the North Sea," *EWEC, Athens*, 2006.

[29] V. Botan, J. Waldmeyer, M. Kunow, and K. Akurati, "Six inch thyristors for UHVDC transmission," in *PCIM Europe 2010*, 2010.

[30] L. Zehong, G. Liying, W. Zuli, Y. Jun, Z. Jin, and L. Licheng, "R&D progress of 1100 kV UHVDC technology," in *CIGRE Paris 2012 session, paper B4.201*, 2012.

[31] C. Harvey, K. Stenseth, and M. Wohlmuth, "The Moyle HVDC interconnector: project considerations, design and implementation," in *AC-DC Power Transmission, 7th International Conference on (Conf. Publ. No. 485)*. IET, 2001, pp. 145–149.

[32] G. Daelemans, K. Srivastava, M. Reza, S. Cole, and R. Belmans, "Minimization of steady-state losses in meshed networks using VSC HVDC," in *Power Engineering Society General Meeting*. IEEE, 2009, pp. 1–5.

[33] J. Graham, T. Holmgren, P. Fischer, and N. Shore, "The Rio Madeira HVDC System, Design aspects of Bipole 1 and the connector to Acre-Rondonia," in *CIGRE Paris 2012 session, paper B4.111*, 2012.

[34] N. Flourentzou, V. G. Agelidis, and G. D. Demetriades, "VSC-based HVDC power transmission systems: an overview," *Power Electronics, IEEE Transactions on*, vol. 24, no. 3, pp. 592–602, 2009.

[35] P. Haugland, "It's time to connect: Technical description of HVDC light® technology," ABB, Tech. Rep., 2006.

[36] B. Jacobson, B. Westman, and M. Bahrman, "500 kV VSC transmission system for lines and cables," in *Proc. CIGRE B4 Colloquium, San Francisco, USA*, 2012.

[37] N. Mohan, T. M. Undeland, and W. Robbins, *Power electronics: converters, applications, and design*. Wiley, 2003.

[38] D. Das, J. Pan, and S. Bala, "HVDC Light for large offshore wind farm integration," in *Power Electronics and Machines in Wind Applications (PEMWA)*. IEEE, 2012, pp. 1–7.

[39] B. Stott and O. Alsaç, "Optimal power flow–basic requirements for real-life problems and their solutions," in *SEPOPE XII Symposium, Rio de Janeiro, Brazil*, 2012.

[40] J. A. Momoh, *Electric power system applications of optimization*. CRC Press, 2001, vol. 11.

[41] J. D. Weber, "Implementation of a Newton-based optimal power flow into a power system simulation environment," Ph.D. dissertation, University of Illinois, 1997.

[42] D. P. Bertsekas, *Nonlinear programming*. Athena Scientific, 1999.

[43] N. S. Rau, *Optimization principles: practical applications to the operation and markets of the electric power industry*. John Wiley & Sons, Inc., 2003.

[44] R. D. Zimmerman and C. E. Murillo-Sánchez, "MATPOWER 4.1 User's Manual," *Power Systems Engineering Research Center (PSERC)*, 2011.

[45] R. H. Byrd, J. Nocedal, and R. A. Waltz, "KNITRO: An integrated package for nonlinear optimization," in *Large-scale nonlinear optimization*. Springer, 2006, pp. 35–59.

[46] D. W. Marquardt, "An algorithm for least-squares estimation of nonlinear parameters," *Journal of the Society for Industrial & Applied Mathematics*, vol. 11, no. 2, pp. 431–441, 1963.

[47] R. D. Zimmerman, C. E. Murillo-Sánchez, and R. J. Thomas, "MATPOWER's extensible optimal power flow architecture," in *Power Engineering Society General Meeting*. IEEE, 2009, pp. 1–7.

[48] W. Rosehart, A. Schellenberg, and C. Roman, "New tools for power system dynamic performance management," in *Power Engineering Society General Meeting*. IEEE, 2006, pp. 7–14.

[49] H. Wang, C. E. Murillo-Sánchez, R. D. Zimmerman, and R. J. Thomas, "On computational issues of market-based optimal power flow," *Power Systems, IEEE Transactions on*, vol. 22, no. 3, pp. 1185–1193, 2007.

[50] H. Wang, "On the computation and application of multi-period security-constrained optimal power flow for real-time electricity market operations," Ph.D. dissertation, Cornell University, 2007.

[51] M. Bjelogrlic, M. S. Calovic, P. Ristanovic, and B. Babic, "Application of Newton's optimal power flow in voltage/reactive power control," *Power Systems, IEEE Transactions on*, vol. 5, no. 4, pp. 1447–1454, 1990.

[52] S. Ge and T. Chung, "Optimal active power flow incorporating power flow control needs in flexible AC transmission systems," *Power Systems, IEEE Transactions on*, vol. 14, no. 2, pp. 738–744, 1999.

[53] S. Teerathana and A. Yokoyama, "An optimal power flow control method of power system using interline power flow controller (IPFC)," in *TENCON 2004. IEEE Region 10 Conference*, vol. 100. IEEE, 2004, pp. 343–346.

[54] L. Vanfretti, D. Van Hertem, and J. O. Gjerde, *Smart Grids and Sustainable Energy Transformation*. Springer, 2014, ch. A smart transmission grid for Europe: challenges in developing grid enabling technologies.

[55] P. Guha Thakurta, J. Maeght, D. Van Hertem, and R. Belmans, "Increasing Transmission Grid Flexibility of CWE through TSO Coordination to Integrate More Wind Energy Sources while Maintaining System Security," *Sustainable Energy* Special Issue*, IEEE Transactions on*, 2014, submitted.

[56] D. Van Hertem, J. Rimez, and R. Belmans, "Power flow controlling devices as a smart and independent grid investment for flexible grid operations: Belgian case study," *Smart Grid, IEEE Transactions on*, vol. 4, pp. 1656 – 1664, 2013.

[57] J. Warichet, J. Leonard, J. Rimez, O. Bronckart, and J. V. Hecke, "Grid implementation and operational use of large phase shifting transformers in the Belgian HV grid to cope with international network challenges," in *CIGRE Paris session 2010, paper C2.207*, 2010.

[58] G. Li and J. Zhang, "Available Transfer Capability Calculation for AC/DC Systems with VSC-HVDC," in *Electrical and Control Engineering (ICECE), International Conference on.* IEEE, 2010, pp. 3404–3409.

[59] I. Das and J. E. Dennis, "Normal-boundary intersection: A new method for generating the pareto surface in nonlinear multicriteria optimization problems," *SIAM Journal on Optimization*, vol. 8, no. 3, pp. 631–657, 1998.

[60] M. Farina and P. Amato, "A fuzzy definition of optimality for many-criteria optimization problems," *Systems, Man and Cybernetics, Part A: Systems and Humans, IEEE Transactions on*, vol. 34, no. 3, pp. 315–326, 2004.

[61] P. Ngatchou, A. Zarei, and M. El-Sharkawi, "Pareto multi objective optimization," in *Intelligent Systems Application to Power Systems, Proceedings of the 13th International Conference on.* IEEE, 2005, pp. 84–91.

[62] F. Milano, C. A. Cañizares, and M. Invernizzi, "Multiobjective optimization for pricing system security in electricity markets," *Power Systems, IEEE Transactions on*, vol. 18, no. 2, pp. 596–604, 2003.

[63] A. Kumar and W. Gao, "Voltage profile improvement and line loss reduction with distributed generation in deregulated electricity markets," in *TENCON, IEEE Region 10 Conference.* IEEE, 2008, pp. 1–6.

[64] Y. Jin, M. Olhofer, and B. Sendhoff, "Dynamic weighted aggregation for evolutionary multi-objective optimization: Why does it work and how?" in *Genetic and Evolutionary Computation, Conference on*, 2001.

[65] J. G. Vlachogiannis and K. Y. Lee, "Coordinated aggregation particle swarm optimization applied in reactive power and voltage control," in *Power Engineering Society General Meeting.* IEEE, 2006, pp. 6–pp.

[66] F. Zaro and M. Abido, "Multi-objective particle swarm optimization for optimal power flow in a deregulated environment of power systems," in *Intelligent Systems Design and Applications, 2011 11th International Conference on.* IEEE, 2011, pp. 1122–1127.

[67] C. B. M. Oliveira, M. de Medeiros, and J. T. de Oliveira, "New method based in particle swarm optimization for power factor remote control and loss minimization in power systems with wind farms connected," in *Intelligent System Applications to Power Systems. 15th International Conference on.* IEEE, 2009, pp. 1–6.

[68] J. Liao, Wu, "Multi-objective optimization by reinforcement learning for power system dispatch and voltage stability," in *IEEE PES Innovative Smart Grid Technologies Conference Europe (ISGT Europe)*, 2010.

[69] M. Abido, "Multiobjective evolutionary algorithms for electric power dispatch problem," *Evolutionary Computation, IEEE Transactions on*, vol. 10, no. 3, pp. 315–329, 2006.

[70] K. Morison, L. Wang, and P. Kundur, "Power system security assessment," *IEEE Power and Energy Magazine*, vol. 2, no. 5, pp. 30–39, 2004.

[71] D. Layden and B. Jeyasurya, "Integrating security constraints in optimal power flow studies," in *Power Engineering Society General Meeting.* IEEE, 2004, pp. 125–129.

[72] F. Capitanescu, M. Glavic, D. Ernst, and L. Wehenkel, "Applications of security-constrained optimal power flows," in *Modern Electric Power Systems Symposium, Proceedings of*, 2006.

[73] Y. Fu, M. Shahidehpour, and Z. Li, "Security-constrained unit commitment with AC constraints," *Power Systems, IEEE Transactions on*, vol. 20, no. 2, pp. 1001–1013, 2005.

[74] O. Alsaç and B. Stott, "Optimal load flow with steady-state security," *Power Apparatus and Systems, IEEE Transactions on*, no. 3, pp. 745–751, 1974.

[75] K. Karoui, L. Platbrood, H. Crisciu, and R. A. Waltz, "New large-scale security constrained optimal power flow program using a new interior point algorithm," in *Electricity Market, 5th International Conference on European.* IEEE, 2008, pp. 1–6.

[76] S. Grijalva and A. Visnesky, "The effect of generation on network security: Spatial representation, metrics, and policy," *Power Systems, IEEE Transactions on*, vol. 21, no. 3, pp. 1388–1395, 2006.

[77] S. Grijalva, S. R. Dahman, K. J. Patten, and A. M. Visnesky Jr, "Large-scale integration of wind generation including network temporal security analysis," *Energy Conversion, IEEE Transactions on* , vol. 22, no. 1, pp. 181–188, 2007.

[78] H. Gil, M. El Chehaly, G. Joos, and C. Canizares, "Bus-based indices for assessing the contribution of DG to the voltage security margin of the transmission grid," in *Power Engineering Society General Meeting*. IEEE, 2009, pp. 1–7.

[79] F. Milano, C. A. Canizares, and M. Invernizzi, "Voltage stability constrained opf market models considering "N-1" contingency criteria," *Electric Power Systems Research*, vol. 74, no. 1, pp. 27–36, 2005.

[80] A. Alessandri, S. Grillo, S. Massucco, F. Silvestro, and G. Vimercati, "ANN application for on-line power system security assessment," in *Probabilistic Methods Applied to Power Systems, International Conference on*. IEEE, 2006, pp. 1–6.

[81] S. Massucco, S. Grillo, A. Pitto, and F. Silvestro, "Evaluation of some indices for voltage stability assessment," in *PowerTech, IEEE Bucharest*. IEEE, 2009, pp. 1–8.

[82] L. Platbrood, H. Crisciu, C. Merckx, P. Panciatici, S. Fliscounakis, F. Capitanescu, L. Wehenkel, D. Kirschen, and M. Ortega-Vazquez, "Deliverable D3.3: Prototypes for European transmission system steady-state optimisation, PEGASE project," Online, www.fp7pegase.eu/, 2011.

[83] F. Capitanescu, J. L. Martinez Ramos, P. Panciatici, D. Kirschen, A. Marano Marcolini, L. Platbrood, and L. Wehenkel, "State-of-the-art, challenges, and future trends in security constrained optimal power flow," *Electric Power Systems Research*, vol. 81, no. 8, pp. 1731–1741, 2011.

[84] T. Mikolinnas and B. Wollenberg, "An advanced contingency selection algorithm," *Power Apparatus and Systems, IEEE Transactions on*, no. 2, pp. 608–617, 1981.

[85] R. Sunitha, K. Sreerama, and T. M. Abraham, "Development of a composite security index for static security evaluation," in *TENCON 2009-2009 IEEE Region 10 Conference*. IEEE, 2009, pp. 1–6.

[86] Y. Makarov and N. Moharari, "A generalized power system reliability and security index," in *Electric Power Engineering, PowerTech Budapest. International Conference on*, 1999, p. 136.

[87] J. F. Benders, "Partitioning procedures for solving mixed-variables programming problems," *Numerische mathematik*, vol. 4, no. 1, pp. 238–252, 1962.

[88] W. Qiu and A. J. Flueck, "A new technique for evaluating the severity of generator outage contingencies based on two-parameter continuation," in *Power Engineering Society General Meeting.* IEEE, 2004, pp. 150–156.

[89] A. Monticelli, M. Pereira, and S. Granville, "Security-constrained optimal power flow with post-contingency corrective rescheduling," *Power Systems, IEEE Transactions on*, vol. 2, no. 1, pp. 175–180, 1987.

[90] M. Aragüés-Peñalba, J. Beerten, J. Rimez, D. Van Hertem, and O. Gomis Bellmunt, "Optimal power flow for hybrid AC/DC systems," in *Power Engineering Society General Meeting.* IEEE, July 2014.

[91] X. Wei, J. H. Chow, B. Fardanesh, and A.-A. Edris, "A common modeling framework of voltage-sourced converters for load flow, sensitivity, and dispatch analysis," *Power Systems, IEEE Transactions on*, vol. 19, no. 2, pp. 934–941, 2004.

[92] J. Beerten, "Modelling and Control of DC Grids (Modellering en controle van DC netten)," Ph.D. dissertation, Katholieke Universiteit Leuven, Belgium, 2013.

[93] S. Cole, "Steady-state and dynamic modelling of VSC HVDC systems for power system Simulation," Ph.D. dissertation, Katholieke Universiteit Leuven, Belgium, 2010.

[94] A. Pizano-Martinez, C. Fuerte-Esquivel, H. Ambriz-Perez, and E. Acha, "Modeling of VSC based HVDC systems for a Newton-Raphson OPF algorithm," *Power Systems, IEEE Transactions on*, vol. 22, no. 4, pp. 1794–1803, 2007.

[95] J. Cao, W. Du, H. Wang, and S. Bu, "Minimization of Transmission Loss in Meshed AC/DC Grids With VSC-MTDC Networks," *Power Systems, IEEE Transactions on*, vol. 28, no. 3, pp. 3047–3055, Aug 2013.

[96] K. Padiyar and N. Prabhu, "Modelling, control design and analysis of VSC based HVDC transmission systems," in *Power System Technology. International Conference on*, vol. 1. IEEE, 2004, pp. 774–779.

[97] M. Baradar, M. Ghandhari, and D. Van Hertem, "Modeling multi-terminal VSC-HVDC in power flow calculation using unified methodology," in *IEEE-PES ISGT Europe 2011*, Dec. 2011.

[98] J. Beerten, S. Cole, and R. Belmans, "Implementation aspects of a sequential AC/DC power flow computation algorithm for multi-terminal VSC HVDC systems," in *ACDC2010, Proceedings in*, London, October 20-21 2010.

[99] S. Cole, J. Beerten, and R. Belmans, "Generalized dynamic VSC MTDC model for power system stability studies," *Power Systems, IEEE Transactions on*, vol. 25, no. 3, pp. 1655–1662, August 2010.

[100] J. Beerten, S. Cole, and R. Belmans, "A sequential AC/DC power flow algorithm for networks containing Multi-terminal VSC HVDC systems," in *Power Engineering Society General Meeting*. IEEE, 2010.

[101] T. Chung and G. Shaoyun, "Optimal power flow incorporating FACTS devices and power flow control constraints," in *Power System Technology, International Conference on*, vol. 1. IEEE, 1998, pp. 415–419.

[102] J. Rimez and R. Belmans, "A combined AC/DC Optimal Power Flow Algorithm for meshed AC and DC Networks linked by VSC Converters," in *International Transactions on Electrical Energy Systems, Wiley (accepted)*, 2014.

[103] S. De Boeck and D. Van Hertem, "Coordination of multiple HVDC links in power systems during alert and emergency situations," in *PowerTech (POWERTECH)*. Grenoble: IEEE, June 2013, pp. 1–6.

[104] G. W. Stagg and A. El-Abaid, *Computer Methods in Power System Analysis*. McGraw-Hill, 1968.

[105] T. Athay, R. Podmore, and S. Virmani, "A practical method for the direct analysis of transient stability," *Power Apparatus and Systems, IEEE Transactions on*, no. 2, pp. 573–584, 1979.

Curriculum vitae

ir Johan Rimez
Born: November 8th, 1977 in Halle (Belgium)
Married to: Erika Plaitin

1989 - 1995	Secondary School Onze-Lieve-Vrouwe College (Halle, Belgium) Latin-Mathematics (8h) Special awards for Mathematics and Aesthetics
1995 - 2000	Master Degree in Applied Sciences Vrije Universiteit Brussel (Brussels, Belgium) Electro-mechanical engineering Graduated with great distinction
2000 - 2004	Project engineer Tractebel Engineering, afterwards BEL Engineering
2004 - 2008	Expert HV equipment Elia Engineering
2008 -	Senior Expert Simulations and special grid phenomena Elia Engineering
2008 - 2014	PhD Researcher KULeuven - ESAT - ELECTA (Leuven, Belgium)
2012 -	Observer member of the CIGRE B4 study committee “HVDC and Power Electronics” for Belgium

List of publications

Published papers

J. Rimez e.a., "Grid implementation of a 400MVA phase shifting transformer for power flow control in the Belgian Network : specification and operational considerations", in *CIGRE Paris 2006 session, paper A2.202*, 2006

J. Rimez e.a., "Impact of furan analysis on asset management of high voltage transformers in the Belgian transmission network", in *CIGRE Colloquium A2-D1, paper PS1-19*, Brugge, 2007

J. Warichet, J. Rimez, e.a., "Grid implementation and operational use of large phase shifting transformers in the Belgian HV grid to cope with international network challenges", in *CIGRE Paris 2010 session, paper C2.207*, 2010

D. Van Hertem, J. Rimez, R. Belmans, "Power flow controlling devices as a Smart and Independent Grid Investment for flexible grid operations: Belgian Case Study", in *Smart Grid, IEEE Transactions on*, vol. 4, pp. 1656-1664, 2013

Papers under review

J. Rimez, R. Belmans, "A combined AC/DC Optimal Power Flow Algorithm for meshed AC and DC Networks linked by VSC Converters", in *Electrical Energy Systems, International Transactions on*, Wiley, 2013 (accepted for publication)

J. Rimez, J.L. Limelette, B. Brijs, "The first Belgian HVDC Link NEMO: technical choices, obstacles and future developments", *CIGRE Belgium Conference*, Brussels, 2014

J. Rimez, B. Genêt, J.F. Goffinet, D. Moers, L. Uyttersprot, C. Engelbrecht, S.G. Kim, "Design of the assets of a mixed 380 kV link using a risk-based approach, the STEVIN project", *CIGRE Belgium Conference*, Brussels, 2014

M. Aragüés-Peñalba, J. Beerten, J. Rimez, D. Van Hertem, O. Gomis Bellmunt, "Optimal power flow for hybrid AC/DC systems", *Power and Energy Society General Meeting*, IEEE, July 2014 (submitted)

FACULTY OF ENGINEERING SCIENCE
DEPARTMENT OF ELECTICAL ENGINEERING
DIVISION ELECTA
Kasteelpark Arenberg 10, box 2445
B-3001 Heverlee
info@esat.kuleuven.be
http://www.esat.kuleuven.be